DEVELOPMENT OF PROCESS TO SIMULTANEOUSLY SCRUB NO_2 AND SO_2 FROM COAL–FIRED FLUE GAS

A.B. Evans, R.K. Lyon, J.N. Pont, G.C. England, W.R. Seeker
Energy and Environmental Research
18 Mason
Irvine, CA 92718

V. Zamansky
Research Cottrell
P.O. Box 1500
Somerville, N.J. 08876

Key Words: NO_2 scrubbing, CombiNO_x, Na/Ca based scrubbers.

INTRODUCTION

The CombiNO_x process is being developed to provide a low-cost method of controlling the NO_x emissions of coal–fired utility boilers to very low levels. This process incorporates a family of NO_x reduction technologies including staged combustion, Advanced Reburning (i.e. reburning combined with selective non–catalytic reduction) and methanol injection to convert NO to NO_2 which can then he removed by wet scrubbing. While individually these technologies are limited in their NO_x reducing capabilities, in combination they are capable of reducing NO_x emissions to extremely low levels at a fraction of the cost of selective catalytic reduction.

The methanol injection step, however, is subject to the limitation that one must have a scrubber that will remove NO_2. The removal of SO_2 and NO_2 by sodium-based wet scrubbers is a well -established technology, but the majority of wet scrubbers currently in use are calcium based. Accordingly, this study was undertaken to determine whether or not the chemistry which occurs in calcium based scrubbers could be modified to allow removal of NO_2 as well as SO_2.

Bench-scale experiments were performed in conjunction with chemical computational modeling to evaluate the effect of scrubbing solution composition on SO_2 and NO_2 scrubbing efficiency. In addition, potential by-products were identified. Finally, larger pilot-scale tests were performed with a packed tower scrubber to address scale–up issues and confirm the bench-scale results.

BENCH-SCALE STUDIES

The bench-scale NO_2 scrubbing apparatus is displayed in Figure 1. A simulated flue gas containing variable amounts of NO_2 and SO_2 was flowed through a constant temperature, 80 cubic centimeter, bubbler containing the scrubbing solution to be evaluated. After passing through the "scrubber", the gas was analyzed for O_2, NO_x, N_2O, and SO_2 to determine removal efficiencies.

Figure 2 graphically summarizes the bench-scale results. The numbers symbolize various cases that were performed while varying slurry composition, the lines show the resulting performance as a

function of time. A $Ca(OH)_2$ solution (2 percent $Ca(OH)_2$ by weight) achieved 99+ percent SO_2 reduction, indicating that the scrubber provides good mass transfer. However, only 50 percent of the NO_2 was removed. Reference 1 indicates that the crucial reaction for NO_2 scrubbing is:

$$NO_2 + SO_3^{--} = NO_2^{-} + SO_3^{-}. \qquad (1)$$

With pure $Ca(OH)_2$ solution, the necessary sulfite ion (SO_3^{--}) tends to precipitate out as calcium sulfite, instead of reacting, as desired, with NO_2.

Since sodium sulfite (Na_2SO_3) can provide the necessary sulfite ions for NO_2 absorption, a 2 percent solution was evaluated. 99+ percent SO_2 and 89 percent NO_2 capture was obtained initially, however, this performance decreased after approximately 2 minutes of run time. After these 2 minutes, SO_2 reduction became negative and NO_2 reduction dropped to 17%. SO_2 is captured via the reaction

$$SO_2 + SO_3^{--} = 2HSO_3^{-} \qquad (2)$$

and NO_2 via reaction (1). Unfortunately, the SO_3^{-} generated by NO_2 removal is a chain carrier in the oxidation of sulfite and bisulfite ions to sulfate and bisulfate ions. Oxidation of the bisulfite ion to the bisulfate ion acidifies the solution, forcing SO_2 back into the gas phase.

Adding $Ca(OH)_2$ to the Na_2SO_3 scrubbing solution eliminates the problem of SO_2 rejection by keeping the solution basic, however the NO_2 capture remains poor and short lived. Replacing the highly soluble $Ca(OH)_2$ with very low solubility $CaCO_3$ increases the concentration of sulfite ion that stays in solution. This improves NO_2 absorption, but the sulfite ion quickly oxidizes to sulfate, hampering NO_2 removal. Experiments were conducted under conditions which inhibited the oxidation of sulfite to sulfate (i.e. decreasing reaction temperature and/or flue gas oxygen content). Even though these conditions can not be applied to a real application, they did show that if sulfite ion stays in solution, NO_2 capture improves and can be sustained for a longer period of time.

Sodium thiosulfate ($Na_2S_2O_3$) has been proposed as a method of inhibiting the oxidation of sulfite to sulfate (2). We found that by adding this compound to the scrubbing solution (1% by weight), 95% NO_2 capture was achieved and this capture was sustained for the duration of the test. Based on these results, the recommended slurry solution to achieve 99+ percent SO_2 and 95 percent NO_2 at bench -scale level is:

9% Na_2CO_3
9% $CaCO_3$
1% $Na_2S_2O_3$.

This scrubbing mixture was studied computationally using the mechanism of Chang et al. (1). For the batch experiments, the reaction was found to proceed in three stages. During the first stage, carbonate ion concentration falls while the concentrations of sulfate, bisulfate and sulfite ion increase. This first stage ends when the ratio of carbonate to sulfite ion becomes so low that calcium carbonate starts to dissolve while calcium sulfite precipitates. During the second stage, the ratio of the concentrations of carbonate and sulfite ion are constant and the pH remains fairly steady. The

concentration of sulfate ion increases until calcium sulfate starts to precipitate. The second stage ends when the calcium carbonate is exhausted. When this happens the pH begins to rise until it reaches a level at which SO_2 absorption fails and scrubbing solution is spent.

The model predicts that NO_2 capture will remain effective through these three stages of the process, but the fate of absorbed NO_2 changes. During the first and second stages nearly all of the absorbed NO_2 will be present as nitrite ion, with only trace amounts of the complex nitrogen sulfur ions being formed. During the third stage, however, the nitrite ion is converted to complex nitrogen sulfur ions, chiefly the aminetrisulfonate ion. Near the end of the third stage the aminetrisulfonate ions are hydrolyzed to sulfate ion and sulfamic acid.

While the model contains reactions which are capable of forming N_2O and nitrate ions, these reactions are only significant at very low pH. During the bench-scale experiments samples were taken of the bubbler's exhaust and, consistent with the models predictions, no significant N_2O production was observed. Measurements were also made with EM Quant test strips on spent scrubbing solution. As one would expect from the model, nitrite ion was found in fresh solution but not in solution which had been allowed to age. Nitrate ions were not detected in the spent solution.

PILOT-SCALE STUDIES

Scale-up effects were investigated in two different pilot-scale facilities corresponding nominally to heat inputs of 2 MMBtu/hr and 10 MMBtu/hr. The small pilot-scale scrubber tests were performed by Research Cottrell using the facility illustrated in Figure 3. The small pilot- scale scrubber consists of a propane combustor, absorber tower, absorber feed tank, analytical train, and solid disposal system. To simulate a coal–fired flue gas, variable amounts of SO_2 and NO_2 were doped into the exhaust upstream of the absorber tower. At the absorber tower exit, NO_x, SO_2, CO, and O_2 were measured. The absorber tower is a vertical, stainless steel, 16 inch diameter tube, approximately 20 feet in height. The simulated flue gas enters the tower from the bottom, travels through five sections to the top, and exits to the gas sample conditioning systems and analyzers. The first two sections can be packed with a light packing material to provide improved gas/liquid contact. Sections of the tower may also be removed, if desired, to reduce absorber tower residence time. The scrubber slurry is continually being mixed with dry limestone, sodium salts, and water in the absorber feed tank. From the 200-gallon feed tank, the slurry is pumped to the top of the absorber tower and dispensed in counter flow to the flue gas with a single slurry nozzle. The slurry solution is drained by gravity from the bottom of the tower back to the feed tank.

The first tests were performed to verify that SO_2 removal was possible on the pilot-scale scrubber. For a 6 percent limestone slurry, flue gas flow rates were varied between 127 - 140 cfm, and slurry flow rates were maintained at 12 gpm. Up to 99 percent SO_2 removal was obtained indicating satisfactory mass transfer.

Simultaneous scrubbing of NO_2 and SO_2 was evaluated using scrubbing salts consisting of 49.5 percent $CaCO_3$, 49.5 percent Na_2CO_3, 1 percent $Na_2S_2O_3$. Note this is approximately 1/5 of the concentration of $Na_2S_2O_3$ utilized in the bench-scale tests. During this test series, the following parameters were varied: liquid/gas ratio (liquid flow and gas flow were independently varied),

concentration of sodium carbonate in slurry, concentration of sodium thiosulfate in slurry, and initial NO_2 concentration. NO_2 removal efficiency ranged between 65 and 90 percent while maintaining 97 - 99 percent SO_2 removal.

The ratio of slurry flow rate to flue gas flow rate is defined as the liquid to gas ratio (L/G), and is expressed here in units of (gallons of slurry)/(1000 cubic feet of gas). The slurry flow and gas flow were varied independently of one another. Figure 4 summarizes the effects of L/G ratio on NO_2 scrubbing efficiency. As would be expected, a larger L/G ratio results in higher NO_2 removal. Even though not depicted in the figure, data indicate that gas flow rate has a larger affect on the NO_2 scrubbing efficiency than slurry flow rate. By decreasing the gas flow rate by a small fraction (from 135 to 115 cfm), efficiency increased from 77 to 84 percent. However, when the slurry flow rate was nearly doubled (11.4 to 20 gpm), the efficiency only increased by approximately the same amount, 77 to 85 percent.

Experiments were performed to determine the effect of initial NO_2 concentration on NO_2 scrubbing efficiency. Slurry flow rate remained approximately constant as inlet NO_2 concentration was varied by adjusting the doping gas flow rate. Results are displayed in Figure 5. The general trend shows that scrubbing effectiveness drops as initial NO_2 concentrations increase.

The effect of Na_2CO_3 concentration on NO_2 and SO_2 scrubbing efficiency was evaluated by diluting the scrubbing solution by a factor of two, while continuing to add limestone to maintain pH and ion concentration. Figure 6 shows that even though scrubbing efficiency was initially hampered by the dilution that occurs 200 minutes into the test, with time the NO_2 removal efficiency rose again to approximately the same level as before the dilution. Even after diluting the slurry a second time, the NO_2 scrubbing efficiency returned to almost the original value. These data indicate that NO_2 removal efficiency is not sensitive to Na_2CO_3 concentration in this range.

The effect of sodium thiosulfate concentration was tested by adding an additional 3.8 mmol of sodium thiosulfate per liter of solution. As expected, NO_2 removal efficiency jumped from 65 percent to 89-90 percent within 15 minutes, and SO_2 removal efficiency remained at 99+ percent. The thiosulfate inhibits oxidation of sulfite to sulfate, sustaining the presence of sufficient sulfite ions for NO_2 capture.

Throughout the experiments discussed above, scrubbing solution composition measurements were periodically taken. In general, these observations were consistent with the model and the assumption that the scrubber was operating in the second stage (see previous discussion). The model is, however, limited in its ability to account for sulfite ion oxidation, therefore, not surprisingly, sulfite to sulfate conversion was much higher than predicted. The small pilot-scale studies also show nitrate ion as a major product, contradicting both model's prediction and the bench-scale results.

A single test was performed in EER's large pilot-scale facility. The large pilot-scale scrubber facility consists of a simple spray tower with a pad-type demister. The spray tower is 6 ft in diameter and 16 ft high, with an array of 16 spray nozzles. Natural gas combustion products were doped with NO_2 to a concentration of 74 ppm. SO_2 was not added. The test was conducted at an L/G ratio of approximately 30 gal/1000 acf and the scrubbing solution was 9 percent $CaCO_3$/9 percent NaOH/1

percent $Na_2S_2O_3$. The test results are also shown in Figure 4. Much higher NO_2 removal was achieved than was expected based on the small pilot-scale results. This may have been due to the much higher concentration of sodium thiosulfate used in the large pilot-scale test. However, additional tests are necessary to validate this hypothesis. The results do indicate that high NO_2 removal efficiencies can be achieved even with a relatively primitive scrubbing system operating at L/G ratios similar to that of large commercial scrubbers.

DISCUSSION

The primary goal of this research, demonstration of efficient NO_2 and SO_2 scrubbing in a calcium based wet limestone scrubber, has been achieved. Two important questions, however, remain with respect to the disposability of the products produced by this modified scrubber. First, there is the question of whether or not using sodium compounds in the scrubbing solution will result in unacceptable sodium contamination of the calcium sulfate/sulfite product. Since wet scrubbers require considerable amounts of makeup water, it is theoretically possible to solve this problem by washing the calcium sulfate/sulfite with the makeup water, but this option would require an engineering design study which has not been done.

The second question of disposability regards the formation of nitrate ion seen in the pilot-scale experiments. This ion formation was not detected during bench-scale or computer modeling studies. One possible explanation for this discrepancy is that as the scrubbing liquid passes downward through the absorber tower, it reaches a point at which its ability to absorb SO_2 is completely exhausted. This low pH condition was not considered in the modeling study, yet it may responsible for the increase in nitrate concentration. Mechanisms within the computer model do, in fact, show nitrate ion formation at low pH levels.

While the possible formation of nitrate ion will require further research, there are a number of ways in which this problem might be solved. Adjustment of scrubbing conditions so that the solution is prevented from over-reacting may prevent nitrate formation. Alternatively, if nitrate forms by oxidation of nitrite ion, the removal of nitrite ion by reaction with NH_2SO_3H may prevent nitrate formation, or, all else failing, nitrate ion could be removed by selective reduction with scrap aluminum (3). In a brief study the authors found that this method works quite well with shredded soda cans as the source of aluminum.

ACKNOWLEDGMENTS

This work was funded under DOE Contract No. DE-AC22-90PC90363, Development of Advanced NO_x Control Concepts for Coal–Fired Utility Boilers. Mr. Charles E. Schmidt of Department of Energy Program Coordinator. The small pilot-scale experimental scrubbing studies were conducted by Research Cottrell under subcontract to EER.

REFERENCES

1. S.C. Chang, D. Littlejohn and N.H. Lin, *Flue Gas Desulfurization*, ACS Symposium Series 188, American Chemical Society, p. 128 - 152, (1982)
2. E. Gorin, M.D. Kulik, R.T. Struck, U.S. Patent 3,937,788 (1976).
3. A.P. Murphy, *Chemical Removal of Nitrate from Water*, Nature 350, 223-225, (1991).

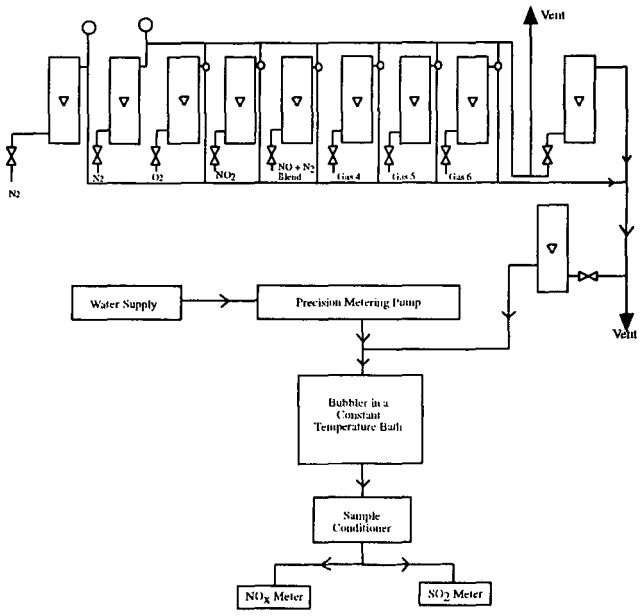

Figure 1. Experimental set–up for NO_2/SO_2 scrubbing experiments.

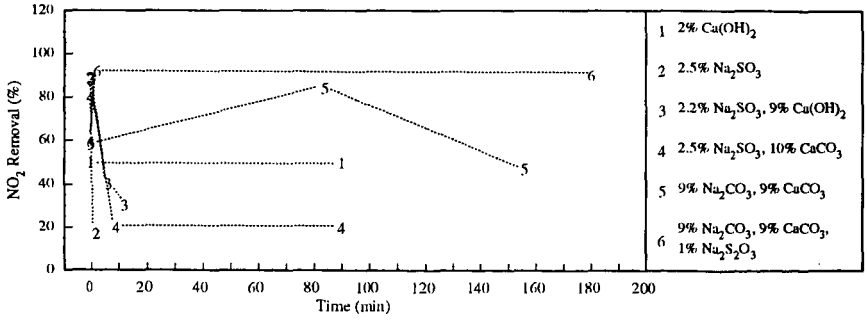

Figure 2. Bench-scale scrubbing studies results.

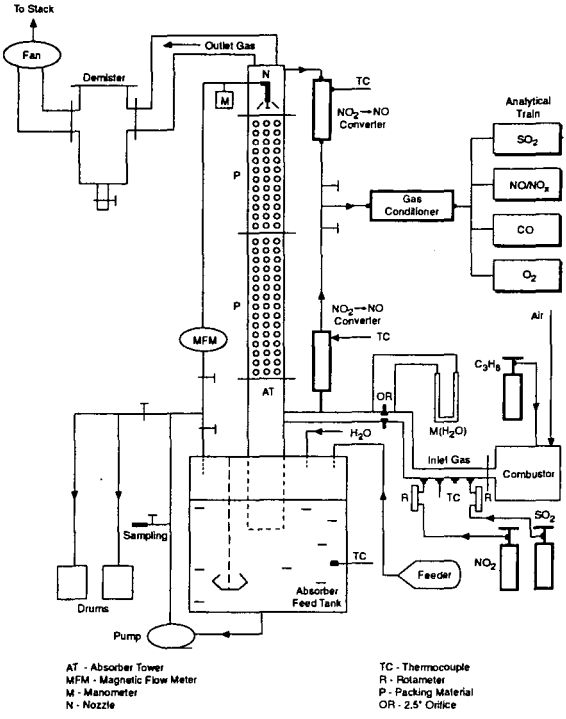

Figure 3. Schematic of the pilot-scale scrubber.

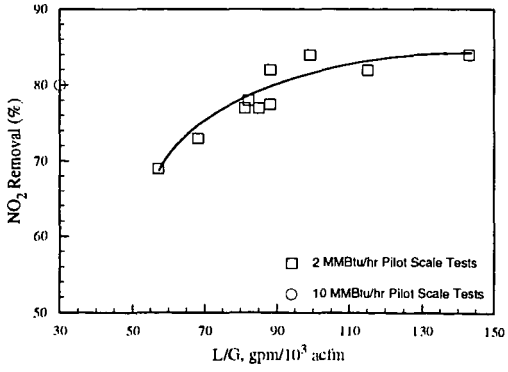

Figure 4. Effect of liquid to gas ratio on NO_2 removal.

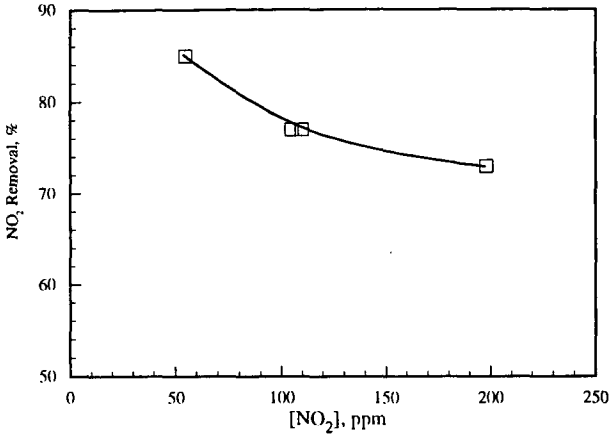

Figure 5. Effect of initial NO_2 concentration on NO_2 removal.

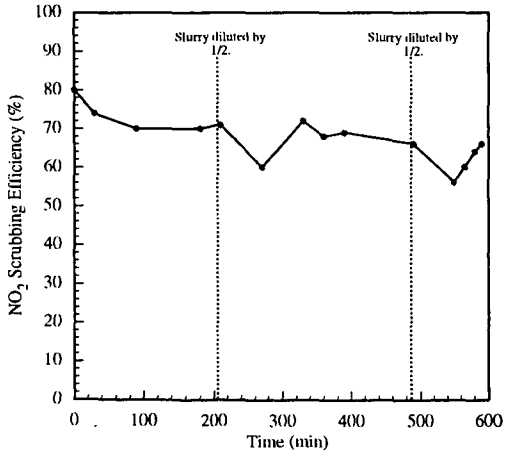

Figure 6. Effect of Na_2CO_3 dilution on NO_2 scrubbing performance.

THE CHEMISTRY OF ELECTROSTATIC PRECIPITATION

P. L. Feldman and K. S. Kumar
Research-Cottrell
Somerville, NJ

Keywords: Electrostatic precipitation; corona; electrical breakdown; resistivity; chemical conditioning

ABSTRACT

Electrostatic precipitation is a leading means of particulate emissions control for large industrial and utility plants. It effects collection of the particulate matter by charging the particles in a corona discharge and causing them to migrate to a grounded collecting surface under the influence of an electric field. At first it may appear that this process is strictly electrical in nature, but in reality the chemistry of the process is just as important, if not moreso, as the electrical aspects are to the efficiency of the process. The important chemical effects are seen primarily in the gas phase chemistry as it influences electrical breakdown, or sparking, and particle surface chemistry as it influences conductivity and cohesivity. This paper presents examples of the use of chemical methods to enhance the precipitation process including the use of chemical conditioning agents to improve particle conductivity or cohesivity or to increase gas breakdown strength. Also discussed are specific effects of sulfur, sodium, carbon and various metals in determining the viability of electrostatic precipitation in a given application. A section is also devoted to a discussion of the use of corona discharge to promote chemical reactions for air pollution control.

THE ELECTROSTATIC PRECIPITATION PROCESS

Electrostatic precipitation is a leading means for the control of particulate emissions from large industrial and power generation sources. It is capable of very high particulate removal efficiencies, including the control of the submicron particulate fraction. The electrostatic precipitation process is different from other mechanical means of particulate control, such as filters and cyclones, in that it uses electrical forces to separate the particles from the gas stream. These electrical forces are applied by exposing the particles to a corona discharge, therby charging them electrically, and then placing them in a zone of high electric field strength. The resultant electrical force, proportional to the product of the particle charge and the field strength, moves the particles towards a grounded collecting surface where they are held until periodically rapped into hoppers for disposal. Modern industrial precipitators use the single-stage design which accomplishes the corona discharge and electric field functions simultaneously in a single geometry consisting of high voltage discharge electrodes placed between grounded collecting plates. The discharge polarity in these precipitators is negative. The discharge electrodes themselves are either small-diameter wires or more rigid bodies with points or sharp edges. A sharp radius of curvature

is necessary to concentrate electric field strength to allow corona discharge.

Although electrostatic precipitation is electrophysical in nature, the process efficiency and viability are strongly influenced by other scientific disciplines, especially gas and surface chemistry. In fact much of the original development work of the precipitator was carried out by chemists and metallurgists. Dr. Frederick Cottrell is credited with developing the first practical electrostatic precipitator in the early 1900's. The importance of chemistry in electrostatic precipitation can be understood by looking more closely at some of the performance-limiting aspects of the process, namely gas-phase breakdown, dust layer breakdown and particle reentrainment. Enhancement of the precipitation process can then be achieved by altering the system chemistry toward more favorable conditions.

ELECTRICAL BREAKDOWN OF THE GAS PHASE

Electrical breakdown of the gas phase as manifested by sparking limits the operation of the precipitator by imposing a maximum to the voltage which can be applied to the discharge electrodes, thereby limiting the power input to the precipitator as well as the field strength and the supply of corona-generated ions necessary to the process. Since precipitator efficiency can be correlated with power input, this limitation is very important. The levels of voltage and corona current at which sparking will occur is determined by gas density and electrode spacings as well as the chemistry of the gas flowing through the precipitator. In the corona zone, electrons are emitted from the discharge points and move toward the grounded electrode under the influence of the electric field between the discharge electrode and the collecting plate. As they lose their initial energy they tend to attach to gas molecules they encounter on the way, forming negative ions which then travel at much lower velocities toward the grounded electrode, resulting in a more controlled corona current. Gas molecules differ in their receptiveness to attachment of electrons. Nitrogen for example is not receptive. Therefore in pure nitrogen no ions are formed and the current is totally electronic, resulting in high current (because of the high electron velocities) and breakdown at voltages only slightly above corona start. The precipitation process is not practical under these circumstances.

For effective electrostatic precipitation, small amounts of electronegative gases must be present in the gas stream to attach the electrons and, through their lower ionic mobility, provide controlled corona current over a wide range of voltage before breakdown occurs. Such gases include oxygen, water, ammonia, sulfur dioxide, many organic vapors and others. Normal industrial flue gases contain adequate amounts of electronegative gases so generation of stable corona is not usually a problem. However, there are situations in which gas conditioning can be employed to reduce the net ion mobility and achieve more stable operation. An important example is precipitation at low gas density. Such applications include high temperature operations such as precipitators on fluid cat cracker exhaust in the petroleum industry. These precipitators normally operate at about 700°F and

frequently are limited by premature breakdown because of the low gas density. Addition of ppm amounts of ammonia is found to remedy the situation and allow operation at higher power input levels, thereby restoring efficient operation.

In other applications the addition of percentage amounts of water vapor can have significant benefits to electrostatic precipitation by allowing operation at higher voltage and power input levels because of the net reduction of ionic mobility. Practical increases in power input of 20% or more can be achieved in this way.

ELECTRICAL BREAKDOWN OF THE DUST LAYER

Another important performance limitation encountered by electrostatic precipitators is the electrical breakdown of the dust layer deposited on the collecting electrode. This condition arises when the resistivity of the dust layer is high. Generally when the resistivity is above 10^{11} ohm-cm, electrical breakdown of the dust layer occurs before gas-phase breakdown. Dust layer breakdown is caused by the development of a high voltage gradient across the dust layer which exceeds the breakdown strength of the gas in the interstices of the dust layer. The voltage gradient is due to current flow through the layer, and is equal to the product of resistivity and current density. As resistivity increases, the allowable current before breakdown decreases, and, in extreme cases, operation of the precipitator is seriously impaired. Dust layer breakdown may manifest itself as premature sparking or as back corona. Back corona is a phenomenon in which a stable discharge of positive ions originates from the dust layer because of the high voltage gradient present there. The positive ions then tend to neutralize the negative particle charge achieved by the forward corona and thereby defeat the particle collection process.

Dust layer resistivity is dependent on the chemical composition of the dust and its temperature. For coal combustion flyash, several models and rules-of-thumb exist for relating flyash resistivity to ash composition, gas chemistry and temperature. For example a computer model developed by Southern Research Institute uses a large database to derive correlations for resistivity with virtually all the constituents of flyash. In addition there are many indices which have been published in the literature for relating various key components to resistivity. Examples include the alkali-silicate index relating resistivity to the ratio of sodium + potassium to silica + alumina; the Soviet index which uses the ratio of silica + alumina times ash content to moisture + hydrogen times sulfur content; the Bureau of Mines oxide index which uses the ratio of calcium + magnesium oxides to sodium oxide + sulfur trioxide; and many more. Also it is generally true that coals high in sulfur content produce ashes which are not of high resistivity. The point to be made is that the chemical composition of the dust to be precipitated determines its resistivity, and therefore determines whether or not the precipitator will have difficulty in operating effectively.

Temperature determines the mode of electrical conduction through the layer; at higher temperatures, e.g. above 400°F, volumetric

conductivity of the particles is controlling, and, at lower temperatures, e.g. below 300°F surface conductivity is controlling. In the transition range between about 300°F and 400°F a maximum in resistivity usually occurs. For power generation applications, flue gas temperature is normally around 300°F and, depending on ash composition, may be subject to high resistivity problems. Although it may appear that an easy solution is to either raise or lower the temperature of operation of the precipitator, this is not necessarily a practical solution. Lowering the temperature may result in acid dew point problems, and operation at higher temperature, though sometimes effective, carries with it other problems including the possibility of the sodium depletion phenomenon. Sodium depletion refers to the migration of sodium out of a thin sublayer of ash next to the collecting surface under the influence of the electric field at high temperature. The resulting sodium-poor layer, for many ashes, is itself highly resistive and presents the same high resistivity limitation the high temperature operation was intended to solve. The sodium depletion problem, however, has been found to be treatable by the addition of sodium compounds to the coal feed, although this is objectionable to many boiler operators.

An effective remedy for high resistivity and one that is practiced widely is chemical conditioning of the flyash. Chemical conditioning is effective in enhancing the surface conductivity of the ash and is thus generally used at temperatures of 300°F and below. Sulfur trioxide is the most used conditioning agent. The addition of ppm levels of sulfur trioxide to the flue gas can reduce resistivity out of the problem range by depositing a conductive layer of sulfuric acid on the ash surface. Not all ashes are easily conditioned by SO_3 however. For example the acidic Eastern bituminous ashes are more difficult to condition, often requiring higher levels of SO_3 to be effective. On the other hand the alkaline Western coal ashes are easily conditioned by low ppm of SO_3. To improve the conditionability of the Eastern ashes it has become common to consider the use of dual conditioning, using low ppm levels of ammonia injection in the flue gas in addition to the SO_3. The effect of the ammonia is probably to increase the pH of the ash surface so that it is more receptive to the acid.

Although most commonly used, sulfur trioxide is not the only conditioning agent found effective for reducing resistivity. Others include sulfonic acid, sulfamic acid, ammonium sulfate and bisulfate, sodium carbonate, triethylamine, and various proprietary chemicals. In some cases moisture addition alone is effective.

PARTICLE REENTRAINMENT

Proper operation of an electrostatic precipitator involves periodic rapping of the collecting plates to jar loose the collected dust and allow it to fall into the hoppers for subsequent removal. Before the collectee dust is finally removed from the precipitator, however, it is subject to reentrainment back into the gas stream by three mechanisms: scouring of the dust off the collecting surface by the gas flow itself; electrical reentrainment caused by inductive reversal of charge on the

collected dust because of inadequate electrical current; and reentrainment induced by the rapping blow itself. The effect of reentrainment is to reduce the net collection efficiency of the precipitator. This can be a serious limitation in achieving modern high efficiency particulate control requirements in a reasonably sized precipitator.

The reentrainment problem can be greatly reduced by agglomeration of the particles on the collecting surface. This is because the agglomerates will tend to cake and fall to the hoppers more readily than the non-agglomerated fine particles. Also the agglomerates, because of their larger size, are more easily recollected in the remaining precipitator than the fine particles. It has been found that certain chemical additives are effective in promoting this desired agglomeration by enhancing the surface cohesivity of the particles. Some of these are ammonia, dual injection of ammonia and sulfur trioxide, moisture, sodium sulfate and others. Through use of these chemicals, reduction of reentrainment results in a marked decrease in emissions from the electrostatic precipitator. It is interesting to note that the precipitator's chief rival for high-efficiency particulate control, the fabric filter, also benefits from conditioning to increase particle cohesivity; the benefits to the fabric filter include higher collection efficiency and reduced pressure drop because of the formation of a more porous filter cake.

CORONA CHEMISTRY

The region immediately surrounding the corona discharge point on the precipitator's discharge electrode is a region of intense electron activity. Electrons are emitted with high enough energy to create reactive species such a OH and O radicals when colliding with the constituent gas molecules. These radicals in turn can initiate reactions leading to the production of ozone and the oxidation of various flue gas components, e.g. NO and SO_2, therefore presenting the possibility of gaseous pollutant control by corona initiated reactions. Various investigators have realized this potential and work is ongoing to develop practical corona systems for the control of SO_2 and NO. EPA and others are investigating the use of corona for VOC destruction, claiming destruction of benzene, toluene and other organics at very high efficiencies.

Normal electrostatic precipitator configurations are far from optimum for taking advantage of corona chemistry. The active corona region occupies only a small fraction of the volume of the interelectrode space. Therefore the opportunity and time for exposure of the gaseous components to the active species is not adequate for good removal. Changes away from normal precipitator design have to be made to evolve into a practical contactor for the purpose of gaseous pollutant control. Electrode spacings have to be reduced to increase the fraction of volume occupied by the active species; very sharp discharge points have to be used to concentrate the electric field strength and deliver high energy electrons; and pulse enegization should be used to maximize the applied discharge voltage.

Further work is needed to develop the use of corona initiated reactions for gaseous pollutant control. It will not be done in a conventional precipitator design. Attention will also have to be paid to the energy requirement for achieving high levels of pollutant removal. Some of the reported work indicates that this requirement may be high depending on the pollutant to be removed.

INVESTIGATION INTO THE DISCREPANCY BETWEEN MWI AND MWC CDD/CDF EMISSIONS

W. Steven Lanier, T. Rob von Alten, and Richard K. Lyon
Energy and Environmental Research Corporation
Irvine, California 92718

INTRODUCTION

On February 11, 1991, the EPA promulgated standards of performance for new municipal waste combustors (MWC's) and emission guidelines for existing MWC's with a unit capacity greater than 250 tons/day of waste. These standards included limitations on total dioxins (tetra- through octa-chlorinated dibenzo-p-dioxins or CDD) and dibenzofurans (tetra- through octa-chlorinated dibenzofurans or CDF). For new units the CDD/CDF stack emission limit was set at 30 nanograms/dry standard cubic meter (ng/dscm) (12 gr/billion dscf), corrected to 7 percent oxygen (dry basis), and was based on use of a spray dryer/fabric filter (SD/FF) emission control system. For existing systems the CDD/CDF emission guideline was established at 125 ng/dscm (50 gr/billion dscf) and was based on use of a dry sorbent injection/fabric filter (DSI/FF) emission control system. In the Federal Register, the EPA concludes that "all types of existing MWC's . . . applying . . . a . . . DSI/FF system can meet a dioxin/furan emission level of . . . 50 gr/billion dscf at 7 percent [oxygen]." Based on limited emissions test data, it was believed that this emission level reflected a nominal 75 percent reduction in CDD/CDF emissions.

The EPA is currently developing emission standards for new and existing medical waste incinerators (MWIs). An initial belief was that MWIs and MWCs equipped with similar air pollution control devices (APCDs) would have similar CDD/CDF emission reductions and stack CDD/CDF removal being effected. This paper compares available CDD/CDF emission data from MWCs and MWIs and examines various parameters which could potentially contribute to higher emissions from MWIs. Based on this examination, a possible explanation was developed involving the partitioning of CDD/CDF between the stack gases and the captured fly ash. Data is then presented from subsequent testing which supports the hypothesis.

This study was funded by the U.S. Environmental Protection Agency through a subcontract to EER from Mid West Research Institute. The effort was coordinated by Mr. Ken Durkee at EPA and Mr. Roy Neulicht at MRI.

EMISSION COMPARISON: MWI vs. MWC

In the discussion that follows it is important to establish that with similar APCDs, stack CDD/CDF concentrations from MWIs are greater than from MWCs. To accomplish this objective, it is important to institute a frame of reference and a set of terminology reflecting the potential for formation of CDD/CDF in APCDs. Figure 1 illustrates the various chemical processes and the bifurcation of material within the APCD. Both solid and gas phase material exit the furnace (either MWI or MWC) and enter the APCD. CDD and CDF may be in either the gas phase or may be directly associated with solid phase material. Both phases of materials entering the APCD may also provide precursor materials or catalytic surfaces for formation of CDD/CDF in the APCD.

Within the APCD, many complex processes may occur. Surface catalyzed reactions can cause formation of CDD/CDF with key constituents supplied from either the gas phase or from material associated with the particulate or both. When the CDD/CDF, is formed it may be retained on the particle surface or desorbed to the gas phase. Any gas phase CDD/CDF entering the APCD may pass directly through the control device or may be absorbed on solid surfaces. From a mass balance perspective, there is a flow of CDD/CDF into the APCD with additional CDD/CDF formed in the control device. The inflow plus generated CDD/CDF will exit the APCD through the stack or with the collected fly ash. CDD/CDF in the gas phase will exit the APCD with the flue gas while the majority of the solid phase CDD/CDF will exit with the collected fly ash.

Historically, the effectiveness of APCD systems to "control" CDD/CDF emissions has been based on concentration measurements in the stack and at the APCD inlet, ignoring the quantity of CDD/CDF associated with the collected fly ash. The current study examines the available data from MWC and MWI

facilities within the broader framework and attempts to identify process parameters that could be responsible for apparent differences in emission performances between the two classes of incinerators.

APCD INLET CONCENTRATIONS

The initial point of comparison between MWCs and MWIs is to compare the CDD/CDF concentration in the gases leaving the incinerator -entering the APCD system. Figure 2 provides a compilation of inlet CDD/CDF data for a variety of MWIs[1-5] and MWCs[6,7,8]. A relatively wide variation in inlet CDD/CDF concentration is observed indicating differences in equipment design and possibly mode of operation. The important issue, however, is that no trend is observed indicating significantly higher CDD/CDF concentrations coming from either type of combustion equipment.

APCD OUTLET CONCENTRATIONS

There is a relatively small body of data defining the CDD/CDF emission performance of MWIs with APCDs and an even smaller body for units equipped with dry sorbent injection and a fabric filter. One such facility is the MWI at the Borgess Medical Center in Michigan. The Borgess Medical Center incinerator uses dry hydrated lime injection upstream of a baghouse for control of acid gas and particulate matter. A complete description of the Borgess facility and the test program is given in Volume II of the *Michigan Hospital Incinerator Emissions Test Program* [1].

The initial expectation was that CDD/CDF emission rates and APCD collection efficiency for the Borgess facility would be generally consistent with emissions from MWC facilities equipped with DSI/FF. Figure 3 illustrates outlet CDD/CDF concentrations for Borgess[1] and various MWCs[6,7,8] with DSI/FF. The CDD/CDF concentration from all the MWCs tested were under 60 ng/dscm while the outlet concentration measurements at the Borgess MWI ranged between 250 and 650 ng/dscm. Clearly the stack CDD/CDF emission concentrations from Borgess are significantly higher than emissions from MWCs with similar APCDs. Moreover, comparison of the data in Figures 2 and 3 indicates that the "Control Efficiency" of the DSI/FF at Borgess was extremely low and, on certain tests, was negative.

CDD/CDF FORMATION IN APCDs

The above comparisons indicates that stack CDD/CDF emissions from MWIs are higher than from MWCs. Two obvious explanations include the potential that more CDD/CDF is formed in the APCD system of MWIs or that DSI/FF is less effective on MWIs than on MWCs. The following section discusses the possibility that more CDD/CDF is formed in the APCD of medical waste incinerators.

APCD Temperature Formation of CDD/CDF can occur in the APCD and the formation rate generally increases with increasing temperature. Several laboratory studies suggest that peak formation rates occur when the reaction temperature is on the order of 300°C (572°F)[9]. Figure 4 presents the stack outlet CDD/CDF concentration versus APCD temperature for various MWI and MWC facilities utilizing PM control both with dry sorbent injection (DSI) and without acid gas control. The clearly illustrates the trend of increased CDD/CDF emission at higher APCD operating temperature. More importantly, the data tend to fall into two distinct groups. At any given APCD operating temperature, MWIs emit higher CDD/CDF concentrations than MWCs. Based on this comparison the APCD temperature does not provide a reasonable basis for explaining why MWIs have higher CDD/CDF stack emissions.

Surface Area Numerous process parameters have been suggested as key variables influencing low temperature formation of CDD/CDF. Since the basic formation reaction process is believed to be catalytic, one of the key parameters should be the amount of surface area provided by the fly ash. In general, the uncontrolled (inlet to the APCD) particulate matter (PM) loading from an MWC will be about an order of magnitude higher than from a MWI (1-2 gr/dscf for MWCs[10] vs. ~0.1 gr/dscf for MWIs[1,3]). However, the PM emitted by typical MWIs tends to be highly skewed toward submicron particles. Thus, it is possible that the shift in size distribution could more than offset the reduced mass loading.

Only limited size distribution data is available from either MWC or MWI[11] units. By combining actual or typical particle size distridution data with mass loading data it was posible to broadly PM surface area

variation. This process indicated that there is not major difference between MWCs and MWIs as regards the amount of PM surface area available for low temperature formation of CDD/CDF.

Presence of Chlorine and Catalysts The low temperature reactions to form CDD/CDF clearly involve surface reactions, but there is more than one way in which the surface could potentially participate. Researchers have shown a significantly greater formation of chlorinated organics when passing concentrations of Cl_2 rather than HCl over synthetic ash [12]. In these tests, the organic precursor to CDD/CDF was supplied by the particulate, but tests suggest an additional role for the particulate. Specifically, one of the standard processes for forming Cl_2 is to pass HCl over a copper catalyst. Copper or other catalysts in the particulate could enhance formation of Cl_2 and thereby increase CDD/CDF formation. Laboratory experiments using synthetic fly ash have shown that increasing the quantity of copper increased CDD/CDF formation[9]. Further studies examining fly ash from many incinerators found a moderate correlation between copper in ash and CDD/CDF[13].

Based on the above studies, there is at least a possibility that MWIs produce greater quantities of CDD/CDF because of enhanced formation of Cl_2. Medical waste incinerators typically have double the uncontrolled HCl emission compared to MWCs. The difference is due to the higher chlorine content of medical waste. The limited data on the amount of Cu in fly ash is not sufficient to draw conclusions on the comparative role of chlorine and catalysts in the formation of CDD/CDF. Although it remains possible that the higher chlorine content of medical waste (in conjunction with a catalyst) may influence the formation of CDD/CDF, there is a strong opinion that this is not the source of the observed variation in MWI and MWC CDD/CDF emissions. The HCl concentration from MWIs is probably no more than a factor of 2 greater than that from MWCs, and yet the CDD/CDF emissions are increased by a factor of 5 to an order of magnitude.

SYSTEM MASS BALANCE

The preceding evaluation, though not exhaustive, provides no explanation for the observed higher CDD/CDF concentration in MWI stack gases. Those evaluations, however, tend to focus on comparison of inlet and stack outlet CDD/CDF concentrations and do not include consideration of the CDD/CDF associated with the collected fly ash. For a limited number of facilities it is possible to estimate the actual formation of CDD/CDF in APCDs. The calculation requires that a mass balance be performed for the APCD. The amount formed equals the total CDD/CDF leaving the system (both in solid residue and in stack gases) minus the quantity entering the system. While portions of this data are available for many facilities, very few data sets contain all the required data. Three data sets which did contain all the necessary information are Borgess (MWI)[1], Montgomery County (MWC)[6], and Quebec City pilot study[8] (MWC).

For the three facilities with sufficient data, the total CDD/CDF generated is determined by adding all of the exit streams and subtracting the inlet concentrations. Data for all streams were normalized by the volumetric flow rate of flue gas for that facility, corrected to 7% O_2. Results are presented in Figure 5 and show that CDD/CDF formation is consistent between the comparable APCD systems at Borgess (MWI) and Quebec City (MWC) as well as with the DSI/ESP equipped Montgomery County facility. By comparing total CDD/CDF formation in the APCD the broad groupings of data observed in Figure 4 is collapsed into a single line.

GAS/SOLID CDD/CDF SPLIT IN APCDs

The preceding discussion has first shown that there is no significant difference between MWCs and MWIs relative to the concentration of CDD/CDF exiting the incinerator. Next it has been shown that there is no significant difference MWCs and MWIs relative to the mass of CDD/CDF formed in similar APCD systems. Thus, it is strongly suggested that the source of the discrepancy between MWC and MWI stack concentrations is the split between CDD/CDF captured with the fly ash and CDD/CDF which escapes with the flue gas. In general, it is expected that CDD/CDF in the gas phase within the APCD will be released with the flue gas while that associated with the PM (fly ash and sorbent) will likely be captured and exit the APCD with the solid residue. This section examines the issue of CDD/CDF partitioning in MWIs and MWCs.

A common perception is that under the low temperature conditions in an APCD, CDD and CDF will condense onto fly ash or onto injected sorbent material. A brief examination of the CDD/CDF vapor pressure characteristics shows that, in fact, condensation is not the controlling process. Figure 6 illustrates the variation in tetra and octa CDD vapor pressure as a function of temperature[14]. As shown, at 300°F the vapor pressure of octa CDD is > 10^{-3} atmospheres and the vapor pressure of tetra CDD is about 10^{-4} atmospheres. Thus, at 300°F, if the concentration of octa CDD is less than 1000 parts per million, it will remain in the vapor phase or be evaporated if it is a free liquid on the surface of a particle. By comparison, 1000 ng/Nm^3 of tetra CDD is equivalent to a concentration of about 50 parts per trillion.

Based on the above data, it is clear that within APCDs, CDD/CDF does not condense onto the surface of particles and remains as a free liquid or solid. It is also a fact, however, that substantial concentrations of CDD/CDF are found in fly ash collected from MWCs and MWIs. For this to occur it is necessary that the CDD/CDF be chemically or physically bonded to the PM. The implications of this requirement will be examined below.

If CDD/CDF is chemically bound to the surface of particulate matter (chemisorption), one would expect that bonding to be influenced by temperature and by the nature of the particle surfaces. As regards temperature, one would anticipate that the bonds would tend to break as the temperature increases. This possibility is evaluated by examining experimental data from the MWC in Montgomery County, Ohio where CDD/CDF concentrations were determined in both the collected fly ash and stack gas at several different APCD operating temperatures. These data are important in that tests were conducted both with and without sorbent injection. Further, the Montgomery County MWC is equipped with a water quench upstream of the ESP which tends to remove most of the large diameter particulate. In fact, this MWC has a PM size distribution entering the ESP which is quite similar to an MWI controlled-air system.

Table 1 and Figure7 illustrate data from the Montgomery County MWC. The data have been converted such that both the fly ash and stack CDD/CDF concentrations are normalized to the volume of dry flue gas, corrected to 7% oxygen. These data illustrate that greater amounts of CDD/CDF are formed at higher temperatures but also show how temperature impacts the bifurcation. As shown in Figure 7, all of the data without duct injection of sorbent exhibit a linear relationship. As APCD temperature increases, there is a substantial increase in the fraction of the total CDD/CDF which escapes with the stack gas. This is precisely the anticipated trend discussed earlier.Test point TC-5 was the only condition in the Montgomery County test series where hydrated lime was injected into the duct leading to the ESP. Table 1 and Figure 7 illustrate two important trends. First, the total quantity of CDD/CDF leaving the ESP (both gas and solid phase) was significantly reduced relative to the tests without duct sorbent injection at an equivalent temperature (test point TC-4). Additionally, however, of the total CDD/CDF from test TC-5, a much larger fraction was released to the gas phase. In test condition 5, 57% of the total CDD/CDF was released with the stack gas as compared to 22% in test condition 4.

The above described Montgomery County MWC data make two very important suggestions. Reducing APCD temperature will decrease the total quantity of CDD/CDF formed and will also reduce the fraction of that organic which will be released to the gas phase. The other key indication from this single test point is that hydrated lime injection greatly reduces total CDD/CDF formation. Further, the presence of hydrated lime appears to increase the percentage of total CDD/CDF released to the gas phase. The increase in percent released with stack gas was not nearly significant enough to offset the decrease in total formation and, hence, a reduction in stack gas concentration was observed.

Measurements similar to those discussed above for Montgomery County were taken at several other facilities. The Borgess MWI facility tests provide both ash and stack data but the testing covered only a relatively narrow band of fabric filter temperature. For the series of five tests at Borgess, the average CDD/CDF concentration at the APCD inlet, in the stack, and in the ash were 459, 452, and 355 ng/ dscm of flue gas respectively. Thus, the ratio of CDD/CDF in the fly ash to CDD/CDF in the stack gas is 0.78. Since the APCD temperature at Borgess was nominally 320°F, the tendency for CDD/CDF to be retained with the ash is almost identical to that observed at Montgomery County (with duct sorbent injection).

The other facility for which there is a large body of data is the Quebec City MWC which was tested as part of Environment Canada's NITEP program. Table 2 presents the CDD/CDF data in ng/dscm of flue gas basis at several locations in the pilot scale DSI/FF tests. In all cases, there was a substantial concentration of CDD/CDF leaving the fabric filter but essentially all of the organic was retained with the collected

solids. Note that even with the fabric filter operating at 408°F, only 7.3 ng/dscm were in the stack gas as compared to 2383 ng/dscm of total CDD/CDF exiting the fabric filter in the ash and stack gas combined. When compared to the previously described results, the data in Table 2 suggest that perhaps there is something different about the Quebec City Data. Duct injection of sorbent certainly did not significantly suppress the total CDD/CDF formation in the fabric filter. In fact, much more CDD/CDF was formed in the bag house at Quebec City than was formed at Borgess. What is totally different, however, is the fraction of that CDD/CDF that is released to the gas phase.

CARBON LOADING

The current study is unable to prove why the Quebec City MWC retained nearly all of its CDD/CDF with the collected solids. We can, however, suggest that carbon in the fly ash could be a controlling parameter and suggest that this parameter is the key difference between MWCs and MWIs.

Several field tests have demonstrated that injection of small quantities of activated carbon can have a significant impact on the emission of CDD/CDF from both MWC's and MWI's. Activated carbon injection is currently used at a few incinerators for mercury and volatile organic control. Typically, a small amount of carbon is injected into the flue gas and adequately mixed. Effort is made to assure good mixing prior to a moisturizing environment since water is believed to plug the pores and reduce the reactivity of the activated carbon. The small amounts of carbon (typically 20-400 mg/Nm^3 with an average of ~70 mg/Nm^3) are believed to provide a large amount of active surface area for chemisorption of CDD/CDF. Results from a hospital incinerator test in Sweden showed that activated carbon reduced outlet CDD/CDF emissions by 76 to 92% over tests without activated carbon[16]. A full scale MWC in Zurich reduced outlet CDD/CDF by 57 to 93%.

The relevance of the above data to the Quebec City MWC is that the pilot scale tests described in Table 2 were performed prior to completing extensive hardware modifications to improve combustion performance. In fact, personnel from the facility and from Environment Canada described the plume for the Quebec City MWC as containing many "black birds" -- thin, large diameter pieces of black material escaping the ESP. The carbon content of the particulate from this MWC (prior to the facility modification) is not reported in the various Environment Canada (EC) documentation. It is safe to assume, however, that the carbon in the uncontrolled ash was at least at the upper end of the range observed for other MWCs tested in recent years (1 to 5%). EC does report the uncontrolled PM concentration for the pilot scale DSI/FF tests. The average concentration reported was 6700 mg/Nm^3. If the carbon in ash was only 5%, then the total solid phase carbon loading entering the Quebec City pilot-scale fabric filter would be 335 mg/Nm^3. Thus, the "naturally occurring " carbon concentration is, as a minimum, consistent with the level of activated injected into the above MWI in Sweden or the MWC in Zurich.

In contrast to the situation at Quebec City, controlled air incinerators such as the Borgess facility have very low uncontrolled PM concentrations. At Borgess the average carbon content of the fly ash was approximately 5% (not including injected sorbent) and the average PM loading was 253 mg/dscm. Thus, at Borgess the solid phase carbon flow into the fabric filter is only 13 mg/dscm. That is significantly less than at Quebec City. There may be several phenomena which can explain the CDD/CDF retention discrepancy between Borgess and Quebec City, but clearly the flow of solid carbon to the particulate control device is a leading contender. In fact, it is the only phenomena uncovered thus far which can explain the observed discrepancy between MWC and MWI stack CDD/CDF emissions.

TESTING

The Borgess incinerator was retested to evaluate the impact of activated charcoal injection. The system was modified to inject activated carbon upstream of the fabric filter. Eight tests were completed. Three tests were run without carbon injection, two tests with carbon injection at 1 lb/hr, and three tests with carbon injection at 2.5 lb/hr. The test condition averages are illustrated in Figure 8. Carbon injection at 1 lb/hr reduced stack emissions by 88% from baseline average. With carbon injection at 2.5 lb/hr, stack emissions were reduced by 95% from baseline average. The results support the hypothesis that the amount of unburned carbon influences CDD/CDF stack emissions. The complete data set was not yet available to analyze the impacts of carbon injection on the split between captured fly ash and stack gases.

However, it is believed that the observed reduction is due to the carbon adsorbing the CDD/CDF from the gases and transferring it into the captured fly ash stream.

SUMMARY

The preceding material has examined a variety of phenomena in an attempt to explain a major inconsistency between CDD/CDF emissions from MWCs and MWIs utilizing similar pollution control systems and operating under similar conditions. The available data indicates that a larger portion of the CDD/CDF formed in the APCD of MWIs is released with the flue gas. For MWCs the larger fraction appears to be retained with the collected fly ash. The data also indicates that CDD/CDF leaving the APCD with the solid material is chemisorbed to the surface and not merely condensed on the surface. Increasing APCD temperature weakens those bonds and causes more of the CDD/CDF to be released to the gas phase. Further, it was shown that the strength of this bonding appears to depend on the nature of the particulate surface. Injected sorbent material tends to reduce the total quantity of CDD/CDF formed but the sorbent apparently does not provide a strong bonding between the CDD/CDF and the surface.

The issue of surface bonding led to a reexamination of DSI/FF pilot tests at the Quebec City MWC. The data shows three important trends. First, the total amount of CDD/CDF formed in the APCD system at Quebec City is greater than the quantity formed at the Borgess MWI. Secondly, almost all of this CDD/CDF was retained on the particulate matter and not released with the flue gas. This is very different than the situation with MWIs or with the Montgomery County MWC. Finally, it was shown that the Quebec City pilot-tests had a quite high concentration of carbon in the fly ash. In fact, the carbon levels are at least as high as in tests conducted in Europe where activated carbon was injected into the APCD. Those European tests showed major reduction in exhaust CDD/CDF concentration. In contrast to the Quebec City pilot test, typical MWIs (and the MWC test at Montgomery County) have very low solid carbon loading entering the APCD. The carbon in fly ash levels for MWIs are on the same order or less than in MWCs but the total particulate loading in MWIs is about a factor of 10 to 20 less than for MWCs. The low concentration of solid carbonaceous material, with strong bonding to gaseous hydrocarbons like CDD/CDF, could result in more of the formed CDD/CDF being released to the gas phase.

This theory was evaluated by retesting the Borgess incinerator. Tests were conducted with and without activated carbon injection. The results showed that the injection of activated carbon did reduce CDD/CDF stack concentrations to less than 20 ng/dscm @ 7% O_2. Those concentrations are approximately what is expected for a MWC with dry sorbent injection. Therefore, it is believed that the higher CDD/CDF stack emission concentrations observed at MWIs utilizing similar control technologies as a MWC, is due to the lower amount of unburned carbon loading in an MWI. The lower carbon loading in an MWI results in a greater fraction of the CDD/CDF escaping with the flue gas rather than be adsorbed and collected with the fly ash as in an MWC.

References

1. England, G., D. Hansell, J. Newhall and N. Soelberg. Draft Report " Michigan Hospital Incinerator Emissions Test Program Volume II: Site Summary Report, Borgess Medical Center Incinerator." April 15, 1991.
2. Radian Corporation. Draft Report " Medical Waste Incineration Emission Test Report, Volume I Jordan Hospital, Plymouth, Massachusetts." May 1991.
3. England, G., D. Hansell, J. Newhall, and N. Soelberg. Draft Report " Michigan Hospital Incinerator Emissions Test Program, Volume III: Site Summary Report, University of Michigan Medical Center Incinerator." April 25, 1991
4. Jenkins, Al, C. Castronovo, G. Lindner, P. Ouchida, and D. C. Simeroth. "Evaluation Test on a Hospital Refuse Incinerator at Cedars Sinai Medical Center, Los Angeles, CA." Test Report. April 1987.
5. Jenkins, Al, P. Ouchida, and G. Lew. "Evaluation Test on a Refuse Incinerator At Stanford University Environmental Safety Facility." California Air Resources Board, ARB/ML-88-025, August 1988.

6. Radian Corporation. " Draft Emissions Test Report for the Parametric Test Program at the Montgomery County South Facility, Unit 3, Dayton Ohio Volume I: Summary of Results." October, 1989.
7. P.J. Schindler. " Municipal Waste Combustion Assessment: Combustion Control at Existing Facilities." EPA Report No. 600/8-89-058. August 1989.
8. Environment Canada. " The National Incinerator Testing and Evaluation Program: Air Pollution Control Technology, Summary Report." EPS 3/UP/2. September 1986.
9. Stieglitz, L. and H. Vogg. " New Aspects of PCDD/PCDF Formation in Incineration Processes." Formation and Decomposition of Polychlorodibenzodioxins and -furans in Municipal Waste Incineration. February 1988.
10. Radian Corporation. " Municipal Waste Combustors - Background Information for Proposed Standards: Post-Combustion Technology Performance." EPA Report No. 450/3-89-27c. August 1989.
11. Brady, Jack. " Submicron Aerosol Generation and Aerosol Emission Control in Infectious Waste Incinerators." Presented at the Second International Conference on Municipal Waste Combustion. Tampa, Florida. April 16-19, 1991.
12. Gullet, Brian, K. Bruce,, and L. Beach. " Formation of Chlorinated Organics During Solid Waste Combustion." Waste Management and Research, Vol. 8, pp. 203-214 (1990).
13. Hinton, W. S. and A.M. Lane. " Characteristics of Municipal Solid Waste Incinerator Fly Ash Promoting the Formation of Polychlorinated Dioxins." Chemosphere, Vol. 22, pp. 473-483 (1991).
14. Rordorf, Berchtold. " Prediction of Vapor Pressures, Boiling Points and Enthalpies of Fusion for Twenty-Nine Halogenated Dibenzo-p-Dioxins and Fifty-Five Dibenzofurans by a Vapor Pressure Correlation Method." Chemosphere, Vol. 18, pp. 783-788 (1989).
15. Brown, B. and K.S. Felsvang. " Control of Mercury and Dioxin Emissions From United States and European Municipal Solid Waste Incinerators By Spray Dryer Absorption Systems." Presented at Second International Conference on Municipal Waste Combustion. Tampa, Florida. April 16-19, 1991.
16. Skovde Hospital Waste Incinerator. Performance Test Data.

Table 1 Montgomery County CDD/CDF Behavior

* (ng/dscm) corrected to 7% O_2

	Test Condition 1	Test Condition 2	Test Condition 3	Test Condition 4	Test Condition 5	Test Condition 6
Flue gas flow rate (dscm/min)	713	756	922	859	805	779
Oxygen concentration (%)	13.09	13.50	13.61	13.43	12.47	14.50
ESP temperature (°F)	571	396	394	298	306	534
Fly ash collection rate (g/min)	548	398	994	955	2270	436
Fly ash CDD/CDF conc. (ng/g)	2539	1761	2323	1179	9	4399
Fly ash CDD/CDF (ng/min)	1390220	700856	2309592	1125379	20433	1918123
CDD/CDF in fly ash *	3449	1731	4743	2424	42	5304
Stack CDD/CDF emissions *	17109	866	1480	673	57	14517
Total CDD/CDF out *	20558	2596	6223	3097	99	19821
Uncontrolled CDD/CDF conc.*	252	33	38	14	5	214
Total CDD/CDF Generated*	20306	2563	6185	3083	94	19607

Table 2 Complete CDD/CDF Behavior at Quebec City Pilot Study

* (ng/Nm^3) corrected to 7% O_2

Uncontrolled CDD/CDF *	880	2340	2300	1590
Fly ash CDD/CDF*	2076	2589	2576	2376
Stack CDD/CDF*	2.5	0.2	1.1	7.3

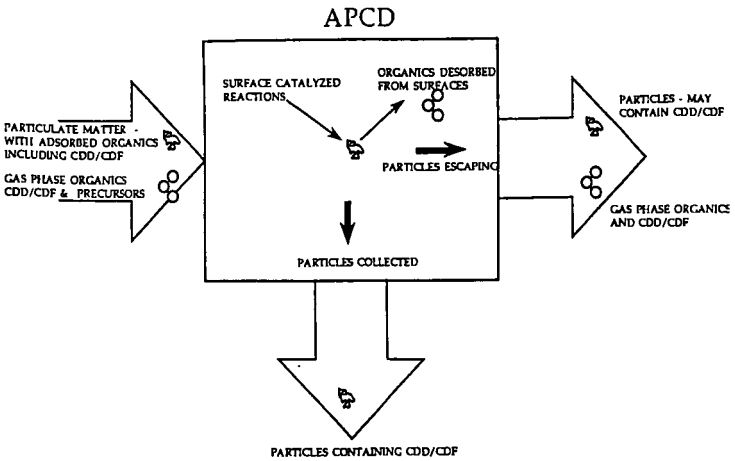

Figure 1 CDD/CDF Behavior in an APCD

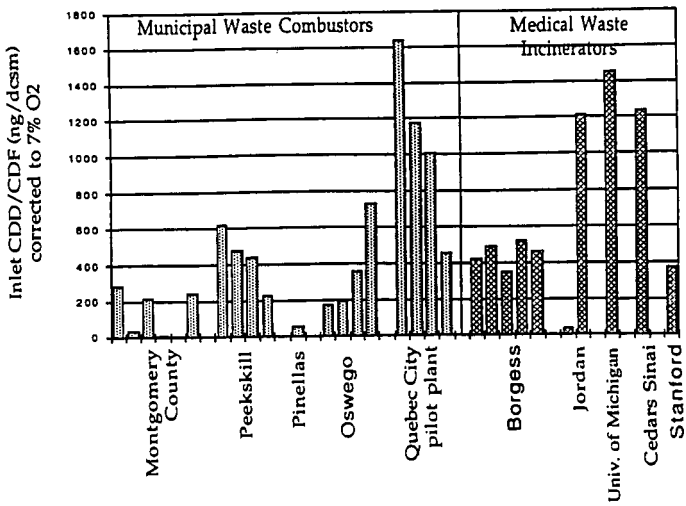

Figure 2 APCD Inlet CDD/CDF Concentrations

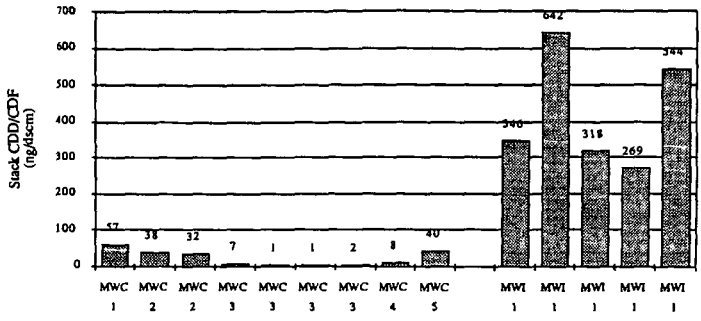

Facility code	Facility name	combustor type	APCD
MWC1	Montgomery County, OH	rotary kiln	WQ/DSI/ESP
MWC2	Claremont	mass burn	DSI/FF
MWC3	Quebec City pilot test	mass burn	WQ/DSI/FF
MWC4	St. Croix	MOD/EA	DSI/HE/FF
MWC5	Wurzburg	mass burn	WQ/DSI/FF
MWI1	Borgess	MOD/SA	DSI/FF

Figure 3 Comparison of Outlet CDD/CDF Concentrations for an MWI and MWCs with Dry Sorbent Injection

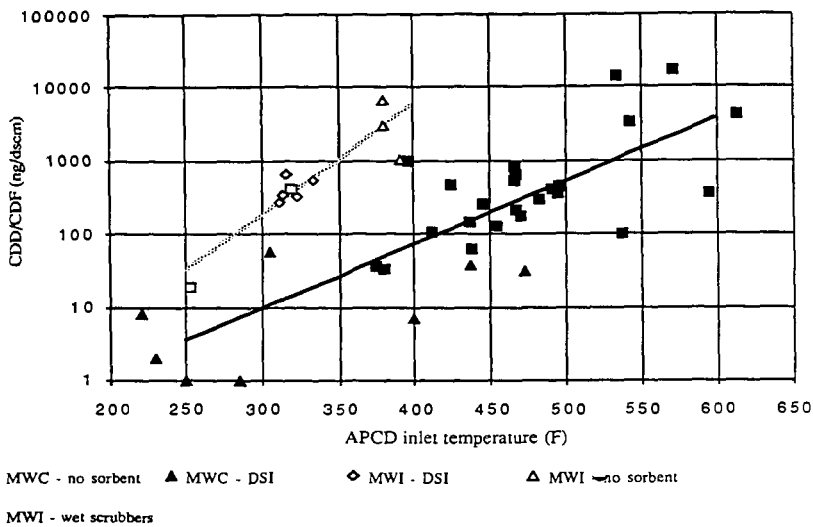

Figure 4 Effect of APCD Temperature on CDD/CDF Outlet Concentration

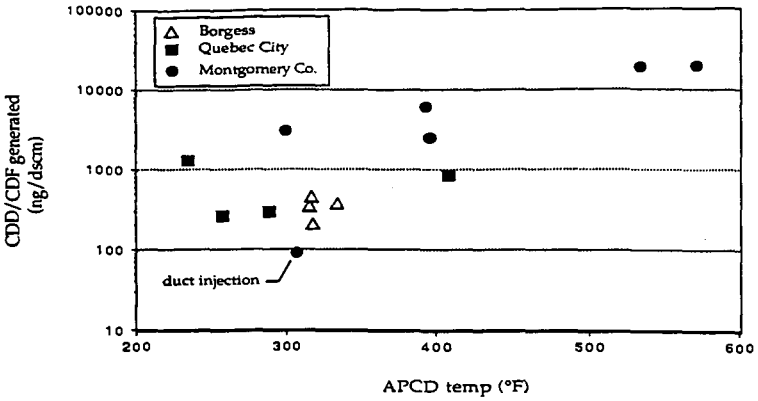

Figure 5 Comparison of Total CDD/CDF Generated in APCDs

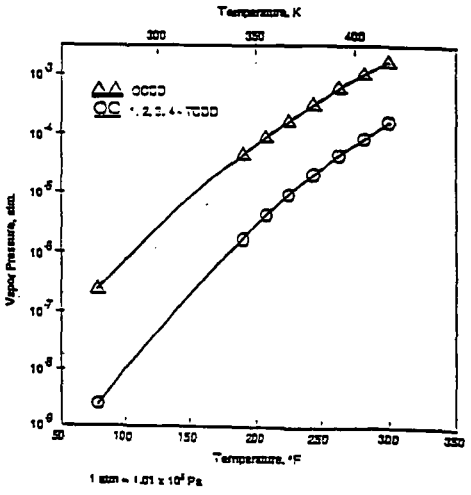

Figure 6 Vapor Pressure of Octa- and Tetra-chlorodibenzo-(p) dioxins

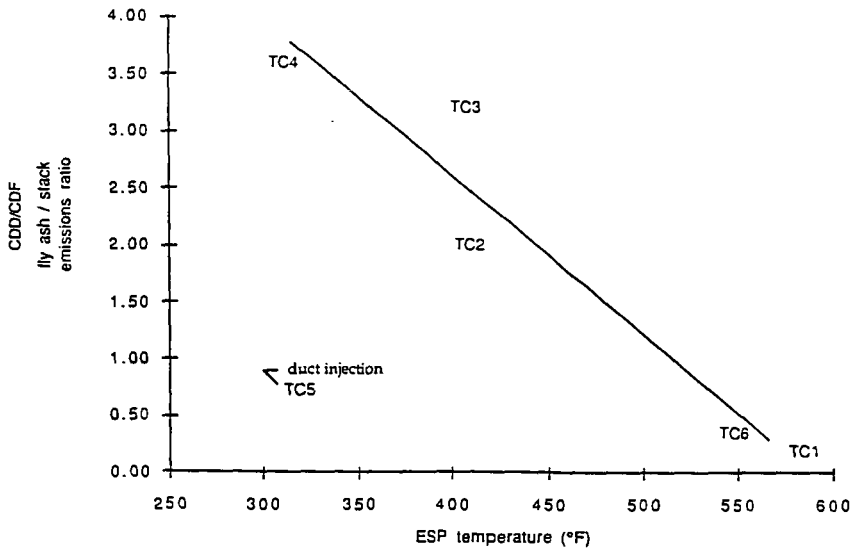

Figure 7 Effect of Temperature on Bifurcation of CDD/CDF in an ESP

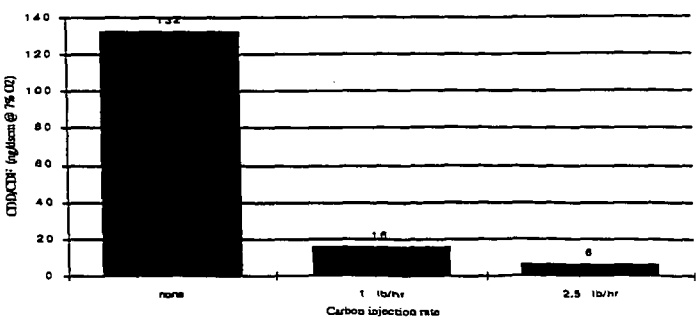

Figure 8 Effect of Activated Carbon on CDD/CDF Stack Concentration

UNMIXED COMBUSTION: A NEW TECHNOLOGY FOR PREVENTION OF PUFFING BY ROTARY KILN INCINERATORS AND OTHER APPLICATIONS

Richard K. Lyon
Energy and Environmental Research Corp
18 Mason
Irvine, CA. 92718

Key words: copper oxide, puffing, incinerator

INTRODUCTION

The Problem of Puffing in Civilian Incinerators The United States currently produces 265 million tons per year of hazardous waste. In most instances the toxicity of this waste come from toxic organic materials which, in principle, can be completely destroyed by incineration. Since all other disposal technologies involve the risk that some of the toxic materials will return to the environment incineration is, in principle, the ideal solution to the problem. Presently available incinerator technology is subject to a number of limitations, one of the most important of these limitations being the puffing problem of rotary kiln incinerators, i.e. these incinerators are observed to occasionally emit puffs of toxic organic materials. This is a serious failure since as discussed by Oppel (1) rotary kiln incinerators are a substantial fraction of total U. S. incineration capacity. Detailed mathematical models of this puffing phenomenon has been presented in references 2, 3, and 4. As these references discuss rotary kiln incinerators handle both solid and liquid wastes. For combustible liquid wastes the practice is to mix the liquid waste with a sorbent, which is then placed in a container (typically a cardboard, plastic, or steel drum), and feed to the rotary kiln incinerator. These large closed containers are heated until the vapor pressure of the liquid is sufficient to cause them to rupture. This results in a sudden discharge of a large amount of combustible vapors into the incinerator. The supply of combustion air can be much less than sufficient for complete oxidation of these suddenly released vapors and this can cause substantial amounts of these toxic organic vapors to be discharged from the incinerator into the environment.

Disposal of Chemical Weapons A problem very similar to puffing is likely to occur during the U.S. Army's planned incineration of its stockpile of chemical weapons. If during the unpacking of these weapons a live munition were inadvertently included in the packing material sent to the dunnage incinerator most of the nerve agent it contains would be discharged to the environment. A risk analysis by GA Technologies (5) estimates a probability of 0.01 per year per site for such a mishap. Since there are nine sites and the destruction of the munitions will require a number of years, the probability of such an accident happening at least once is significant.

Puffing Control via CuO In both civilian and military incinerators the fundamental problem is that organic matter can go into the combustion chamber in slugs while combustion air is supplied continuously. It occurred to the author that this problem of mismatch between the supplies of fuel and air could be solved by using a bed of copper oxide. Organic matter passing through copper oxide at elevated temperatures is rapidly oxidized and air readily reoxidizes the copper to copper oxide. Thus a bed of copper oxide can, in effect, provide a means of storing an inventory of combustion air.

The Concept of Unmixed Combustion The research reported herein was initiated to test on a laboratory scale the feasibility of this method of controlling puffing. During the course of this work, however, it was recognized

that the use of copper oxide to maintain an inventory of combustion air make s possible a novel type of combustion system, one in which the fuel and air do not mix. Such an unmixed combustion system would be unique in that in all other combustion systems the stiochiometric ratio (i.e. the fuel/air ratio) is a critical parameter but in unmixed there are two stiochiometric ratios each of which is important, the ratio of the amount of fuel passed through the bed during a cycle to the maximum capacity of the bed to oxidize fuel and the ratio of the amount of air passed through the bed during a cycle to the maximum capacity of the bed to reduce O_2.

Preliminary experiments were done to examine the properties of such an unmixed combustor and are reported below.

APPARATUS AND EXPERIMENTAL PROCEDURES

Three sets of experiments were done, two to demonstrate puffing control with a fixed bed and and fluid bed CuO on high surface area alumina and one to explore unmixed combustion.

Fixed Bed Experiments for Puffing Control In the former experimental setup rotameters were used to prepare a flowing gas mixture containing oxygen and nitrogen in known proportions. For experiments involving volatile organic compounds a third rotameter was used to send a measured flow of nitrogen through a bubbler partially filled with the volatile organic compound and this stream of nitrogen saturated with the volatile organic was added to the flow of the oxygen/nitrogen mixture. A fourth rotameter was then used to take a measure portion of this flowing mixture and the rest was sent to vent via a back pressure regulator. For experiments with materials which are not readily volatile, i.e. phosphonoacetic acid, a precision metering pump send a flow of an aqueous solution of the material to the top of the fixed bed where the temperature was high enough to cause it to vaporize.

From the fourth rotatmeter the flowing gas mixture was sent to a three way valve and thence either went downward though the fixed bed and then to the analytical instruments or went directly to the analytical instruments. In these experiments the fixed bed was housed in a 1" OD stainless steel tube inside an electrically heated furnace. Two type K thermocouples were used to monitor and control its temperature.

The analytical instruments used were a Beckmann 400 Hydrocarbon analyzer (i.e. a flame ionization detector) and a Teledyne O2 analyzer.

The fixed bed consisted of 25.5 wt% CuO supported on 5/16" alumina rings and was prepared by the incipient wetness method. In this method a solution of copper nitrate was added to the alumina with constant stirring until the bed could not absorb more without becoming macroscopically wet. The alumina rings were then heated to 800°C to drive off water and decomposed copper nitrate to copper oxide. Manufacturer's specifications on these alumina rings list them to have a surface area of 284 M^2/gm, total pore volume, H_2O, of 1.10 cc/gm, total pore volume, Hg, of 1.038 cc/gm, and a median pore diameter of 0.009 microns.

In doing these experiments the following procedure was used: an oxygen/nitrogen mixture without organic matter was passed through the bed and the oxygen level measured for the gas exiting the bed. Initially the concentration of oxygen in the gas going out of the bed could be extremely low because all the input oxygen was reacting will copper metal formed in the previous experiment. The oxygen level in the output gas would remain very low until virtually all of the metallic copper was consumed then would rise rapidly to equal the input level. Once the level of oxygen in the output gas was stable organic matter could

be added via either the bubbler or the metering pump and the change in the oxygen level of the exit gas noted. Since flame ionization detector was limited to concentrations less than 1000 ppmC, the change in the oxygen content which occurred when organic matter was added was used to calculate the input concentration of the organic matter. After making these observations the oxygen content of the gas going into the bed was reduced to zero and the flame ionization detector was used to measure the amount of organic matter which survived passage through the copper oxide bed as a function of time.

Fluid Bed Experiments for Puffing Control For fluid bed experiments the experimental apparatus and procedures were the same the following exceptions. The fluid bed was housed in a 26mm ID, 91 cm long, quartz tube which was placed inside an electric furnace with a 30 cm. heated length. The bed had a settled height of 13 cm. It operated in a slugging mode with a height of 30cm. Gases flowing out of the quartz tube went directly into a laboratory hood. Sample gas for the analytical instruments was obtained by a probe. The material in the fluid bed was 16.8 wt% CuO supported on Alcoa type F-1 activated alumina, 28-48 mesh. A single batch of this material was prepared, loaded into the fluid bed reactor, and used for all fluid bed experiments.

Examination of Unmixed Combustion For these experiments a setup was used in which flows of methane and air were measured by two rotameters and then each went to the common inlet of an electrically activated three way valve. (The use of three way valves allowed the flow through the rotameters to be continuous and hence more accurately measurable.) One of the flows was passed through the three way valve to vent while the other was passed through a 0.902 ID steel tube in an electric furnace, the heated length of this tube having a volume of 160cc and containing 87grams of 25.5% copper oxide on alumina rings. An electrical cycle timer was used to switch the three way valve at predetermined intervals.

RESULTS

Demonstration of Puff Suppression Figure 1 shows raw data from a packed bed experiment, i.e. in this experiments a mixture of 2520ppm C_5H_5N, 3.6% O_2, balance N2, the O_2 was shut off, and the flame ionization detector is used to measure the amount of C_5H_5N surviving passage through the bed as a function of time. From the known initial and observed final concentrations of the C_5H_5N one can calculate as a function of time both the DRE and the extent to which the bed's oxidation capacity have been used. Figure 2 shows the data from Figure 1 recalculated in this manner. Using this procedure the experimental results from the fixed bed and fluid bed experiments were reduced to determine the initial DRE and the extent to which the oxidation capacity of copper oxide can be used before the DRE falls below some predetermined value. Capacity of the copper oxide bed is conveniently expressed in terms of the volume of combustion air a volume of the bed is equivalent to. The results of these calculations are shown in Table 1.

The following observation is also to be reported: when oxygen was present in the gas going into the hot copper oxide bed the amount of organic matter surviving passage through the bed was zero within the noise level of the FID. This was found in all experiments with one exception: during the experiments with CCl_3F 76% of the input CCl_3F survived passage through the bed both in the presence and absence of oxygen.

Using the unmixed combustion setup the bed of CuO was subjected to approximately 5400 puffs of pure CH_4 and showed no signs of mechanical deterioration or of its losing chemical activity. On completion of this test a

series of experiments was done to examine the operational characteristics of the unmixed combustor. Figure 3 shows the variations in the oxygen level of the postcombustion gases when the bed was operated at a fuel to capacity ratio less than one but an air to capacity ratio much greater than one. Figure 4 also shows oxygen level but with the combustor operating at fuel to capacity and air to capacity ratios which are both less than one. Figure 4 also shows the amount of NOx being produced by unmixed combustion.

A series of experiments was done in which the variations of levels of NOx and oxygen in the postcombustion gases was measured over a range of overall fuel to air stiochiometric ratios with the results shown in Figures 5 and 6

In another experiment the electrical furnace was shut off and the combustor was allowed to operate autothermally with a CH_4 input of 3212 cc/min for 2 seconds, off for 15 seconds, and an air input of 3000cc/min for 15 seconds, off for 2 seconds. Initially the bed temperature in this experiment was 775°C. After dropping to 635°C the bed temperature wandered, slowly rising to 681°C. At 2.8 hours after shutting off the electric furnace the run was voluntarily terminated .

DISCUSSION

Laboratory Scale Demonstration of Puffing Control The results in Table 1 show that for a considerable variety of compounds (i.e. hydrocarbons and organic compounds containing nitrogen, phosphorous, chlorine and sulfur) copper oxide can provide both the DRE and the capacity needed in a practical method of puffing control. While the results for C_6H_5F were not as good, they still indicate that this technique may be useful for fluorine containing hydrocarbons. Similarly the results for CCl_3F were arguably positive. Freons are extremely refractory materials and even in the absence of puffing would normally be expected to pass unchanged through an incinerator. Thus in addition to providing a solution to the occasional problem of puffing, the use of a copper oxide bed also provides a means of substantially reducing the continuous emission of freons from incinerators.

Controlling NOx production by Unmixed Combustion The data reported above show that it is in principal possible to use supported CuO as the basis for a novel combustion system, one in which the fuel and air are largely unmixed. During unmixed combustion the production of NOx was found to be extremely low. Given the generally accepted mechanisms for NOx production this result is not surprising. For fuels which do not contain chemically bound nitrogen it is generally agreed that NOx is chiefly thermal NOx, i.e. most of the NOx is produced by the "extended" Zeldovitch mechanism, $O + N_2 = NO + N$, $N + O_2 = NO + O$, $OH + N = NO + H$. The other source of NOx is the prompt NOx mechanism, i.e. the attack of hydrocarbon radicals such as CH on N_2 to produce HCN which is then oxidized to NO. Both these mechanisms are strongly disfavored at lower temperatures and both depend on the superequilibrium concentrations of free radicals which conventional combustion produces. By eliminating direct contact between the fuel and air both the extremely high temperatures normally associated with combustion and the high free radical concentrations are avoided and thus NOx production is suppressed.

Controlling CO_2 emissions by Unmixed combustion The problem of global warming due to the emissions of CO_2 during combustion has recently begun to receive a great deal of serious attention. In many locations pure CO_2 could economically be used in tertiary oil recovery or put to other use but the possibility of recovering dilute CO_2 from combustion gases have been given little considsration because the expense and large energy consumption involved. In an unmixed combustion system, however, the fuel is converted to CO_2 and water without being diluted with nitrogen. Thus unmixed combustion may, in favorable situations, be the basis of burning fuel without CO_2 emissions.

ACKNOWLEDGMENT The author gratefully acknowledges the support of the U. S. Environmental Protection Agency under the SBIR program, contract 68D20093.

REFERENCES

1 E. T. Oppelt, J. Air Poll. Cont. Assoc., 37, 558 (1987)

2 J. O. L. Wendt, W. P. Linak, Combust. Sci. and Tech, 61, 169-185, (1988)

3 J. O. L. Wendt, W. P. Linak, and P. M. Lemieux, HAZARDOUS WASTE &HAZARDOUS MATERIALS, 7, 41-53, (1990)

4 P. M. Lemieux, W. P. Linak, J. A. McSorley, J. O. L. Wendt,and J. E. Dunn, Submitted to Combust. Sci. and Tech

5 Risk Analysis of the Disposal of Chemical Munitions at National or Regional Sites, ADA 193355

TABLE 1 SUMMARY OF FIXED BED EXPERIMENTS

Puff being Oxidized	Reaction Conditions	Initial DRE	DRE as a function of Bed Oxidation Capacity, Equivalent cc of air per cc of bed
1974 ppmC of C_6H_5Cl	802°C for 0.53sec.	99.9985%	99.99% at 37.3cc/cc
3683 ppmC of C_6H_5Cl	812°C for 0.53sec.	>99.999%	99.9% at 136cc/cc 99% at 207cc/cc
10,000 ppmC of C_6H_6	811°C for 0.53sec.	99.997%	99.9% at 118cc/cc 99% at 197cc/cc
19,000 ppmCof C_5H_4S	814°C for 0.53sec.	99.9999%	99.9% at 186cc/cc 99% at 373cc/cc
7,800 ppmC of C_6H_5F	815°C of 0.53sec.	99.3%	
7,800 ppmC of C_6H_5F	991°C for 0.45sec.	99.94%	99.9% at 2.8cc/cc 99.3% at 59cc/cc
2,520 ppmC of C_5H_5N	817°C for 0.53sec.	99.9968%	99.99% at 99cc/cc
6000 ppmC of CCl_3F	821°C for 0.53sec.	76%	
3110 ppmC of $(HO)_2POCH_2COOH$	818°C for 0.53sec.	99.993%	99.9% at 29cc/cc 99% at 54 cc/cc

SUMMARY OF FLUID BED EXPERIMENTS

8000 ppmC of C_6H_6	806°C for 0.75sec.	>99.994%	99.9% at 43cc/cc 99% at 73cc/cc
3900 ppmC of C_6H_5Cl	805°C for 0.75sec.	>99.95%	99.9% at 169cc/cc 99% at 215 cc/cc

Oxidation of C5H5N by CuO

Run 7

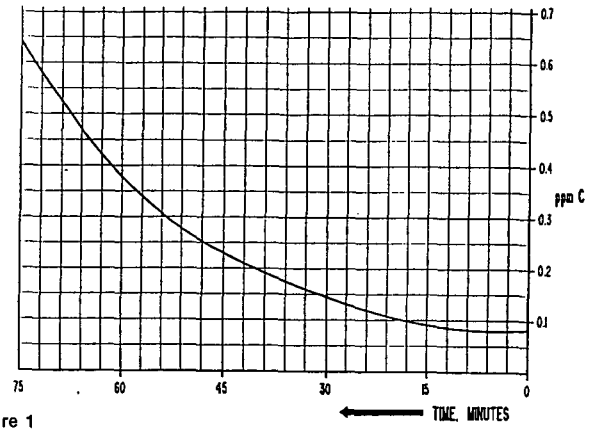

Figure 1

Destruction and Removal Efficiency for Oxidation of C5H5N by CuO

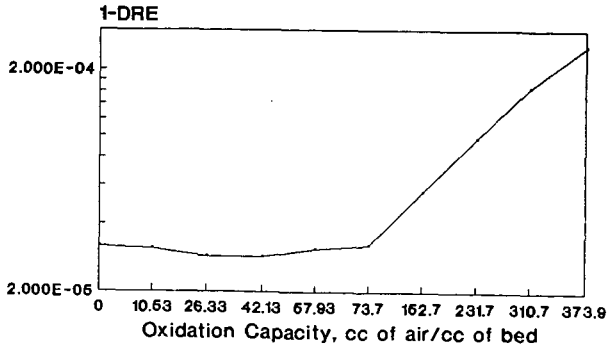

Run 7
Figure 2

Unmixed Combustion

CH4 and Air feed alternately to a bed of CuO on alumina, long pulses of air

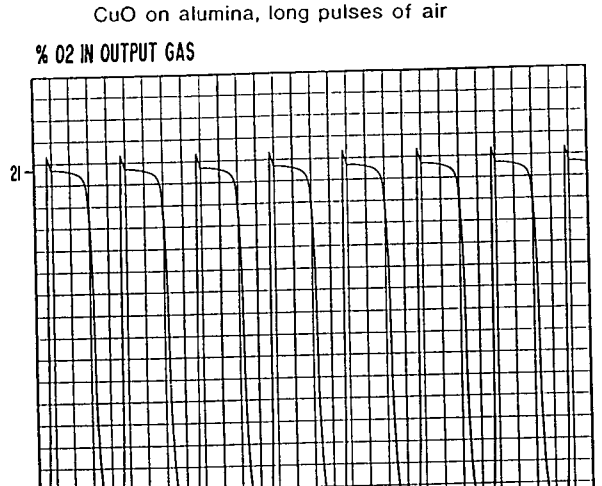

STIOCHIOMETRIC RATIO = 0.315
815C. 87g OF 25.5 WT% CuO IN A 160 cc BED
AIR = 3470 cc/MIN FOR 115 SEC. OFF FOR 5 SEC.
CH4 = 2513 cc/MIN FOR 5 SEC.. OFF FOR 115 SEC.

FIG. 3

Unmixed Combustion

CH4 and Air feed alternately to a bed of CuO on alumina, short pulses of air

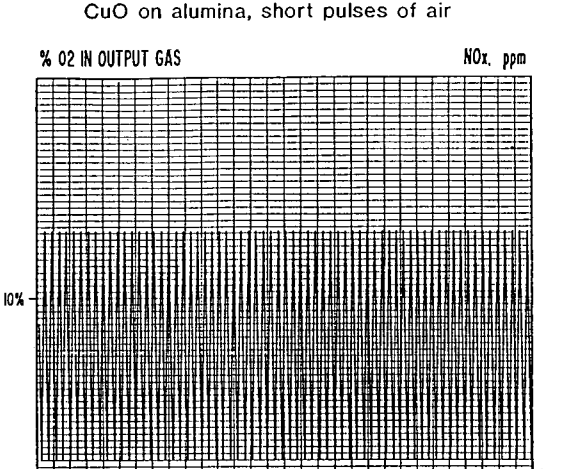

STIOCHIOMETRIC RATIO = 0.458
AIR = 3660 cc/MIN FOR 15 SEC. OFF FOR 1 SEC.
CH4 = 1 SEC ON. 15 SEC OFF

FIG. 4

Effect of Stoichiometric Ratio on the variance of O2 in the output gas from unmixed combustion

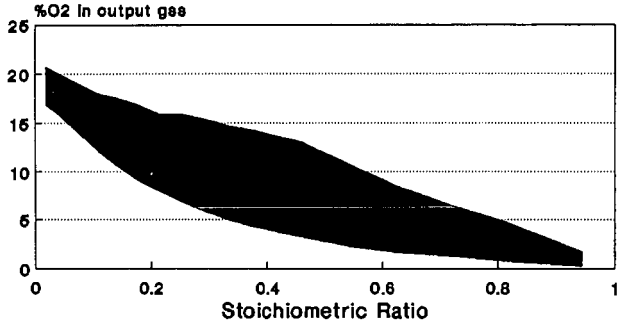

816C, 87g of 25.5wt% CuO in a 160 cc bed
Air = 3660cc/min for 15 sec, 1 sec off
CH4 = 1 sec on, 15 sec off,

Figure 5

Effect of Stoichiometric Ratio on the variance of NOx in the output gas from unmixed combustion

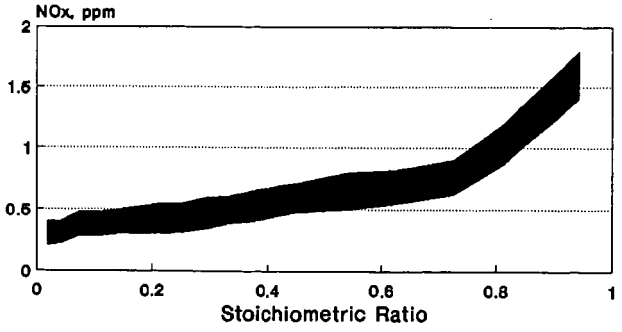

816C, 87g of 25.5wt% CuO in a 160 cc bed
Air = 3660cc/min for 15 sec, 1 sec off
CH4 = 1 sec on, 15 sec off,

Figure 6

ENOx, AN ELECTRONIC PROCESS FOR NOx ABATEMENT

Michael P. Manning
PlasMachines Inc.
11 Mercer Road
Natick MA 01760

Recent revisions of the Clean Air Act have mandated increasingly stringent controls on NOx emissions. Combustion of fuel in engines for transportation and in boilers for electric utility and industrial power generation produce over 90 percent of all NOx emissions. ENOx, a recently discovered electronic process, shows significant promise for reducing NOx emissions from mobile sources such as cars and trucks in the near term and large stationary sources such as boilers in the long term.

The key to PlasMachines ENOx emission control process is the use of a **plasma**, that is an **electronically excited gas**, to cause the decomposition of NO and NO_2. A simplified process diagram is shown in Figure 1. Electrical power feeds a proprietary electronics package which provides the excitation to the process duct. The duct is basically an open chamber with special electrodes and operates at atmospheric pressure or the combustion exhaust stream pressure. The process plasma is an alternating current, discontinuous, multifrequency, non-equilibrium discharge. During operation,

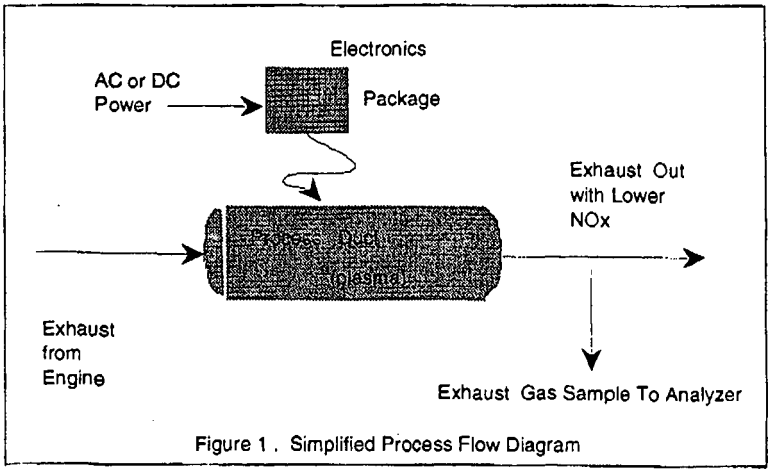

Figure 1 . Simplified Process Flow Diagram

exhaust gas flows through the process duct and constituents of the exhaust stream are activated by collision or ionization with plasma electrons under the influence of the electronic excitation. Molecules of NO and NO_2 are thermodynamically unstable with respect to decomposition back to the elements, nitrogen and oxygen . Hence, after activation by plasma processes, NO and NO_2 undergo decomposition and their concentrations in the exhaust are reduced.

Three engines have been tested using this exhaust treatment process: a 5 hp Briggs and Stratton gasoline engine, an 8 hp Kubota diesel electrical generator set, and a 40 hp Ford multi-fuel industrial engine. The Ford Model VSG-411 is a multi-fuel four cylinder, four stroke, 1.1 liter engine. The engine will accept either gasoline or methanol as liquid fuels and with an IMPCO carburetor will also burn natural gas. Natural gas was used as the fuel for the testing during this experimental work.

PlasMachines current facilities include a complete test facility for dynamometer and emissions testing of engines of all types up to 1000 hp. A Superflow 901 Dynamometer utilizes a water brake to load and measure the output torque of engines, including the Ford engine used in this development work, operating on a test stand under computer control. A photograph of the Ford engine mounted on the dynamometer is shown in Figure 2

Samples of exhaust gas are drawn continuously by vacuum pumps from the engine exhaust line, through a teflon transfer line, and into the emissions analyzers. A small refrigerator with collection trap was used to prevent condensation from the exhaust sample line from entering and interfering with the analyzers.

Emissions monitoring equipment utilized include a Thermo Electron Model 10S NO/NOx Chemiluminescent Analyzer capable of measuring either NO or total NOx concentrations from 1 to 10,000 ppm. An Horiba Model MEXA-554GE NDIR automotive emission analyzer provides capability of continuous or spot monitoring of O_2, CO_2, CO, unburned hydrocarbons (UHC), and calculated air to fuel (A/F) ratio.

The four parallel reactors were each assembled from two stainless steel tees and a single straight length of 1.5 inch tube which were clamped together and clamped to the inlet and outlet manifold. Adapters clamped to each end of the reactor tube served to coaxially locate and support a one inch diameter electrode. Each reactor was connected electrically to a PlasMachines electronic source with two leads - the ground lead was connected to the stainless steel reactor shell while the electronic signal was connected to the electrode. A front view of the parallel reactor array are shown photographically in Figure 3.

The engine and reactors were tested using the following protocol. The Ford natural gas engine was started and run for approximately twenty minutes to ensure that all operating components and fluids including engine oil, cooling and dynamometer water were up to normal operating temperatures. The surface temperatures on the exhaust lines and reactor exterior surfaces were measured. The reactor exterior

surfaces were found to be between 250 and 280 F. The engine was operated at 830 and 1600 rpm with a torque load of 7 ft-lbs. With the PlasMachines electronic sources turned off, the uncontrolled levels of NO and NOx were measured as 300 and 320 respectively. When the electronic sources were turned on, the resulting ENOx process plasma reduced the NO and NOx levels to 60 and 180 respectively. **This demonstrates an 80% reduction in NO and a 44% reduction in NOx.** Power consumption by the electronic unit was 200 W.

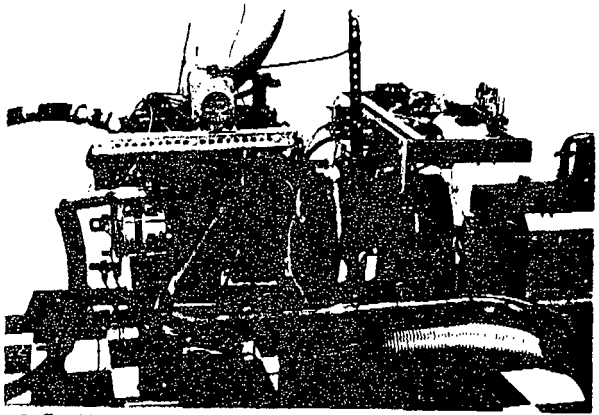

Figure 2. Ford industrial engine mounted on Superflow 901 Dynamometer

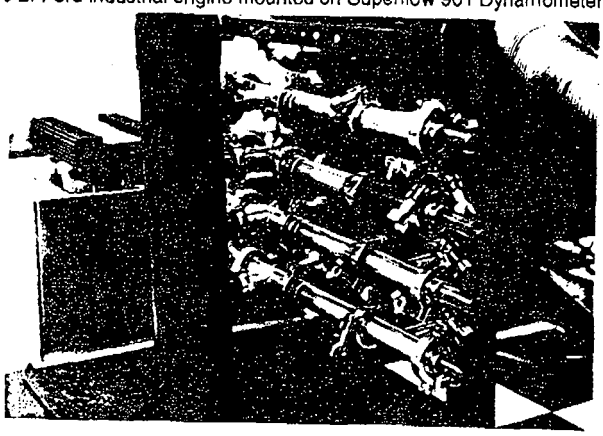

Figure 3. Front view of four parallel reactor units

THE EFFECT OF INITIAL NO_x LEVELS ON SELECTIVE NON-CATALYTIC NO_x REDUCTION PERFORMANCE

Greg C. Quartucy
Tami A. Montgomery
Dr. Lawrence J. Muzio
Fossil Energy Research Corp.
23342-C South Pointe
Laguna Hills, CA 92653

Keywords: Selective Non-Catalytic Reduction, Initial NO_x

ABSTRACT

The primary parameters affecting NO_x reduction performance of SNCR processes include injection temperature and the chemical N/NO_x molar ratio. Previous work showed that SNCR performance was also dependent upon initial NO_x levels. This is of concern for future applications to oil- and gas-fired systems, where initial NO_x levels of 30 to 100 ppm may be anticipated after combustion modifications are implemented.

To quantify the effect of these low initial NO_x (NO_i) levels on SNCR performance, a pilot-scale test program was performed to investigate the effect of NO_x levels with both urea and ammonia injection. This pilot test program evaluated the effect of NO_x levels ranging from 30 to 200 ppm on process performance. A range of temperature and N/NO_x ratios was evaluated for each SNCR chemical. The laboratory effort was supported by chemical kinetic modeling of the SNCR process. Test results included characterization of both the ammonia and urea injection processes. The effect of process parameters on NO_x reduction, and secondary emissions including NH_3, N_2O, and CO emissions was characterized. The laboratory data revealed important information regarding the implementation of SNCR processes at low initial NO_x levels.

INTRODUCTION

Since NO_x plays a major role in the formation of photochemical smog (Ref. 1), regulations requiring NO_x emissions reductions have been enacted in many areas. For example, NO_x emissions from utility boilers in the South Coast Air Quality Management District have been reduced significantly from their baseline, uncontrolled levels through the implementation of combustion modification techniques.

To meet upcoming regulations, which mandate further NO_x emission reductions, alternate control methods may be required. One approach under consideration involves the use of selective non-catalytic NO_x reduction (SNCR) techniques in conjunction with advanced combustion modification techniques. Both urea and ammonia injection have been shown to provide NO_x reductions at full-scale for a variety of combustion devices.

The primary parameters affecting NO_x reduction performance of SNCR processes are the injection temperature and N/NO_x molar ratios. Previous work (Ref. 2) also showed the dependence of process performance on initial NO_x levels. This is a concern for future applications to oil- and gas-fired systems, where initial NO_x levels of 30 to 100 ppm may be anticipated after combustion modifications are implemented.

In order to quantify the effect of these low initial NO_x (NO_i) levels on SNCR performance, a test program investigating the effect of NO_i levels with both ammonia and urea injection was performed. This laboratory test program evaluated the effect of NO_i levels ranging from 30 to 200 ppm on process performance for both urea and ammonia injection. Urea injection tests were performed over a temperature range of 1600 to 2075°F at varying reagent injection rates. Ammonia slip was measured, using wet chemical techniques at selected urea injection conditions. Ammonia injection tests were performed over a temperature range of 1470 to 1900°F. The laboratory experimental effort was supported by chemical kinetic modeling of the urea injection process using CHEMKIN.

FACILITY DESCRIPTION

The tests were performed using a natural gas-fired pilot-scale combustor facility. This facility has a design heat input of 300,000 Btu/hr, and a combustion product flowrate of 47 SCFM. This provides a nominal residence time of 0.5 second in the test section at 1800°F. Combustion gas temperatures entering the test section are controlled by adjusting the firing rate and with a series of adjustable water-cooled probes. Heat removal is controlled by varying the number and insertion depth of individual probes. The unit has a temperature gradient of 400-500°F/second over the test section length. While this is relatively high compared to other laboratory facilities, it was designed to match the temperature gradients typical of utility boiler environments.

Liquid and/or gaseous reagents were injected into the combustion products using water-cooled injectors. Gaseous NH_3 was injected using diametrically opposed injectors. The liquid urea solution was injected using a single small water-cooled atomizer.

A suction pyrometer was used to measure true gas temperatures at the entrance to the test section. For this test program, all gas analysis sampling was performed at the test section exit. A portion of the sample was taken from the sample probe exit and transported to the gas analysis instrumentation by a heated Teflon sample line. Before passing through the analyzers, the sample was dried in a refrigerated dryer. The dried sample was analyzed for NO, NO_x, O_2, CO, CO_2, N_2O and O_2, using continuous electronic gas analyzers. Ammonia concentrations were determined by passing a gas stream through an impinger train containing a dilute sulfuric acid solution. The ammonia concentration was subsequently determined using a specific ion electrode.

NH_3 INJECTION TEST RESULTS

The ammonia injection tests were performed using initial NO_x levels ranging from 30 to 200 ppm. Injection temperatures ranged from nominally 1470 to 1900°F. The N/NO_x ratio, the molar ratio of nitrogen in the SNCR chemical to the inlet NO_x, characterizes the amount of chemical injected. N/NO_x molar ratios of 1.0 and 2.0 were evaluated during these tests.

Figure 1 shows NO_x reduction data plotted versus temperature for tests performed at N/NO_x ratios of 1.0 and 2.0, and varying initial NO_x levels. A number of observations can be made from the data in Figure 1. First, the level of NO_x reduction decreases as the initial NO_x level decreases. Also, the optimum injection temperature appears to shift to higher temperatures as the initial NO_x level increases. Conversely, operation at low initial NO_x levels appears to require injection at reduced temperatures to obtain optimum results. This trend was observed for tests performed at both N/NO_x molar ratios. This temperature shift increases as the N/NO_x ratio increases. A final observation can be made about the effect of initial NO_x level at low injection temperatures. Over the majority of the temperature range, decreasing the initial NO_x level decreased NO_x reduction. However, as can be seen in Figure 1, at temperatures below nominally 1500°F, decreasing the initial NO_x level results in an increase in NO_x removal (albeit the overall levels of NO_x reduction are small).

UREA INJECTION TEST RESULTS

The urea injection tests were conducted using an aqueous urea solution. Solution flow rates were held constant for these tests to maintain a constant thermal environment in the injection zone. To change the N/NO_x ratios, the concentration of the urea solution was varied.

For the urea injection tests, gaseous emissions measurements were made over a temperature range of 1600 to 2075°F. Initial NO_x levels were varied from 30 to 200 ppm, while molar ratios of N/NO_x were varied from 0.5 to 4.0. Byproduct ammonia emission measurements, performed in conjunction with urea injection, were made over a more limited matrix. A temperature range of 1600 to 1940°F was used for performance of the subsequent byproduct NH_3 emissions (NH_3 slip) tests. NH_3 measurements were not made at temperatures in excess of 2000°F, since previous tests have shown that ammonia emissions are negligible at these high temperatures. Molar N/NO_x ratios of 0.5, 1.0 and 2.0 were evaluated during these tests for initial NO_x levels of 30, 70 and 200 ppm (in the present paper, only the results obtained for a N/NO_x molar ratio of 2.0 are shown).

Figure 2 shows NO_x reduction as a function of injection temperature for urea injection tests performed at a N/NO_x molar ratio of 2.0. The results are similar to the ammonia test results shown in Figure 1. These data also show that NO_x reductions decreased with decreasing initial NO_x levels. This trend was evident for all injection temperatures. It was also evident that the optimum injection temperature decreased as initial NO_x levels decreased. Also note that at low temperatures (i.e., less than 1600°F), decreasing the initial NO_x level increased NO_x reduction.

Ammonia slip data are plotted in Figure 3, which shows NH_3 concentration versus temperature as a function of initial NO_x level at a N/NO_x molar ratio of 2.0. As expected, the data show that NH_3 emissions increase with initial NO_x level and decrease with temperature.

N_2O has been found to be a product of the reaction between urea and NO_x. N_2O production is plotted as a function of temperature for operation at a N/NO_x molar ratio of 2.0 in Figure 4. The data show that, below 2010°F, N_2O emissions increased with increasing temperature, regardless of initial NO_x level or N/NO_x ratio. At temperatures above 2010°F, the N_2O emissions decreased. N_2O emissions also increased with both the N/NO_x and initial NO_x levels, as expected. Comparison with data reported previously show that N_2O production peaks at approximately the same temperature as NO_x reduction.

The slope of the N_2O versus temperature curves increased as initial NO_x levels increased for all of the N/NO_x ratios. This change in sensitivity likely reflects the quantity of reagent available to react at the differing injection rates.

CHEMICAL KINETICS MODELING RESULTS

In support of the laboratory urea injection tests, a series of chemical kinetic calculations were performed to investigate the effect of initial NO_x level upon the urea temperature and NO_x reduction, in particular, the behavior of the initial NO_x level at low temperatures. The chemical kinetics calculations were performed over a temperature range of 1472 to 1992°F at initial NO_x levels of 30, 70 and 200 ppm. Urea injection rates were set to give a N/NO_x molar ratio of 2.0. Combustion products were set at a stoichiometry comparable to the pilot-scale work. The urea was assumed to decompose as NH_3 and HNCO.

The chemical kinetics calculations were performed using a PC version of SANDIA's CHEMKIN program. The mechanism used was that of Miller and Bowman (Ref. 3). A residence time of 2.0 seconds was used in the calculations.

Calculated NO_x reductions, NH_3 slip and N_2O production for a N/NO_x ratio of 2.0 are plotted as a function of temperature at three initial NO_x levels (30, 70, and 200 ppm) in Figure 5. For an initial NO_x level of 200 ppm, the calculated chemical kinetics data show that a peak NO_x removal of approximately 100 percent occurred at 1740°F. At an initial NO_x level of 70 ppm, the maximum NO_x removal decreased to approximately 90 percent and occurred at a temperature of 1605°F. When the initial NO_x was decreased to 30 ppm, the maximum NO_x removal decreased to 80 percent and occurred at approximately 1520°F. The calculations indicate that decreasing the initial NO_x concentration shifts the temperature window and reduces the maximum achievable NO_x reduction. In spite of the shift in optimum temperature and maximum reduction, the shape of the window appears to remain essentially the same over the range of conditions evaluated. At low temperatures, the calculated results also show an increase in NO_x reduction with decreasing initial NO_x level (Figure 5).

The model predicts higher NO_x removals and slightly different temperature windows than were seen experimentally. However, the experimental results follow the same trends predicted by the model calculations. As initial NO_x levels decrease, the temperature window shifts to lower temperatures and the maximum amount of NO_x removal decreases.

The NH_3 slip and N_2O levels predicted by the model also support the experimental results (Figure 5). The model predicts the increase in NH_3 and N_2O with increasing NO_x levels, and their decrease with increasing injection temperatures. However, the model predicts lower levels of NH_3 and N_2O than observed experimentally; in addition, the model predicts N_2O production at temperatures lower than those observed experimentally. Part of these differences can be ascribed to the thermal profiles. The calculations were done assuming isothermal conditions while the experimental combustor exhibits a temperature gradient of 400-500°F/second.

CONCLUSIONS

Based on the data presented above, the following conclusions can be drawn for both urea and ammonia injection:

- Reducing initial NO_x levels results in 1) a decrease in NO_x reduction performance, and 2) a decrease in optimum injection temperatures.

The following conclusions can be drawn for urea injection:

- Decreasing temperatures result in increasing NH_3 emissions.
- Below 2010°F, increasing urea injection rates result in increasing N_2O emissions. However, N_2O emissions decrease at temperatures above 2010°F.

Chemical kinetic modeling of the urea injection process showed trends similar to those seen during performance of the laboratory tests.

REFERENCES

(1) Seinfield, J. H., Air Pollution-Physical and Chemical Fundamentals, McGraw Hill, NY, 1975.

(2) Muzio, L. J. and Arand, J. K., "Homogeneous Gas Phase Decomposition of Oxides of Nitrogen," Electric Power Research Institute Report No. EPRI 461-1, July 1976.

(3) Miller, J. A. and Bowman, C. T., "Mechanisms and Modeling of Nitrogen Chemistry in Combustion," Paper Number WSS/CI 88-63, presented at the Fall Meeting of the Western States Section/The Combustion Institute, Dana Point, CA. October 1988.

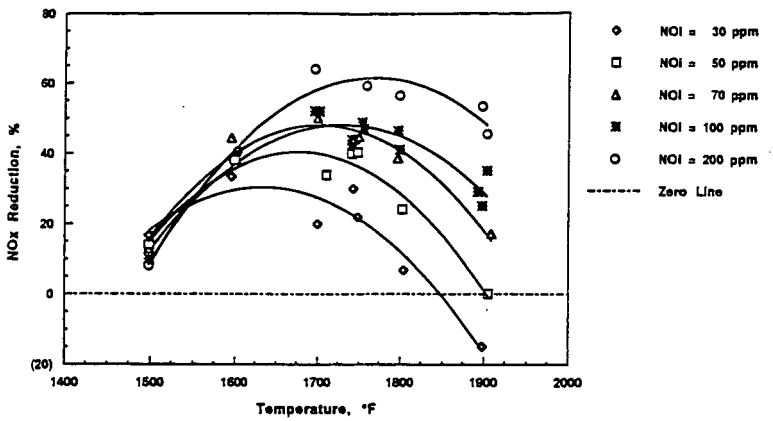

(a) $N/NO_x = 1.0$

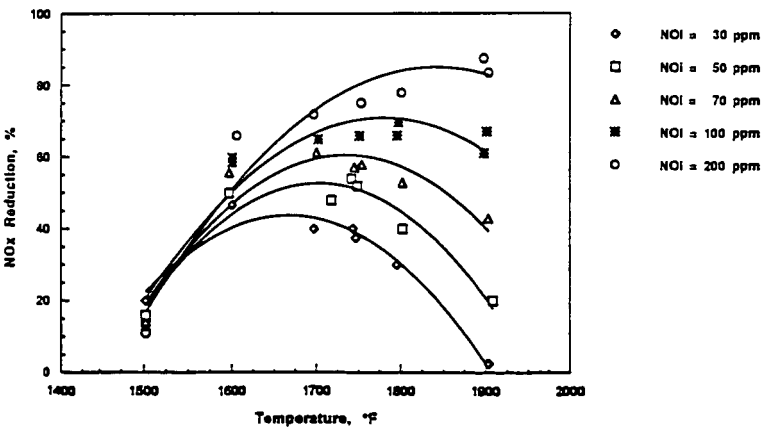

(b) $N/NO_x = 2.0$

Figure 1. Laboratory test results with NH_3 injection. Effect of injection temperature on NO_x removal at variable initial NO_x levels

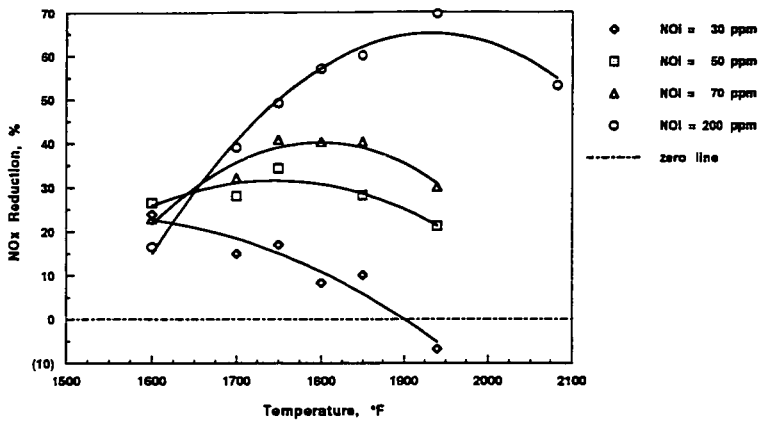

Figure 2. Laboratory test results with urea injection. Effect of injection temperature on NO_x removal at variable initial NO_x levels

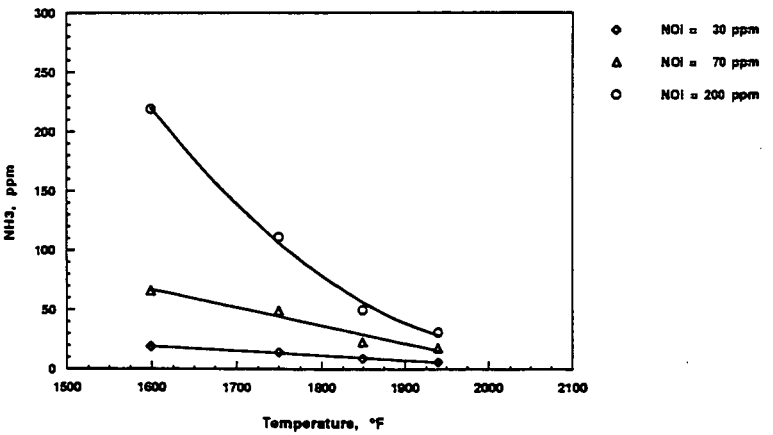

Figure 3. Laboratory test results with urea injection. Effect of injection temperature on NH_3 emissions at variable initial NO_x levels, N/NO_x = 2.0.

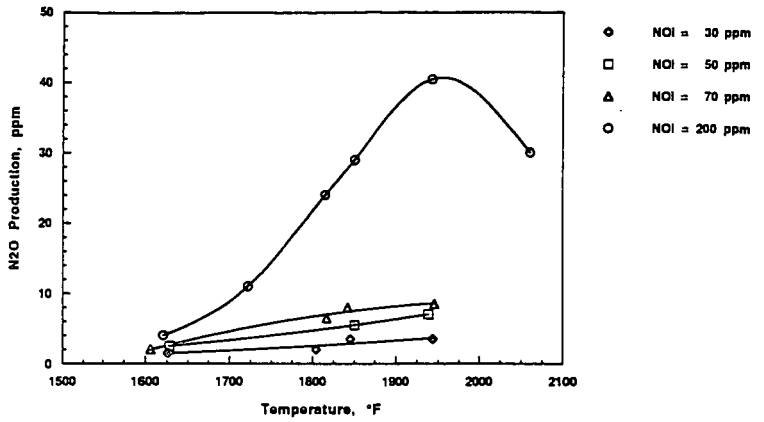

Figure 4. Laboratory test results with urea injection. Effect of injection temperature on N_2O emissions at variable initial NO_x levels, $N/NO_x = 2.0$.

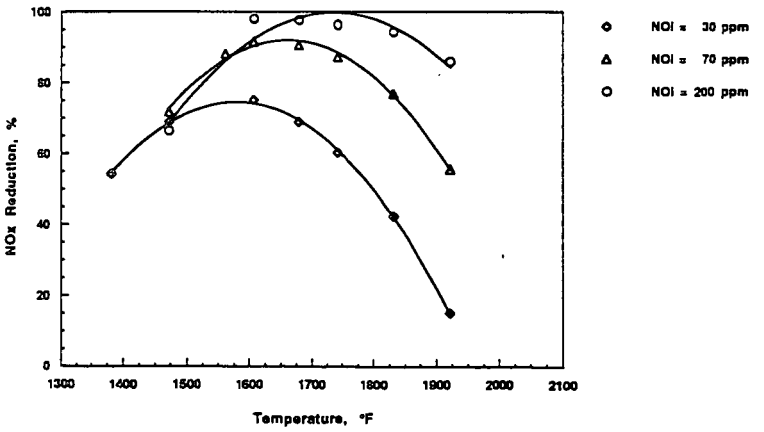

(a) NO_x Reduction

Figure 5. CHEMKIN chemical kinetics modeling results showing the predicted effect of temperature on NO_x reduction with urea injection.

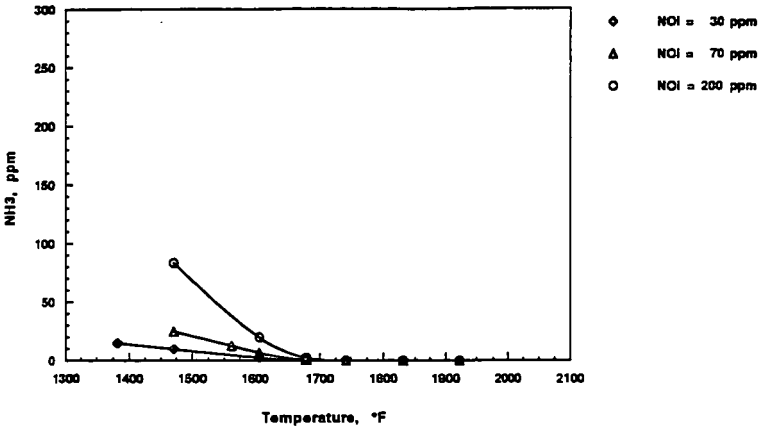

(b) NH_3 Emissions

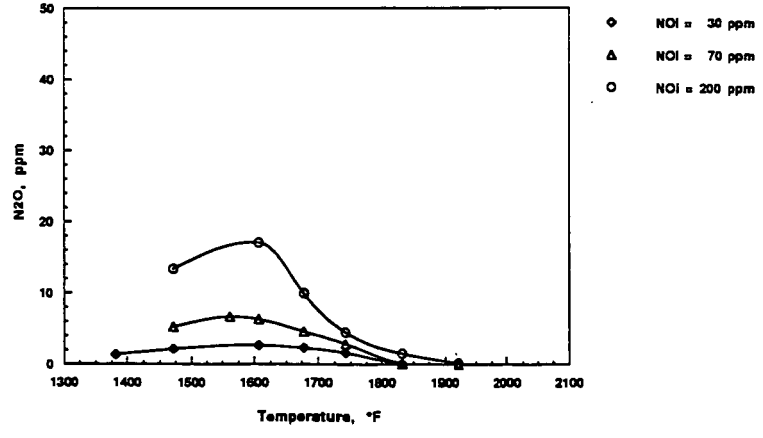

(c) N_2O Production

Figure 5. CHEMKIN chemical kinetics modeling results showing the predicted effect of temperature on NO_x reduction with urea injection.

LIMITS TO NOx REDUCTION BY NH3 INJECTION

John H. Pohl
Energy International
Laguna Hills, CA 92653

Shyh-Ching Yang
Energy and Resources Laboratory
Hsinchu, Taiwan

William A. Sowa and James W. Dill
University of California
Irvine, CA 92717

Keywords: NOx Reduction by NH3

INTRODUCTION

The process to reduce NOx by NH3 was patented by Lyon (1975). The process initially found limited use to control NOx in oil- and gas-fired boilers in Japan. The process was experimentally investigated by Muzio, et al. (1976) and Lyon (1978). Typically the NOx reduction cited in small scale studies or practical application was 40-70 percent. Recently, NH3 injection systems have been installed on a number of incinerators and fluid bed combustors. The measured emission of NOx from some of these operating combustors is below 10 ppm (d, 3% O2). These results implied that better reduction could be achieved than had been thought based on previous small scale results and from field trials.

This paper describes experiments and calculations aimed at establishing the maximum NOx reduction that can be achieved in the absence of mixing limitations and to determine how gas composition, operating parameters, and additives affect the reduction of NOx and the slip of NH3.

EXPERIMENTS

Experiments were designed to be controllable, free of mixing constraints and catalytic influence, and capable of investigating the range of operation of commercial systems. The experimental apparatus, Figure 1., delivers gas from analyzed bottles, mixes and meters the flow through rotometers, adds water vapor as desired from a saturated bath, and passes the gases through a quartz coil reactor in a temperature controlled oven. The bottled gases are mixed to represent the range of flue gases to be treated or the gases after treatment. The gases are analyzed before and after the oven using continuous monitors for NO, NO2, O2, CO, and CO2 and an ion specific electrode for NH3 concentration.

The conditions investigated were (baseline conditions are underlined):

- o residence time: 0.1, 0.2. 0.5, 1.0 seconds
- o temperature: 1061,1116,1144,1172,1200, 1228, 1255, 1283, and 1311 K
- o NO: 100, 200, 300, 400, 600, 800 ppm
- o CO: 0, 100,200,400, 600, 700 ppm

o H2O: 0, 6 %
o CO2: 15 %
o O2: 3 %
0 NH3/NO: 1, 1.5, 2.0, 3.0, 4.0

Calculations were used to interpret and extent the results of the experimental. Calculation were made using the Sandia National Laboratories SENKIN and the extended mechanism of Miller and Bowman (1989). Selected results from the calculations were fit with mathematical expressions. These expressions allow the data to be easily interpolated and possibly to be extended slightly.

RESULTS

The influence of the above conditions on NOx reduction and NH3 slip were determined by experiment and calculations and were compared with previous experimental data. The following conclusions were derived from the range of conditions studied.

Residence Time

Longer residence times generally resulted in slightly increased reduction of NOx and less NH3 slip. However, shorter residence time, occasionally produced slightly greater NOx reductions and the maximum NOx reduction occurs at lower temperatures for shorter residence times.

Temperature

We find an optimum temperature for the reduction of NOx in the range of 1175- 1225 K and the minimum temperature for nearly complete destruction of NH3 to be greater than 1300 K as shown in Figure 2. and in agreement with other literature values. However, our experimental results show much higher reduction of NOx and much greater NH3 slip compared with the measurements of Muzio, et al. (1976). Our results agree with those reported by Lyon (1979) and calculations made using the unaltered Miller and Bowman Mechanism. The differences between our results and those of Muzio, et al. (1976) may result from their injection of aqueous NH4OH solutions instead of gaseous NH3, mixing limitations in their pilot scale combustor compared to our plug flow reactor, temperature gradients in their reactor compared to our constant temperature reactor, and their use of 100 ppm NO compared to our use of 400 ppm.

H2O

The influence of H20 in the range of 0-6 percent was found to be small on NOx reduction and NH3 slip.

CO

Increased concentrations of CO were found to reduce the NOx reduction and create a peak in the NH3 slip as shown in Figure 3. Our results show that increasing CO concentration from 0 to 700 ppm causes a relative small decrease in NOx reduction, where as the results of Teixeira et al. (1991) show a large increase. Conversely, our results show that increasing

the CO concentration from 0 to 100 ppm can result in a four fold increase in NH3 slip: higher concentrations of CO reduce the NH3 slip until the slip reaches a low level at 600 ppm CO. The results of Teixeira et al. show low NH3 slips at all levels of CO. Again, our experimental results agree with calculations obtained from the unaltered Miller and Bowman Mechanism and the difference between our results and those of Teixeira et al. may result from the difference in experimental conditions particularly any imperfect mixing in their experiment.

NO

The fractional NO reduction decreases with decreased levels of initial level of NO concentration below 400 ppm as shown in Figure 4. Conversely, the level of NH3 slip increases with increased level of initial NO concentration. The influence of initial NO concentration on NO reduction and NH3 slip agrees with the results of Muzio, et al. (1976) and the results from calculation based on the Miller and Bowman Mechanism.

NH3/NO

The level of NO reduction increases as the NH3/NO level increases to 1.7 as shown in Figure 5. The amount of NH3 slip increases at NH3/NO ratios greater than 1.0 to 1.5. The results of our experiments agree with those of Teixeira, et al. (1991) and results of calculations made using the Miller and Bowman Mechanism.

Additives

Calculations on the effect of H2, H2O2, and CH4 additives injected after the NH3 injection zone were done to determine the effects of these additives on NOx reduction and NH3 slip. The results of these calculations shown in Figure 6. are based on the effluent from the NH3 reaction zone with a concentration of 8 ppm NO and 81 ppm NH3. The NO reductions reported in Figure 6. is based on the fractional reduction from an original NO concentration of 400 ppm. Therefore, values greater than 0.02 indicate production of NO after the reaction zone. At the temperatures required to reduce NH3 to 5 ppm, injection of H2 and H2O2 both result in increases in NO concentration.

Calculations predict injection of CH4 at a temperature 100 K below the NH3 injection temperature of 1200 K has little effect on NOx emission while reducing the NH3 slip to about 5 ppm. Figure 7. experimentally confirms that CH4 can reduce NH3 slip, although not to the levels predicted by the calculations.

ACKNOWLEDGMENTS

The work reported in this paper was sponsored by the Energy Resources Laboratories in Hsinchu, Taiwan and managed through Energy International of Laguna Hills, California. The work was performed at University of California at Irvine, California.

REFERENCES

Lyon, R.K., "Method for the Reduction of the Concentration of NO in Combustion Effluents Using Ammonia," U.S. Patent 3,900554 (1975).

Lyon, R.K., "Thermal DeNOx: How it Works", Hydrocarbon Processing, October (1979).

Miller, J.A. and C.T. Bowman, "Mechanisms and Modeling of Nitrogen Chemistry in Combustion", Prog. Energ. Comb. Sci., 15, pp. 287-338 (1989).

Muzio, L.J., J.K. Arand, and D.P. Teixeira, "Gas Phase Decomposition of Nitric Oxide in Combustion Products", Sixteenth Symposium (International) on Combustion, pp. 199-207 (1976).

Teixeira, D.P., L.J. Muzio, and T.A. Montgomery, "Effect of Trace Combustion Species on SNCR Performance", International Conference on Environmental Control of Combustion Processes, Joint Meeting of the American Flame Research Committee and the Japanese Flame Research Committee, Honolulu, HI, October (1991).

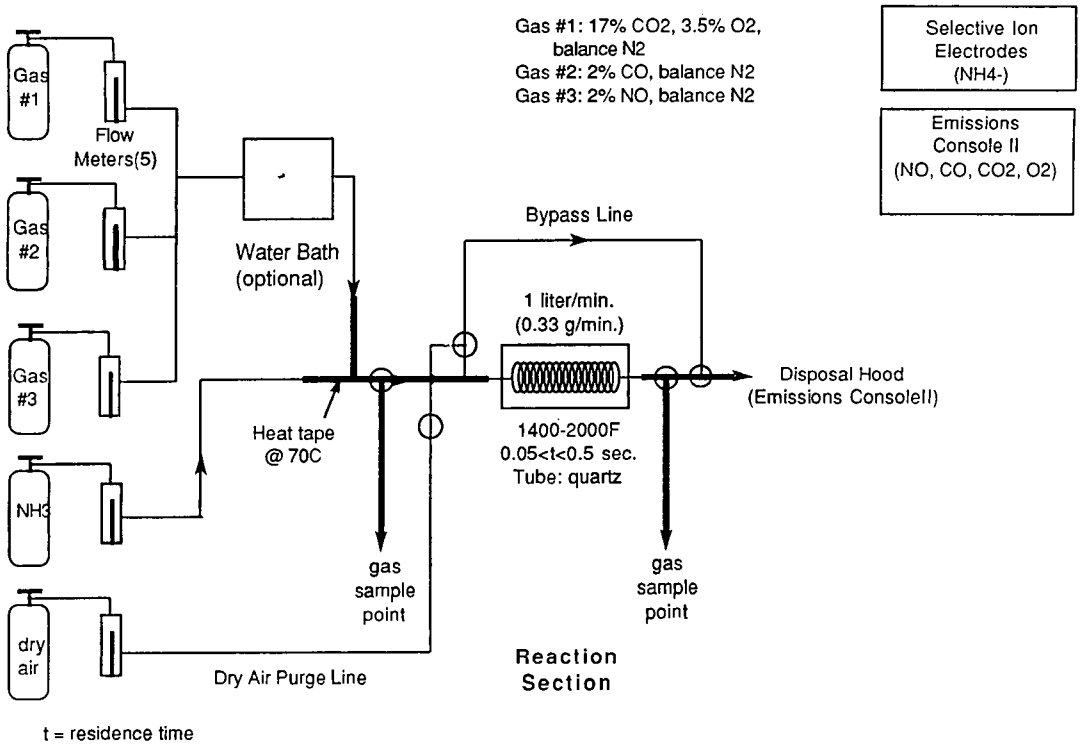

Fig. 1. Experimental Apparatus.

a.) NO Reduction, Experimental Results b.) Residual NH3, Experimental Results

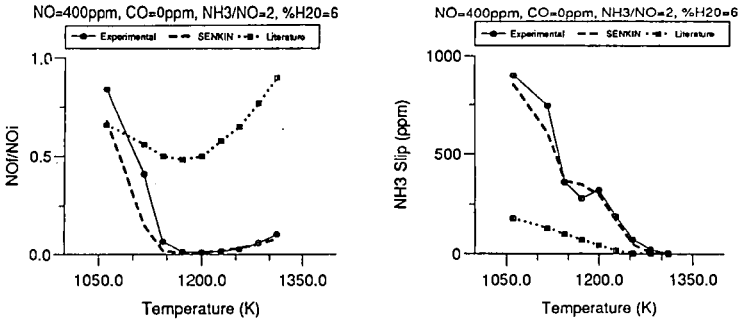

c.) NO Reduction, Modelled (ppm out/in) d.) Residual NH3, Modelled (ppm)

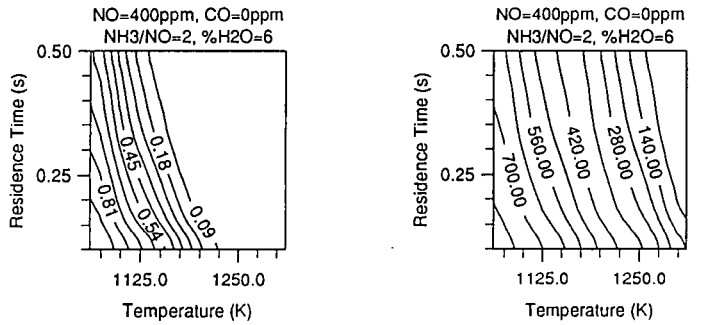

Fig. 2. Effect of Temperature on NOx Reduction and NH3 Slip.

a.) NO Reduction, Experimental Results b.) Residual NH3, Experimental Results

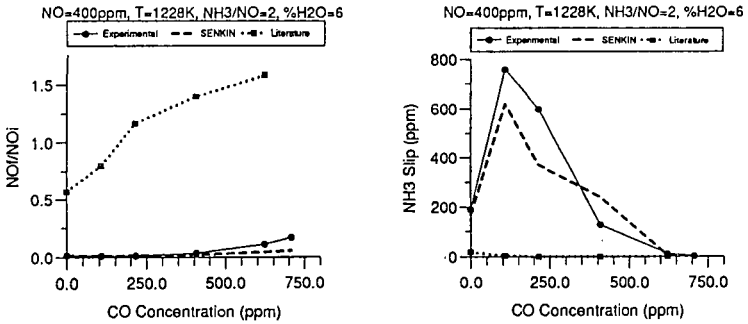

c.) NO Reduction, Modelled (ppm out/in) d.) Residual NH3, Modelled (ppm)

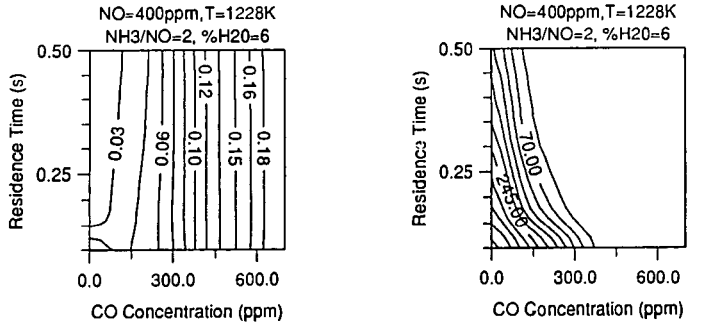

Fig. 3. Effect of CO Concentration on NOx Reduction and NH3 Slip. Teixeira, et al. (1991).

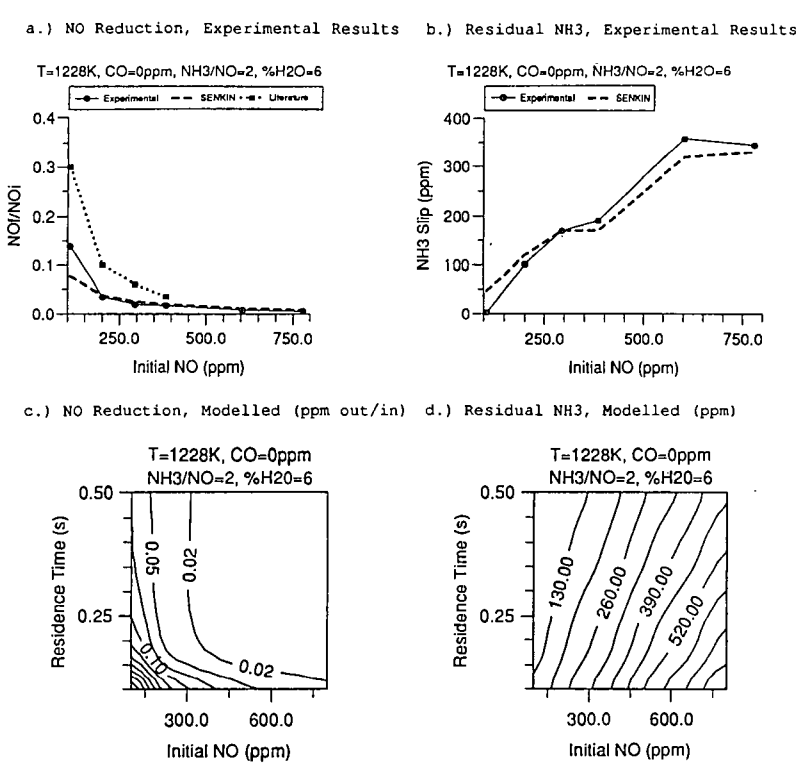

Fig. 4. Effect of Initial NO Concentration on NOx Reduction and NH3 Slip. Muzio, et al. (1976).

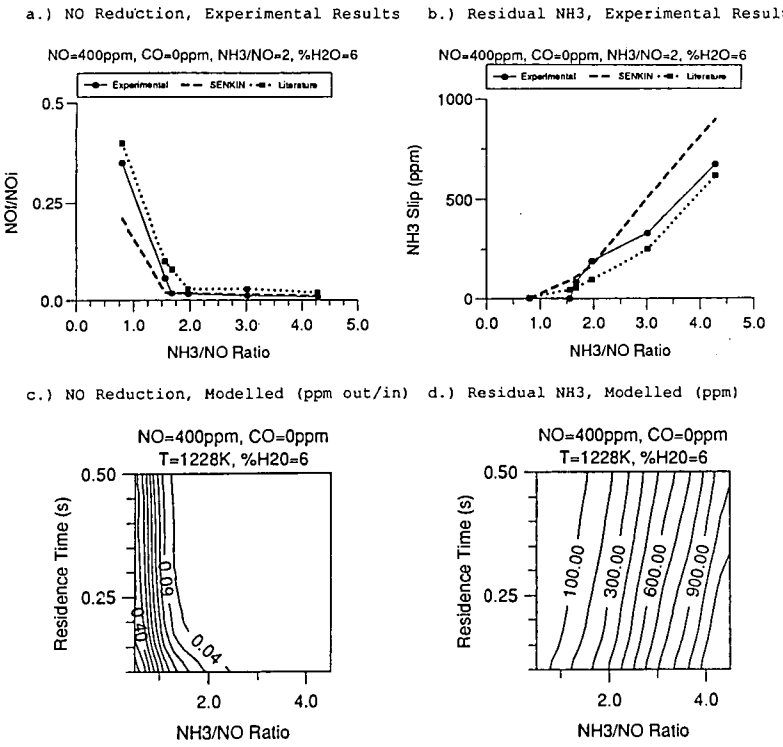

Fig. 5. Effect of NH3/ NO Ratio on NOx Reduction and NH3 Slip. Teixeira, et al. (1991).

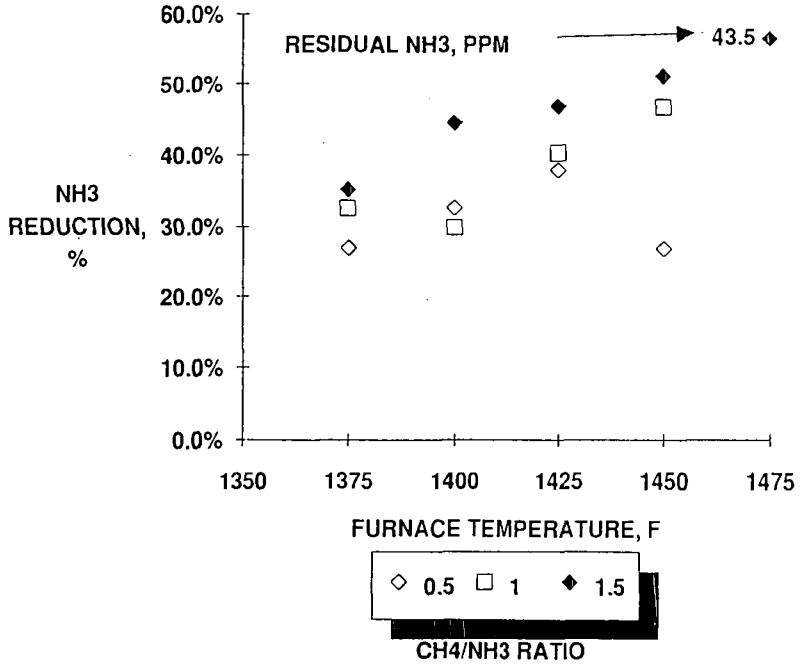

Fig. 6. Effect of CH4 Additive on NH3 Slip.

RESULTS FROM A MODELING AND EXPERIMENTAL EVALUATION OF THE COMBINO$_x$ PROCESS

J.N. Pont, A.B. Evans, R.K. Lyon, G.C. England, D. K. Moyeda, W.R. Seeker
Energy and Environmental Research Corporation
18 Mason
Irvine, CA 92718

Key Words: CombiNO$_x$, NO$_x$ Reduction Technology, Advanced Reburning

INTRODUCTION

Control of emissions of oxides of nitrogen, or NO$_x$, from fossil–fuel fired combustion systems is becoming of increasing interest due to the role of atmospheric nitrogen oxide species in the formation of acid rain and photochemical oxidant or smog. High levels of NO$_x$ removal are typically only achievable with expensive post–combustion technologies employing catalyst beds. This paper describes a process, called "CombiNO$_x$", which is capable of achieving high levels of NO$_x$ reduction at costs significantly below those of catalytic technologies. The CombiNO$_x$ process consists of three NO$_x$ control technologies—reburning, selective non–catalytic reduction ("agent injection"), and NO$_2$ scrubbing—which have been integrated and optimized in a manner which takes advantage of the chemical reactions involved in each process to achieve NO$_x$ reduction approaching 90 percent.

The CombiNO$_x$ process has been studied experimentally using two pilot–scale furnaces. The first series of tests were conducted in a one million Btu/hr down–fired furnace. At this facility, each component of the CombiNO$_x$ process was parametrically evaluated. Results from these studies have been reported elsewhere [1]. Pilot–scale tests at 10 million Btu/hr were also conducted to address process scale–up issues. This paper presents selected results of both series of experimental studies as well as kinetic modeling studies performed to aid in interpretation of the experimental results.

BACKGROUND

The technologies involved in the CombiNO$_x$ process have been extensively studied in small scale combustion tests and demonstrated in a wide range of industrial applications. In general, the global chemical mechanisms involved in the processes are considered relatively well–known. The three technologies used in the CombiNO$_x$ process are described in the following.

Reburning. The reburning concept was first investigated nearly two decades ago [2]. This process consists of injecting a portion of fuel downstream of the primary combustion zone to drive the flue gas stoichiometry slightly fuel rich. In this "reburning zone", the NO$_x$ generated in the primary zone is reduced to molecular nitrogen. Downstream of the reburning zone, additional air is injected to complete combustion of the unburnt products from the reburning zone. Bench and pilot scale studies have identified the general requirements for applying the process to industrial combustion systems [3–4]. Recently, demonstrations of the reburning process employing natural gas as a reburning fuel have been performed on coal–fired utility boilers [5–6].

Agent Injection. Selective non–catalytic reduction, or agent injection, technologies consist of the injection of amine-producing agents into post–combustion flue gases. Typical agents include ammonia

and urea. These agents must be injected into a narrow temperature window generally centered about 1850°F. Injection of the agent at too high of a temperature can cause oxidation of the agent resulting in increased NO_x emissions, while injection of the agent at too cold of a temperature can lead to excessive by-product emissions, such as unreacted NH_3. The fundamentals of the process have been described in the literature [7–8]. Reagent injection for NO_x control has been applied to full–scale utility boilers [9–10]. The results of these and similar tests have shown that the process is extremely sensitive to the gas temperature and that broad temperature distributions at the point of injection of the agent can limit performance.

NO_2 Scrubbing. Studies have shown that it is possible to scrub NO_2 with conventional SO_2 scrubber solutions provided that the solution is slightly modified [11]. The CombiNO$_x$ process exploits this phenomena by injecting methanol into the flue gas downstream of the reburning and agent injection processes to convert any remaining NO to NO_2, and then scrubbing the NO_2 in a conventional wet limestone SO_2 scrubber operating with a modified scrubbing liquor. Although methanol injection has been evaluated at full utility boiler scale as a means of reducing ammonia slip from SNCR systems [12], the integrated NO_2 scrubbing process has yet to be demonstrated in a practical system.

ADVANCED REBURNING

In practice, agent injection performance is extremely sensitive to flue gas temperature at the injection point. However, in the presence of oxidizing CO, the dependence of the process on injection temperature is significantly reduced [12]. The CombiNO$_x$ process furnishes oxidizing CO by injecting reburning fuel upstream of the reducing agent. The EER patented combination of reburning and agent injection, called Advanced Reburning, comprises the first two steps of the CombiNO$_x$ process.

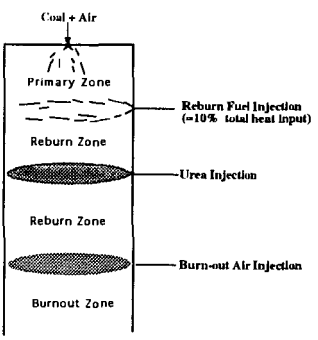

Figure 1. Advanced reburning pilot scale testing schematic.

Figure 1 shows schematically how Advanced Reburning was experimentally evaluated. A high-volatile bituminous coal was used as the primary fuel, while natural gas was used as the reburning fuel. The process can be divided into three zones: the region between the top of the furnace and the reburn fuel injectors is referred to as the primary zone, the region between the reburn fuel injectors and the burnout air ports is the reburning zone, the region downstream of the burnout air ports is referred to as the burnout zone. In these experiments, urea was injected within the reburning zone. The Advanced Reburning parameters evaluated included: reburning zone stoichiometry (or CO level), urea injection temperature, and burnout air injection location.

The effect of reburn zone stoichiometry on urea performance was evaluated to determine the impacts of CO oxidation on the optimal temperature window and achievable NO_x reductions. The chain branching de–NO_x reactions of importance are summarized below [13]:

$$NH_2 + OH \longrightarrow NH_2 + H_2O$$
$$NH_2 + NO \longrightarrow N_2 + H_2O$$

$$NH_2 + NO \longrightarrow NNH + OH$$
$$NNH + M \longrightarrow N_2 + H + M$$
$$H + O_2 \longrightarrow OH + O$$
$$O + H_2O \longrightarrow 2OH$$
$$NH_2 + O,OH \longrightarrow NO$$

The rate limiting step is the oxidation of ammonia to form NH_2. The reducing agent needs to be injected at high enough temperatures to allow the reaction to proceed fast enough to generate sufficient radicals to oxidize NH_3. If temperatures are too hot, the reaction intensity will be too high, and NH_2 will be oxidized rather than react with NO to form molecular nitrogen. If temperatures are too low, the ammonia will not oxidize, and will show in the emissions as ammonia slip. Therefore, there is an optimum agent injection temperature. At temperatures above and below approximately 1850°F, NO reduction efficiency drops off.

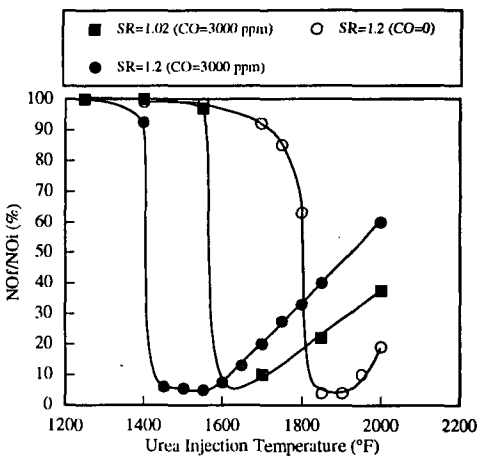

Figure 2. Predicted effect of CO on urea injection performance.

The addition of CO has been shown to shift the reaction window to lower temperatures because carbon monoxide oxidizes and generates additional radicals [13] that support further oxidation of NH_3 in the process. Figure 2 shows predicted NO reduction versus injection temperature using a chemical kinetic model which incorporates a plug flow/stirred reactor algorithm [15]. The plot compares injection of urea without CO to injection of urea with the equivalent of 3000 ppm CO for a stoichiometric ratio (SR) of 1.2. The addition of CO generates additional radicals, which shifts the cold side of the window to lower temperatures. The hot side of the window also shifts to the left, but to a lesser degree because the incremental amount of OH radicals contributed by this small amount of CO is not as great as that from ammonia alone. The net result of these effects is a broader reaction window.

Figure 2 also shows the predicted effect of co-injecting urea with the equivalent of 3000 ppm CO into two different stoichiometric environments. At higher stoichiometries, CO will oxidize more readily and generate more radicals, improving urea performance at lower temperatures, but worsening performance at higher temperatures. At the lower stoichiometry, fewer additional radicals are generated and the curve is not shifted as far to cooler temperatures. An interesting point is that the SR=1.2 curve is broader at the bottom, but rises more steeply as injection temperature increases than the SR=1.02 curve. The explanation may be that the increase in radicals at the high temperature side is relatively less for the SR=1.02 case than for the SR=1.2 case, resulting in relatively less oxidation of NH_2.

The design and operating conditions of a particular actual combustion system will significantly influence the amount of CO produced at a given stoichiometry. In the pilot-scale tests, the reburning zone stoichiometry was varied to evaluate the impact of reburning zone CO and O_2 levels on urea performance. Figure 3 shows the effect of reburn zone stoichiometry on the urea temperature window for the small (one million Btu/hr) pilot-scale tests. As the reburn zone stoichiometry drops, CO increases and O_2 decreases and the temperature window broadens with the optimum injection temperature at 1850°F. For a reburn zone stoichiometry of 1.02, the window not only broadens, but deepens as well, indicating that this unique combination of CO and O_2 provides an optimum amount of radicals. When SR_2 was more fuel-rich than this optimum, the curve shifted to the left rather than broadening. This result is believed to be due to an overabundance of radicals at the high temperature level.

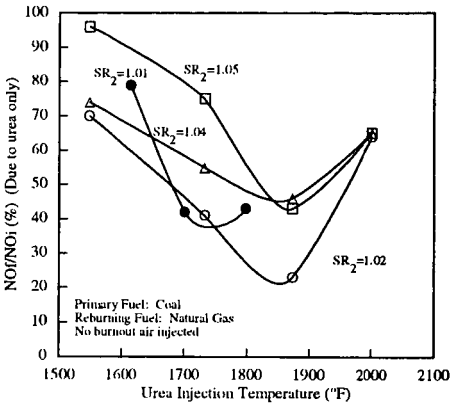

Figure 3. Effect of local CO concentration (SR) on urea performance at small pilot scale.

Because the flue gas flow in the small pilot-scale furnace is laminar, the mixing properties are not representative of a boiler. Also, flue gas temperature quench rates are much lower than on an actual full-scale boiler. Therefore, the 10 million Btu/hr tests were designed to provide information on advanced reburning performance in the presence of large scale turbulent mixing phenomena and at more realistic quench rates. Urea was injected at various temperatures for reburning zone stoichiometries from 1.05 to 0.99, which produced CO concentrations in the reburning zone ranging from 1,500 to 15,000 ppm, respectively. These results are presented in Figure 4. Contrary to the small pilot-scale results, the stoichiometry of the reburning zone did not appear to have a large effect on either the optimum injection temperature or NO reduction. It is hypothesized that the CO enhancement relies on mixing to distribute OH radicals to the SNCR agent uniformly. At large scale, bigger pockets of CO and O_2 co-exist, yielding non-uniform concentrations of radicals, and ultimately failing to promote the $deNO_x$ chemistry as well. It may be stated however, that the SR =

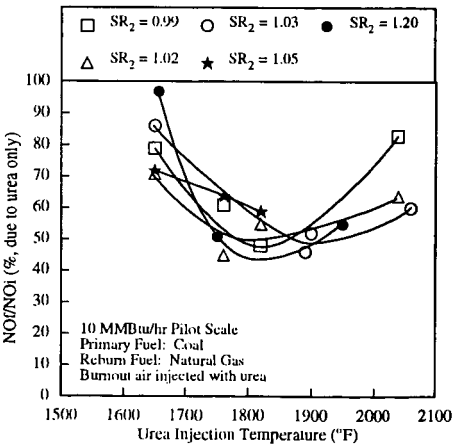

Figure 4. Effect of reburn zone stoichiometry on urea performance at large pilot scale.

1.20 case where no reburning is performed (no CO promotion) upstream of urea injection yielded the narrowest temperature window.

The final Advanced Reburning parameter of interest is the location of burnout air injection to complete combustion of the reburning fuel. Figure 5 shows overall NO_x reduction (due to reburning and urea injection) as a function of burnout air injection temperature (location) for optimum reburn zone stoichiometry and urea injection temperature. At small pilot-scale, NO_x reduction improves as the burnout air is moved away from the urea injection point. This is probably because downstream air prolongs the urea residence time in the "optimum" radical environment. Also shown in the figure are the large pilot-scale data. NOx reduction did not vary with burnout air location at large scale. From an application standpoint, this is important in that it is less expensive to retrofit Advanced Reburning to a boiler if the burnout air and reduction agent can be injected through the same openings.

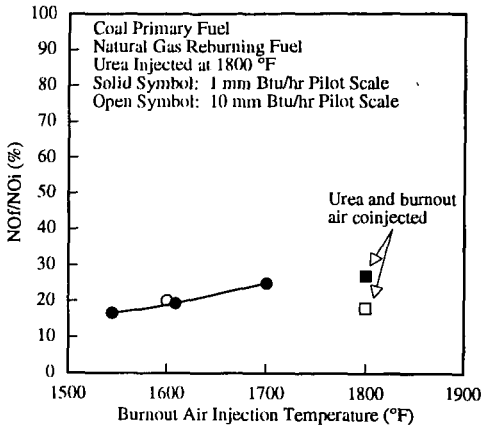

Figure 5. Effect of burnout air injection temperature on Advanced Reburning performance.

Figure 6 presents Advanced Reburning NO_x reduction levels as a function of reburn zone stoichiometry and urea injection temperature at large pilot-scale. Compared to traditional agent injection, the Advanced Reburning process offers a wider range of urea injection temperatures and significantly improved reduction performance up to 84 percent.

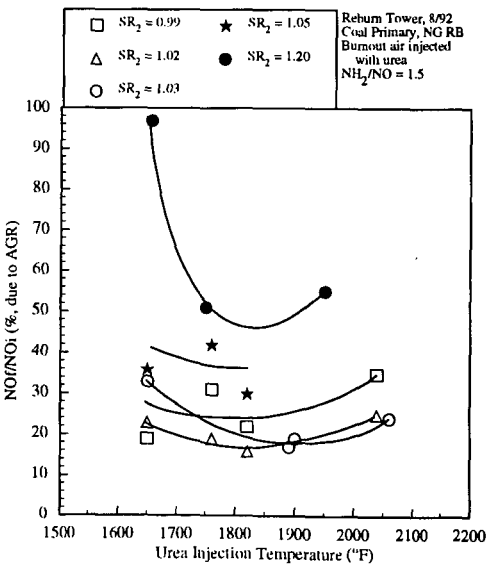

Figure 6. Large pilot scale Advanced Gas Reburning performance

METHANOL INJECTION

The third step of the CombiNO$_x$ pro-

cess, methanol injection, is performed downstream of the Advanced Reburning process. The methanol is intended to convert the NO remaining after Advanced Reburning to NO_2. Since NO_2 is very water soluble, it can subsequently be removed in wet SO_2 scrubber operating with modified liquor. Based on previous kinetic studies, the reaction mechanism for the methanol step is [16]:

$$CH_3OH + OH \longrightarrow CH_2OH + H_2O$$

$$CH_2OH + O_2 \longrightarrow CH_2O + HO_2$$

$$HO_2 + NO \longrightarrow OH + NO_2$$

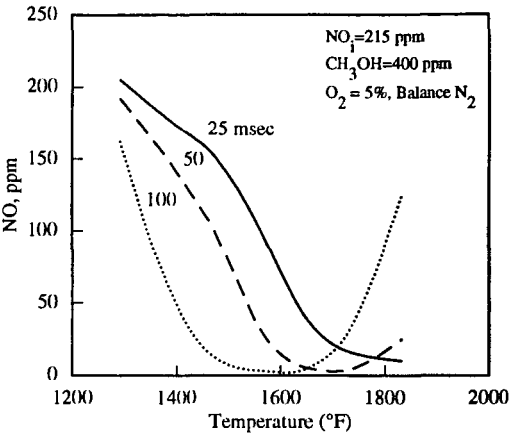

Figure 7. Predicted effect of temperature and residence time on methanol performance.

Figure 7 summarizes the effect of methanol injection temperature on the conversion efficiency of NO to NO_2. Depending on residence time and temperature, the model predicts an optimum injection temperature of between 1500 °F and 1800 °F. Complete conversion was shown to be theoretically possible, with an optimum injection temperature of 1550 °F and a residence time of 0.1 seconds.

Experiments were conducted to verify the modeling results at bench- and one million Btu/hr pilot-scale. At bench-scale, a simulated flue gas was combined with vaporized methanol and introduced into a quartz tube reactor. The reactor temperature and residence times were varied to evaluate their impact on NO conversion. At pilot-scale, methanol was injected into natural gas combustion products at various locations (temperatures) and the resulting NO and NO_x levels were recorded. The residence time at the optimum injection temperature (+/- 50°F) is approximately 600 msec. Figure 8 shows that the pilot-scale result for natural gas combustion products and the bench-scale data for the same residence time agree quite well.

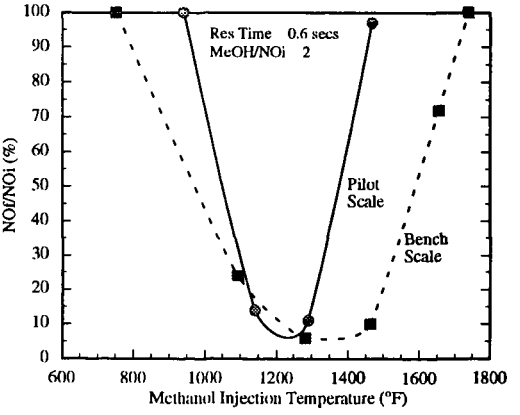

Figure 8. Bench vs Pilot scale methanol performance.

The experimentally-determined opti-

mum methanol injection temperature ranged from 1150°F to 1300°F, which is significantly lower than that predicted by the model. However, the experimental data were obtained at a residence time of 0.6 second residence time, while the predictions were performed for 0.1 second residence time. Additional modelling is planned to determine if increasing the residence time available for methanol reactions shifts the optimum injection temperature to lower levels.

CONCLUSIONS

These studies have shown the influence of the main parameters controlling performance of the Advanced Reburning process. Close coupling of the CO level in the reburning zone and the temperature at which the agent is injected is needed to optimize NO_x reduction. Studies of the methanol injection step in bench- and pilot-scale reactors have shown that conversion of the NO remaining from the Advanced Reburning process to NO_2 is feasible.

In conclusion, the CombiNO_x process, consisting of Advanced Reburning and methanol injection combined with NO_x scrubbing, is a promising retrofit technology for coal fired utility boilers. The Advanced Reburning portion has been demonstrated at 10 millionBtu/hr pilot scale to reduce NO_x emissions by 84 percent. The complete process has the potential to reduce NO_x emissions by 90 percent.

ACKNOWLEDGMENTS

This work was funded under Department of Energy Contract No. DE-AC22-90PC90363, Development of Advanced NO_x Control Concepts for Coal–Fired Utility Boilers. Mr. Charles E. Schmidt is the DOE Program Coordinator.

REFERENCES

1. Pont, J. N., et al. *Evaluation of the CombiNO_x Process at Laboratory and Pilot Scales.* Presented at the AIChE 1992 Summer National Meeting, Minneapolis, Minnesota, August 1992.

2. Wendt, J. O. L. et al. *Reduction of Sulfur Trioxide and Nitrogen Oxides by Secondary Fuel Injection.* Fourteenth Symposium (International) on Combustion, pp. 897–904, The Combustion Institute, 1973.

3. Greene, S. B., et al. *Bench Scale Process Evaluation of Reburning and Sorbent Injection for In–Furnace NO_x Reduction.* ASME Paper No. 84–JPGC–APC–9, 1984.

4. Seeker, W. R., et al. *Controlling Pollutant Emissions from Coal and Oil Combustors Through the Supplemental Use of Natural Gas.* Final Report, GRI Contract 5083–251–0905, 1985.

5. Borio, R. W., et. al. *Reburn technology for Boiler NO_x Control.* Presented at the ASME Winter Annual Meeting, San Francisco, California, December 1989.

6. Moyeda, D. K., et al. *Demonstration of Combined NO_x and SO_2 Emission control Technologies Involving Gas Reburning.* Presented at the 1991 AIChE Annual Meeting, Pittsburgh, Pensylvania, August 1991.

7. Lyon, R. K. Thermal $DeNO_x$, *Controlling Nitrogen Oxides Emissions by a Noncatalytic Process.* Environmental Science and Technology, Volume 21, No. 3, pp. 231–236, 1987.

8. Muzio, L. J., J. K. Arand and D. P. Teixeira. *Gas Phase Decomposition of Nitric Oxide in Combustion Products.* Presented at the Sixteenth Symposium (International) on Combustion, Cambridge, Massachusetts, August 1976.

9. Bartok, W. and G. M. Varga. *Applicability of the Thermal $DeNO_x$ Process to Coal Fired Utility Boilers.* Presented at the American Flame Research Committee International Symposium on NOx Reduction in Industrial Boilers, Heaters and Furnaces, Houston, Texas, October 1979.

10. Abele, A. R., et al. *Performance of Urea NO_x Reduction Systems on Utility Boilers.* Presented at the 1991 Joint EPA/EPRI Symposium on Stationary Combustion NO_x Control, Washington, D. C., March 1991.

11. Evans, A. B, et al. *Development of Process to Simultaneously Scrub SO_2 and NO_2 from Coal–Fired Boiler Flue Gas.* ACS Spring Symposium, Denver, Colorado, March 1993.

12. Irons, M. A., et al. *Tailoring Ammonia-Based SNCR for Installation on Power Station Boilers.* 1991 Joint Symposium on Stationary Combustion NOx Control, Washington D.C., March 25-28,1991.

13. Chen, S. L., et al. *Advanced NO_x Reduction Processes Using -NH and -CN Compounds in Conjuntion with Staged Air Addition.* Twenty–Second Symposium (International) on Combustion, pp. 1135–1145, The Combustion Institute, 1988.

14. Lyon, R.K.: *Kinetic and Mechanism of Thermal $DeNO_x$: A Review.* Preprints: ACS Division of Fuels Chemistry, ACS, 32 (4), 433 (1987).

15. Kau, C.J. and Tyson, T.J. *A Computer Program for General Flame Analysis.* U.S. Environmental Protection Agency Report No. EPA–600/7–87–027 (1987).

16. Lyon, R.K, et al. *The Selective Reduction of SO_3 to SO_2 and the Oxidation of NO to NO_2 by Methanol.* Combustion and Flame, 81, pp. 30–39, 1990.

SYMPOSIUM ON CHEMISTRY OF FLUE GAS CLEANUP PROCESSES
FOR PREPRINTS OF THE FUEL CHEMISTRY DIVISION
AMERICAN CHEMICAL SOCIETY
DENVER, CO MEETING, MARCH 28-APRIL 2, 1993

ACTIVATED CARBON FOR SELECTIVE REMOVAL OF NITROGEN OXIDE FROM COMBUSTION FLUE GAS

By

A.M. Rubel, J.M. Stencel, S. N. Ahmed
University of Kentucky, Center for Applied Energy Research
3572 Iron Works Pike, Lexington, KY 40511-8433

Keywords: NO, selective adsorption, activated carbons

INTRODUCTION

A new concept for non-catalytic NO removal from combustion flue gas is being developed at the University of Kentucky Center for Applied Energy Research (CAER). Flue gas cleanup would be achieved through the use of activated carbons for the selective capture of NO_x at stack temperatures between 70-120°C followed by desorption of a concentrated stream of NO_x at elevated temperatures, near 140-150°C. Processing would involve repeated NO_x adsorption/desorption cycles using the same adsorbent carbon.

Previous work on the removal and adsorption of NO over carboneous materials has focused on the heterogeneous reduction of NO by carbon to CO, CO_2, and N_2[1-6]. The proposed reaction mechanisms involve the chemisorption of NO on carbon at temperatures near 200°C resulting in the formation of a carbon-NO complex which rearranges to form a carbon-oxygen complex and molecular nitrogen[2]. The amount of NO adsorbed was less than 2 wt% of the carbon and, upon desorption, 40-50 wt% of the carbon is gasified[2,6]. Some work has been done toward the use of activated carbon to remove NO_x from moist off-gases in nitric acid plants at ambient temperatures and in the presence of O_2. The NO adsorptive capabilities found were low and near 0.16 to 0.7 mg NO/g carbon[7]. No information has been found in the literature concerning NO/NO_2 adsorption on active carbon under conditions found in combustion flue-gases.

During this study, the mechanisms and kinetics of NO_x adsorption/desorption on activated carbon under conditions typical to combustor stacks were investigated by thermogravimetry/mass spectrometry (TG/MS). Information was obtained concerning the requirements for NO_x capture, the NO_x adsorption capacity of an activated carbon, the effect of repeated adsorption/desorption cycles on NO_x adsorption, and the mechanism of adsorption.

EXPERIMENTAL

Instrumentation

NO_x adsorption/desorption profiles were obtained using a Seiko TG/DTA 320 coupled to a VG Micromass quadrapole MS. The two instruments were coupled by a heated (170°C)

fused silica capillary transfer line leading from above the sample pan in the TG to an inert metrasil molecular leak which interfaced the capillary with the enclosed ion source of the MS. The TG was connected to a disk station which provided for programmable control of the furnace, continuous weight measurements, sweep gas valve switching, data analysis, and export of data to other computers. The MS has a Nier type enclosed ion source, a triple mass filter, and two detectors (a Faraday cup and a secondary emissions multiplier). The MS was controlled by a dedicated personal computer which was also used to acquire and review scans before export to a spreadsheet for data manipulation.

TG-MS procedures

The TG conditions kept constant during the acquisition of adsorption/desorption profiles were: sweep gas flow rate of 200 ml/min metered at room temperature and pressure and a constant carbon sample volume weighing approximately 20 mg. The MS was scanned over a 0-100 amu range with measurement intervals of approximately 30 seconds. NO (mass 30) or NO_2 (mass 30 and 46) were identified by comparing amu 30/46 ion ratios. These ratios were determined for all combinations of gases flowing through the TG-MS system both with and without carbon in the TG sample pan.

The TG heating regime used to produce NO_x adsorption/desorption profiles incorporated segments for outgassing, cooling, adsorption, desorption, and temperature-induced desorption. Table I shows a typical heating program for a single adsorption/desorption cycle. During outgassing and subsequent cooling of the carbon sample to an adsorption temperature (segments a and b, Table I), an inert (He) gas sweep was usually used. However, O_2 and CO_2 pretreatments of the carbon were also done during these steps for some experiments. Maximum outgassing temperature was always the same as the maximum used during temperature programmed desorption (step e). After preconditioning of the carbon, NO or NO_2 was introduced in a simulated flue gas atmosphere containing either O_2 or CO_2, or both O_2 and CO_2. After completion of an adsorption interval (30 or 60 minutes), He was again used to purge the system during segments d and e. Two maximum desorption temperatures were used, 300 and 400°C. Multiple and consecutive adsorption/desorption cycles were performed by recycling the temperature programmer to segment b.

Materials and simulated flue gas composition

A commercially (Carbo Tech) produced coal-based carbon was used. This carbon was produced by physical activation and had a N_2 BET surface area of 450 m^2/g.

During this study, the concentrations of gases used during adsorption and pretreatments were: 2% or 0.3% NO or NO_2; 5% O_2, 15% CO_2 and He as the balance. NO adsorption capacity of the activated carbon studied was determined for the following combinations of gases: 2% NO with O_2 and CO_2; 2% NO in He alone; 0.3% NO in O_2 and CO_2; 0.3% NO in either O_2 or CO_2; 0.3% NO in He with carbon presaturated with either O_2 or CO_2; 0.3% NO in He alone; and 0.3% NO_2 in O_2 and CO_2.

RESULTS AND DISCUSSION

Capacity of activated carbon to selectively capture NO_x

Both single cycle and repeated cycles TG-MS adsorption/desorption profiles were used to show effective and rapid removal of NO from simulated flue gas by activated carbon.

During a single NO adsorption/desorption cycle using a simulated flue gas with a high NO concentration (2% NO, 15% CO_2, and 5% O_2 with a balance of He), 0.14 g NO/g carbon was adsorbed in 30 minutes as evidenced by the increased weight of the carbon (Figure 1). Increasing the adsorption time to 60 minutes only marginally increased NO capture to 0.16 g NO/g carbon. Desorption of NO_x from the carbon through both physidesorption and temperature programmed desorption was confirmed by the mass spectra showing a major peak in the ion intensity of amu 30 (the primary ion mass for both NO and NO_2) coinciding with the TG monitored weight loss. A small peak was also observed for amu 46, a secondary ion mass for NO_2. The temperature of maximum desorption occurred at 140°C.

Repeated cycling of the same carbon through three NO_x adsorption/desorption cycles, resulted in a 15% total loss of adsorptive capacity (Figure 2). The maximum desorption temperature (400°C) used during this experiment was higher than the 250-300°C required for complete NO_x desorption. Since the loss in adsorptive capacity of the carbon coincided with a 0.5-1.0 wt% loss of carbon, possibly through oxidation/gasification, lowering the desorption temperature should reduce this already small loss in adsorptive capacity.

Effect of flue gas constituents on NO_x adsorption

To determine the effect of typical flue gas constituents on the kinetics of NO adsorption, a parametric study was done using 0.3% NO in various combinations with O_2 (5%), CO_2 (15%), and He (balance) (Figure 3). Adsorption time for all experiments was kept constant at 60 minutes. NO capture was dependent on the presence of O_2 but was not significantly affected by the presence of CO_2. Presaturation of carbon with O_2 followed by NO adsorption in He increased adsorption from 1 wt% using He alone to 6 wt% suggesting a carbon surface reaction mechanism. Control experiments without NO present during adsorption showed that 1% or less of the weight gain during NO adsorption resulted from O_2, CO_2, or He adsorption on the carbon(Figure 3).

Possible reaction mechanism

The dependency of NO adsorption on the presence of O_2 suggests that NO must be converted to a surface species similar to NO_2 during the adsorption step. Simultaneous differential thermal analyses (DTA) conducted during these experiments supported such conversion. A significant exotherm accompanied NO adsorption (Figure 4) whereas, no heat of reaction was associated with NO_2 adsorption (Figure 5).

A comparison of MS ion ratios for masses (30/46) for all combinations of NO or NO_2 and O_2 or CO_2 flowing through the TG-MS system with and without activated carbon in the sample pan shows the differences obtained in these ratios (Figure 6). These differences were used to identify the form of NO_x desorbed from the carbon. Since the (30/46) ion ratios for all combinations of NO or NO_2 with O_2 or CO_2 were less than 20, an experiment where desorption occurred in a He sweep with low baseline levels of O_2 and CO_2 was necessary. This requirement was met by presaturating carbon with O_2 followed by adsorption and desorption in He. The ion ratio during desorption for this experiment was 94 and most closely matched the ion ratio for NO_2 in He (Figure 7). For comparison, the desorption ion ratio for a NO, CO_2, O_2 experiment is also shown.

SUMMARY AND CONCLUSIONS

The data presented provides evidence for the selective capture of NO_x by activated

carbons in the presence of typical flue gas components. The NO adsorption capacities approached 0.16 g NO/g carbon. Adsorption of NO was rapid only in the presence of O_2, was not influenced by the presence of CO_2, and involved the exothermic conversion of NO to NO_2-like species at the surface of the carbon. The capacity for NO adsorption was only slightly diminished by repeated adsorption/desorption cycles. At desorption temperature as high as 400°C, the capacity after three cycles decreased to about 85% of the original value with a coincident loss of 0.5-1.0 wt% of the carbon. The results suggested that activated carbon can be used for NO_x flue gas clean-up and would provide a simple alternative to more expensive and complex methods such as selective catalytic reduction.

REFERENCES

1. Smith, R.N., J. Swinehart, and D. Lesnini. *J. Physical Chem.* 63(1959)544.
2. DeGroot, W.F., T.H. Osterheld, G.N. Richards. *Carbon* 29(1991)185.
3. Teng, H., E.M. Suuberg, J.M. Calo, and P.J. Hall. *Proc. 19th Conf. on Carbon*, (1989)574.
4. Suuberg, E.M., H. Teng, and J.M. Calo. *23rd Symposium (International) on Combustion*, The Combustion Institute (1990)1199.
5. Teng, H., E.M. Suuberg, and J.M. Calo. *Preprints of the 200th ACS National Meeting*, Washington, DC, 35,3(1990)592.
6. Gray, P.G., N.J. Desai, and D.D. Do. *Recent Trends in Chem. Rxn Engr.*, B.O. Kkulkarni, R.A. Mashelkar, and M.M. Sharma, eds., Wiley Eastern Ltd., 1(1987)383.
7. Richter, E., R. Kleinschmidt, E. Pilarczyk, K. Knoblauch, and H. Juntgen. *Thermochimica Acta* 85(1985)311.

Table I. Typical TG heating regime for acquisition of NO_x heating profile.

Step	Temp C	Rate C/min	Hold min
a	0-400	20	10
b	400-70	50	10
c	70 (1)	0	30-60
d	70 (2)	0	30
e	70-400	20	10

[1]Adsorption step
[2]Physidesorption step

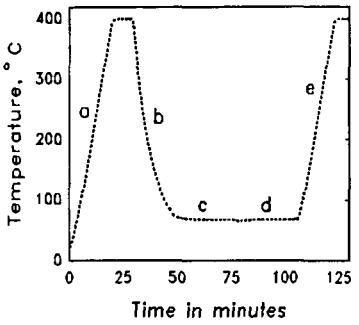

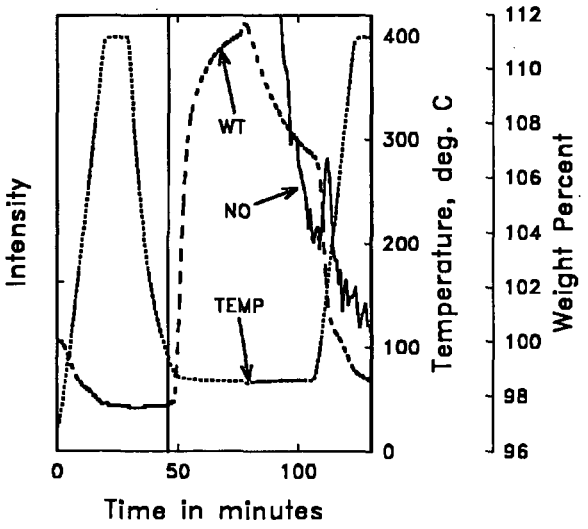

Figure 1. Single adsorption/desorption profile. Adsorption atmosphere: 2% NO, 5% O_2, 15% CO_2, and He balance; adsorption time: 30 min.

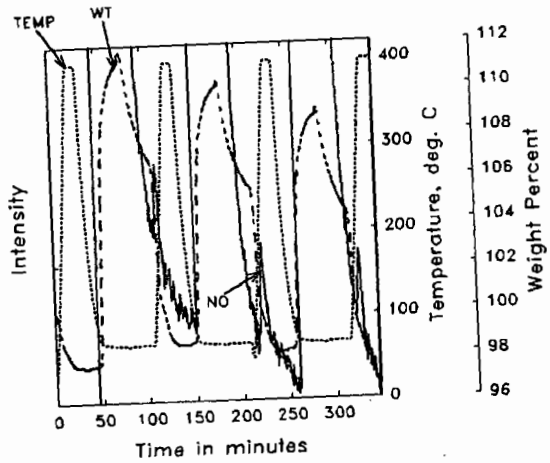

Figure 2. Three consecutive adsorption/desorption cycles using the same carbon sample. Adsorption atmosphere: 2% NO, 5% O_2,15% CO_2, and He balance; adsorption time: 30 min.

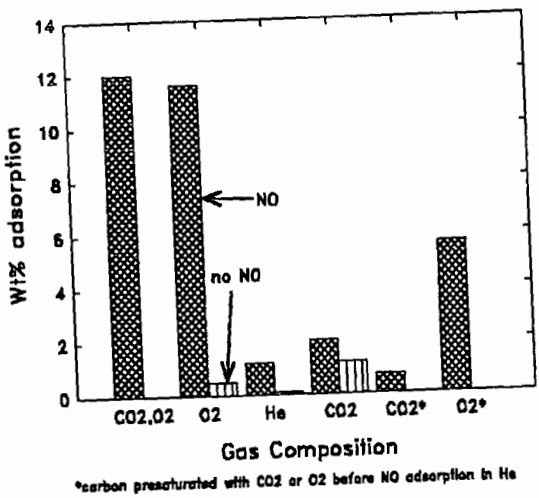

Figure 3. Study of the effect of O_2 and CO_2 on NO adsorption on activated carbon. Gases: 0.3% NO, 5% O_2,15% CO_2, and He balance; adsorption time: 60 min.

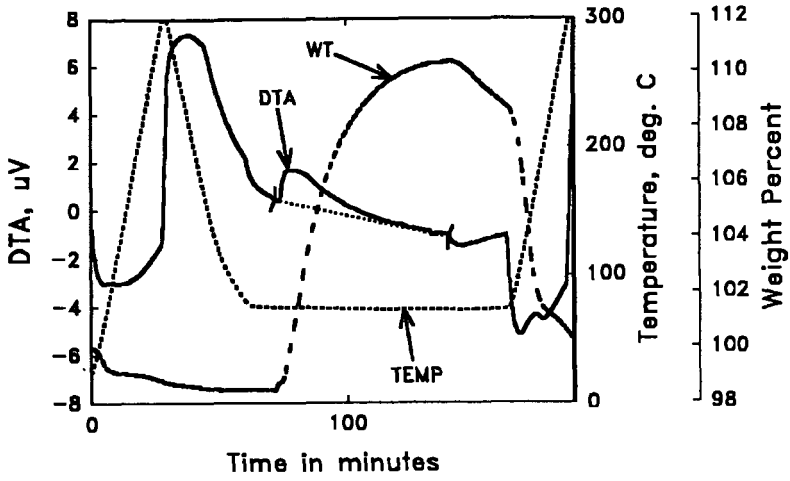

Figure 4. Simultaneous TG/DTA of NO adsorption on activated carbon. Adsorption atmosphere: 0.3% NO, 5% O_2,15% CO_2, and He balance; adsorption time: 60 min.

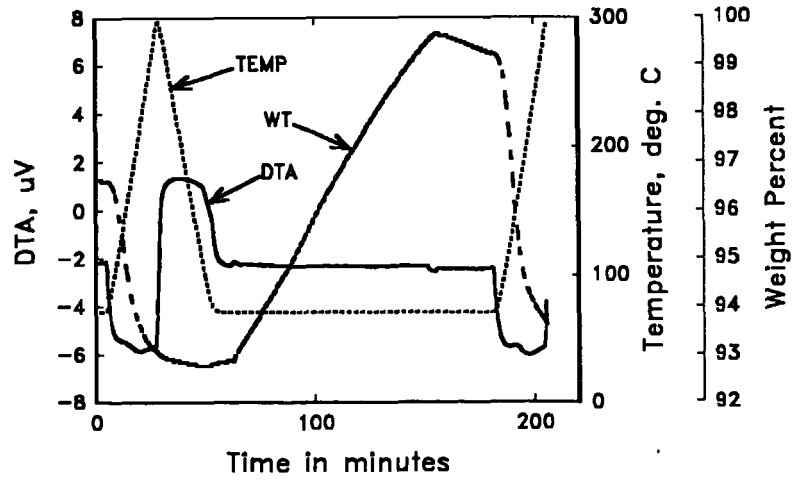

Figure 5. Simultaneous TG/DTA of NO_2 adsorption on activated carbon. Adsorption atmosphere: 0.3% NO_2, 5% O_2,15% CO_2, and He balance; adsorption time: 60 min.

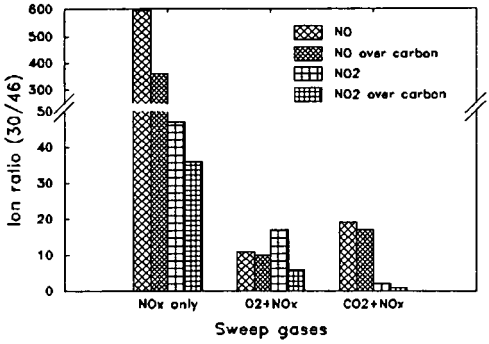

Figure 6. Mass (30/46) ion ratio for various combinations of NO or NO_2 and O_2 or CO_2 with and without the presence of carbon in the TG sample pan as determined by MS.

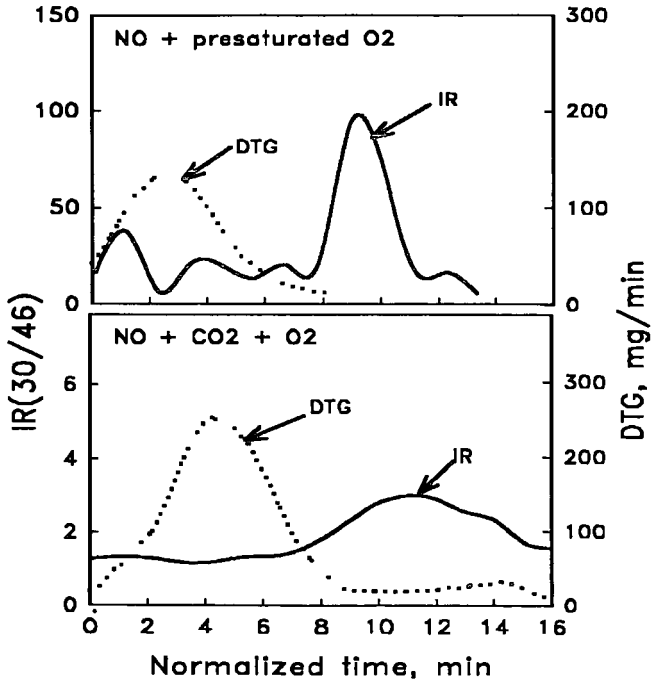

Figure 7. Mass (30/46) ion ratios during desorption of NO_x from activated carbon.

Reaction Kinetics of Selective Non-Catalytic NO_x Reduction with Urea

William H. Sun, Penelope Stamatakis, John E. Hofmann
Nalco Fuel Tech
Naperville, Illinois, U.S.A.

Abstract

Selective Non-Catalytic Reduction (SNCR) of NO_x with urea has proven to be an effective method in controlling NO_x from various stationary combustion sources. The chemistry of this process that is marketed under the name of NO_xOUT®, was modelled to identify major pathways, limitations, and important parameters. The chemical kinetic model includes over 90 elementary radical reactions among various stable and radical species. The developed model has been validated with data generated from a pilot facility.

The model provided understanding of the effects of residence time, treatment rate and baseline NO_x, oxygen and CO concentrations. In addition, the lowest achievable NO_x concentration, referred as 'Critical NO_x', has been identified. This limit is the result of the chemical reaction kinetics. The existence of such limit is explained through reaction chemistry and validated with laboratory and field data.

Introduction

Post combustion NO_x control methods reduce NO_x after its formation is completed. Other methods such as flue gas recirculation and staged combustion limit the formation of NO_x by lowering combustion temperature or by limiting oxygen for N2 oxidation. Once NO_x is formed, post combustion control methods take advantage of the highly selective reactions between ammonia and NO_x or urea and NO_x. These reactions occur at temperatures between 850 - 1100 °C without a catalyst and are called selective noncatalytic reactions (SNCR). Ammonia injection is an Exxon process and has been called the Thermal DeNO$_x$ Process [1,2] while the urea injection was patented by EPRI [3,4]. Nalco Fuel Tech is EPRI's exclusive licensing agent, and the technology is being marketed as NO_xOUT Process. At lower temperatures (300 - 500 °C), various metal and ceramic catalysts are required to reduce NO_x by reacting with ammonia (SCR)[5].

NO_xOUT Kinetic Model

As part of a development effort, a chemical kinetic model has been developed to understand the basic chemistry, to determine important factors and to define the limits of process capability. This model describes an ideal plug flow, i.e., no temperature or species concentration gradient in radial direction and no back-mixing. Chemical reactions along an ideal plug flow can be described by a set of ordinary differential equations. Reaction rates, density, and thermodynamic information are supplied through a library of

gas-phase subroutines called CHEMKIN developed at the Sandia National Laboratories [6]. The CHEMKIN requires a user supplied chemical reaction set and a thermodynamic data set. The resulting set of equations is integrated simultaneously with a numerical integrator called LSODE [7]. The enthalpy equation is neglected in the model. Instead, measured or calculated temperature profiles are required as an input to the model. Computational fluid dynamics modelling is extensively used to provide temperature and residence time relationships for the kinetic model [8]. Initial conditions are the equilibrium concentrations at flue gas temperatures and excess O_2 as measured. Measured NO_x and CO concentrations are also inputs.

The reaction set is adopted from the work of Miller and Bowman [9]. From this set, reactions involving hydrocarbons were neglected. The wet CO oxidation reactions, ammonia oxidation reactions, and HCN oxidation reactions make up the set. Urea decomposition is modelled as a rapid and one step breakdown to NH_3 and HNCO. The reaction set consists of 92 reactions describing interactions among 31 species. The major pathway of urea breakdown and reaction with NO_x is shown in Fig. 1. Ammonia and HNCO, the assumed breakdown products of urea, must react with chain carrier radicals, O, OH, and H, before reacting with NO. Under oxygen rich conditions, OH concentrations are several orders of magnitude higher than O or H. Therefore, reactions involving OH radicals are more important than those involving O or H. Reaction products of NH3 and HNCO with OH are NH2 and NCO. These compounds reduce NO_x or react with OH to form NO_x according to reactions listed below. The balance between formation and destruction of NO_x hinges on concentration of OH and temperature.

```
NH3  + OH = NH2 + H2O          Activation Reactions
HNCO + OH = NCO + H2O

NH2  + NO = NNH + OH
NH2  + NO = N2  + H2O          NOx Destruction Reactions
NCO  + NO = N2O + CO
N2O     --> N2
NNH     --> N2

NH2  + OH = NH  + H2O
NH   + OH = HNO + H            NOx Formation Reactions
HNO  + OH = NO  + H2O
NCO  + OH = NO  + CO  + H
```

Model Validation

Results from a pilot scale combustor are compared with results from the developed model. A schematic of the pilot combustor and the analytical setup is shown in Fig. 2. The test zone of the combustor was kept isothermal by electrical heating. The residence time at this zone was about 0.7 seconds. This is the average residence time between the injection point and the end of the isothermal zone. Urea solution was injected co-flow with an air

atomized nozzle located along the axis of the test zone. Temperature was varied from 700 °C to 1070 °C, baseline NO_x at ~300 ppm, and a treatment rate at NSR of 2. NSR is defined as the actual mole ratio of urea to NO_x divided by the theoretical stoichiometric ratio, which is 0.5 for the reaction between urea and NO_x. Comparison of the model and experimental results is shown in Fig. 3. The available chemical reaction time is less than the residence time because part of the residence time is used to distribute and evaporate droplets. Because of these delays, model results for reaction times of 0.1, 0.3, 0.5, and 0.7 seconds are compared to the experimental results. As shown, the trend and the shape of the experimental results are well modelled.

A range of temperature where significant NO_x reductions are obtained is called the temperature window as indicated on Fig. 3. Within this window, controlled NO_x versus temperature curve consists of three zones: left side, right side and plateau. This shape is a result of competing reactions (formation vs. destruction) on the right side and a limitation of reaction time due to slow reaction rates on the left side. On the plateau zone, destruction reaction rates are sufficiently fast while formation reactions are slow, yielding optimum NO_x reductions. Although the reduction is less than the maximum, operation on the right side is practiced and recommended since byproduct emissions are low on the right side [10].

Treatment Rate

Increasing NSR has a diminishing return in NO_x reduction. In Fig. 4, model results of NO_x concentration as a function of NSR are presented at several temperatures. NO_x decreases with increasing NSR at temperatures within the window; increasing NSR increases NO_x at higher temperatures. At temperatures between 900 and 1200 °C, NO_x reaches a limit at an NSR of about 2. A further increase from NSR of 2 increases NO_x for 1200 °C case but has no effect at lower temperatures.

Residence Time

The temperature window becomes wider with an increase in residence time. As shown in Fig. 5, the window is about 150 °C wide at 0.1 second but the window increases to 300 °C at one second. This widening occurs on the left side only and has virtually no effect on the right side. On the plateau region, reactions are essentially complete after 0.6 seconds and even shorter (0.2 seconds) at temperatures above 1100 °C.

Baseline NO_x

The controlled NO_x is unaffected by the baseline NO_x at the plateau zone, while NO_x increased at higher baselines on the left and right sides. Fig. 6 shows NO_x concentration versus temperature at 100, 200, and 500 ppm baseline NO_x. NSR is kept constant at 2 and residence time is 1 second. At 1200 °C, NO_x increased from 100 ppm

to 120 ppm, but decreased from 500 ppm down to ~300 ppm. This indicates that NO_x can be reduced even at high temperatures provided that baseline NO_x concentrations are also high. In terms of reduction, the temperature window widens toward the higher temperature side with increases in baseline NO_x as shown in Fig. 7.

Excess Oxygen

The effect of excess oxygen is studied by modelling at several levels of excess oxygen and substoichiometric conditions. The fuel equivalence ratio was 1.1 for the substoichiometric case. As shown in Fig. 8, temperature windows are affected slightly as oxygen increased beyond 3%. However, at less than 3% O2, the temperature window shifted about 80 °C for a change in excess oxygen from 0.5 to 0.1%. Under a substoichiometric condition, the window shifted to temperatures above 1200 °C. This shift to higher temperatures is the result of reduction in OH concentration. Under a typical oxygen rich condition, OH concentrations are not strongly affected by O2. Near the stoichiometric condition, however, a slight decrease in excess oxygen directly reduces OH radicals, which in turn, slows the activation reactions and shifts the window to higher temperatures. Experimental investigation of urea injection under oxygen starved condition by Arand and Muzio also indicates that the window exists at much higher temperature under fuel rich conditions [4]. The present reaction set does not address hydrocarbon reactions and therefore the modelling of stoichiometric and fuel rich conditions needs further work. Nevertheless, very low excess oxygen conditions shift a temperature window to higher temperatures.

Carbon Monoxide Concentration

Carbon monoxide oxidizes to generate H, O, and OH radicals through reactions listed below. Overall, one mole of CO generates two moles of OH radicals.

```
CO + OH  ----> CO2 + H     \
H  + O2  ----> OH  + O   --   CO + O2 + H2O ---> CO2 + 2 OH
O  + H2O ----> 2 OH        /
```

This additional source OH increases rates of the activation reactions and the NO_x formation reactions. A net result is shifting of temperature windows to lower temperatures with CO concentration as shown in Fig. 9. Therefore, CO enhances the process performance when operating on the left side, but degrades reductions on the right side.

Critical NO_x

On Fig. 5, part of the curve that represents the controlled NO_x concentrations at 1 second residence time and at temperatures between 900 and 1300 °C is the lowest achievable NO_x concentration curve. Increases in residence time or NSR do not lower NO_x below this curve. On Fig 10, NO_c concentrations are plotted for the

equilibrium concentration of CO at three baseline NO_x concentrations. At temperatures below 900 °C, 10 seconds of residence time are required to determine the lowest achievable concentration. This minimum achievable NO_x concentration through urea injection, is termed as 'Critical NO_x', as first indicated by Fenimore [11] for the Thermal DeNO_x process. Neither an increase in residence time nor treatment rate above a certain value will lower the controlled NO_x below this critical NO_x concentration.

The existence of critical NO_x and its lack of dependencies to residence time and treatment rate are understood through a simplified chemical kinetic analysis. The change of NO concentration with respect to time for following reactions is formulated as equation 1.

NO + NH2 --> --> N2	1
NO + NCO --> --> N2	2
NH2 + OH --> --> NO	3
NCO + OH --> --> NO	4

$$\frac{d[NO]}{dt} = -k_1[NH_2][NO] - k_2[NCO][NO] + k_3[NH_2][OH] + k_4[NCO][OH] \quad (1)$$

With urea injection, NO_x concentration will change from its baseline value to a steady state value. At this point, the lefthand side of the above equation becomes zero. After rearranging, an expression for critical NO_x, $[NO]_c$, is arrived as equation 2.

$$[NO]_c = \frac{[OH]\{k_3[NH_2] + k_4[NCO]\}}{\{k_1[NH_2] + k_2[NCO]\}}; \quad \frac{d[NO]}{dt} = 0 \quad (2)$$

This equation is further simplified for cases where NH_2 is comparable to NCO, NH_2 is in large excess of NCO, and NCO is in large excess of NH_2.

$$[NO]_c = [OH]\frac{(k_3 + k_4)}{(k_1 + k_2)} \qquad NH_2 \sim NCO$$

$$[NO]_c = [OH]\frac{k_3}{k_1} \qquad NH_2 >> NCO$$

$$[NO]_c = [OH]\frac{k_4}{k_2} \qquad NCO >> NH_2$$

These three cases show that NO_c is only a function of OH concentration at a given temperature and does not dependent on residence time or NSR. However, chemicals that generate CO and consequently increase the OH concentration will affect the critical NO_x.

The critical NO_x limits the process on the right side of the window. As shown in Fig. 10, the critical NO_x concentrations are less than 40 ppm at 1050 °C and even lower at temperatures below 1000 °C. These low levels usually do not limit process applications. Instead, the critical NO_x limits achieving low controlled NO_x concentrations at high temperatures where NO_c increases sharply with temperature and baseline NO_x. Finally, reductions are achievable as long as a baseline NO_x is higher than the critical NO_x concentration.

Laboratory and Field Verification

The model study indicates that achievable NO_x concentrations are limited by Critical NO_x and this limit is mainly affected by temperatures. Case 1 and case 2 exhibit the process limitation due to NO_c while case 3 shows that reductions are possible even at high temperatures if baseline NO_x is greater than the NO_c.

Case 1.

A NO_xOUT Process testing on a coal fired boiler revealed that NO_x reduction increased with decreasing boiler load, as shown in Fig. 11. At full load, NO_x reduction remained essentially unchanged in spite of a series of injection optimization tests. However, a slight reduction in boiler load from 100% to 90% increased NO_x reduction. At full load, reaction is occurring at the steep part of the NO_c curve, and therefore, NO_x reduction improved rapidly with decreasing load under an essentially identical injection configuration. The controlled NO_x curve on Fig. 10 virtually represents the critical NO_x curve for this boiler.

Case 2.

During a process demonstration at an ethylene cracker, NO_x reduction was limited regardless of the NO_xOUT Process parameters. The cracker unit operated steadily at a temperature of approximately 1050 °C. When the unit operated at a higher NO_x baseline, NO_x reduction increased, but the lowest achievable NO_x concentration remained the same, as shown in Fig. 12. Increasing NSR or other methods to optimize chemical distribution had no effect on the lowest controlled NO_x. This showed the existence of critical NO_x that is unaffected by NSR, chemical distribution, or baseline NO_x.

Case 3.

An increase in NO_x baseline shifts the right side of the temperature window to a higher temperature. To verify this, a pilot scale combustor was operated at 1200 °C and the baseline NO_x concentration was increased from 150 to 750 ppm. At baseline NO_x below about 200 ppm, NO_x increased with urea injection, while at higher than 200 ppm, NO_x decreased as shown in Fig. 13. Comparison with ammonia injection showed that urea is more effective in reducing NO_x at high temperatures than ammonia.

Conclusions

The reaction kinetic model has proven to be a valuable tool in the development of the NO_xOUT Process. Model predictions with respect to the temperature window, the effect of residence time and CO, the effect of very low excess oxygen, and the phenomenon of critical NO_x, which limits NO_x reduction at the high end of the temperature window, have all been verified in laboratory and field tests. The temperature window is defined primarily by residence time at the low temperature (left) side and by baseline and critical NO_x at the high temperature (right) side of the window.

The model is now used to define temperature/residence time requirements for specific applications and to predict maximum achievable NO_x reduction. The model has also shown that the NO_xOUT Process can be applied at higher temperatures than previously thought applicable provided that the NO_x baseline is sufficiently high.

References

1. Lyon, R.K., U.S. Patent 3,900,559, 1975.
2. Lyon, R.K., "Thermal DeNO_x: Controlling Nitrogen Oxides Emissions by a Noncatalytic Process", Environ. Sci. Technol., Vol. 21, No. 3, p.231, 1987.
3. Arand, J.K., and Muzio, L.J., U.S. Patent 4,208,386, 1980.
4. Arand, J.K., Muzio, L.J., Teixeira, D.P., U.S. Patent 4,325,924, 1982.
5. Benson, C.E., Chittick, G.D., and Wilson R.P., Selective Catalytic NO_x Reduction Technology for Cogeneration Plants, Arthur D. Little Report, Prepared for New England Cogeneration Association, November 1988.
6. Kee, R.J., Miller, J.A., Jefferson, T.H., "CHEMKIN: A General Purpose, Problem-Independent, Transportable, Fortran Chemical Kinetics Code Package", Sandia Laboratories Report #SAND80-8003, Livermore, CA, 1980.
7. Hindmarsh, A.C., "ODEPACK, A Systematized Collection of ODE Solvers", Scientific Computing, R.S. Stepleman et al. (eds.), Vol.1 of IMACS Transactions on Scientific Computation, p.55, North-Holland, Amsterdam, 1983.
8. Sun, W.H., Stamatakis, P., Michels, W.F., Comparato, J.R., Hofmann, J.E., "Selective Non-Catalytic NO_x Control with Urea: Theory and Practice, Progress Update", AFRC 1992 Fall International Symposium, October 1992.
9. Miller, J.A., Bowman, C.T., "Mechanism and Modeling of Nitrogen Chemistry in Combustion", Fall Meeting of the Western States Section/The Combustion Institute, Dana Point, California, October, 1988.
10. Epperly, W.R., O'Leary, J.H., Sullivan, J.C., U.S. Patent 4,780,289, 1988.
11. Fenimore, C.P., "Destruction of NO by NH3 in Lean Burnt Gas", Combustion and Flame, 37, 245, 1980.

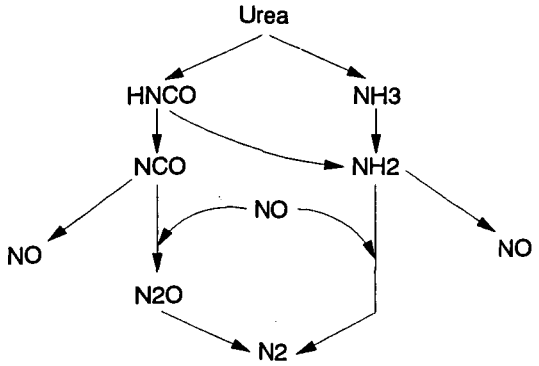
POST COMBUSTION NOx REDUCTION
with UREA
Urea
HNCO
NH3
NCO
NH2
NO
NO
NO
N2O
N2

Fig. 1

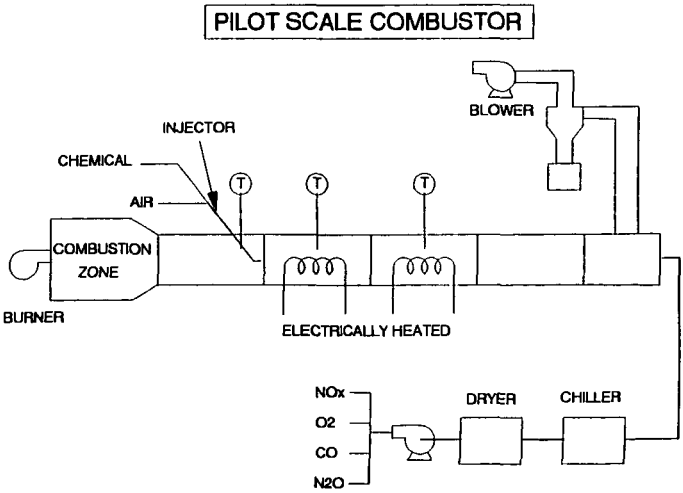
PILOT SCALE COMBUSTOR
BLOWER
INJECTOR
CHEMICAL
AIR
T
T
T
COMBUSTION
ZONE
BURNER
ELECTRICALLY HEATED
NOx
O2
CO
N2O
DRYER
CHILLER

Fig. 2

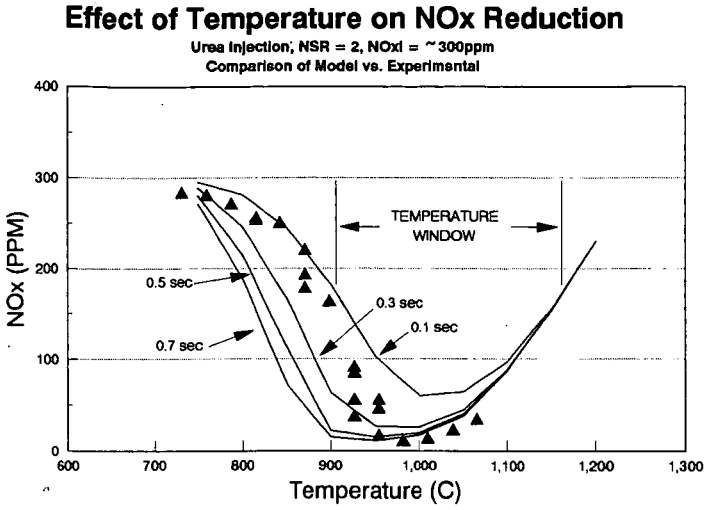
Effect of Temperature on NOx Reduction
Urea Injection, NSR = 2, NOxI = ~300ppm
Comparison of Model vs. Experimental
NOx (PPM)
Temperature (C)
TEMPERATURE WINDOW
0.5 sec
0.7 sec
0.3 sec
0.1 sec
400
300
200
100
0
600
700
800
900
1,000
1,100
1,200
1,300

Fig. 3

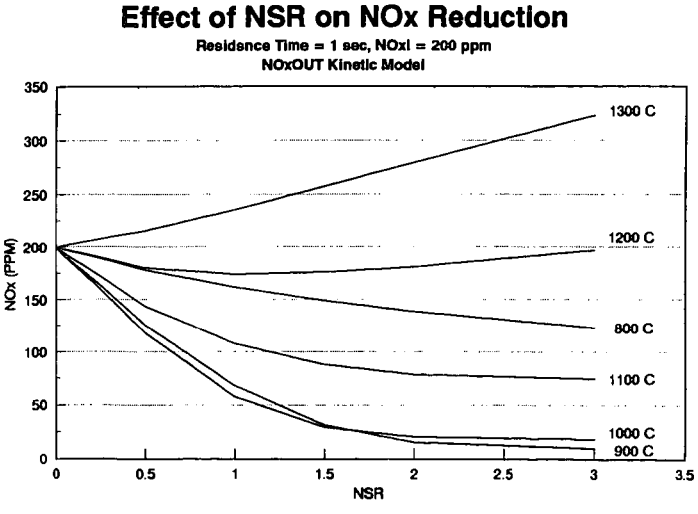
Effect of NSR on NOx Reduction
Residence Time = 1 sec, NOxI = 200 ppm
NOxOUT Kinetic Model
NOx (PPM)
NSR
1300 C
1200 C
800 C
1100 C
1000 C
900 C
350
300
250
200
150
100
50
0
0
0.5
1
1.5
2
2.5
3
3.5

Fig. 4

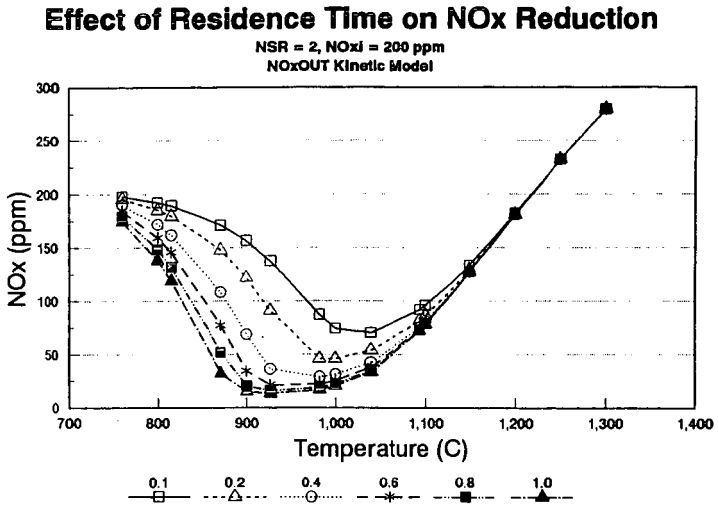
Effect of Residence Time on NOx Reduction
NSR = 2, NOxi = 200 ppm
NOxOUT Kinetic Model
NOx (ppm)
300
250
200
150
100
50
0
700
800
900
1,000
1,100
1,200
1,300
1,400
Temperature (C)
0.1
0.2
0.4
0.6
0.8
1.0

Fig. 5

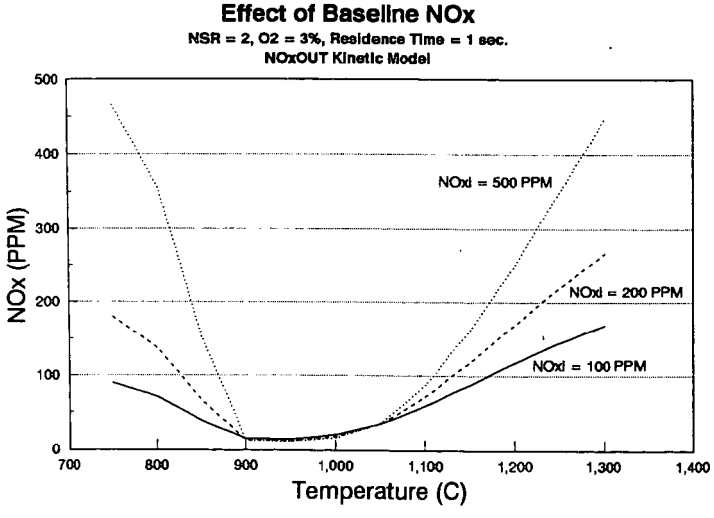
Effect of Baseline NOx
NSR = 2, O2 = 3%, Residence Time = 1 sec.
NOxOUT Kinetic Model
NOx (PPM)
500
400
300
200
100
0
700
800
900
1,000
1,100
1,200
1,300
1,400
Temperature (C)
NOxi = 500 PPM
NOxi = 200 PPM
NOxi = 100 PPM

Fig. 6

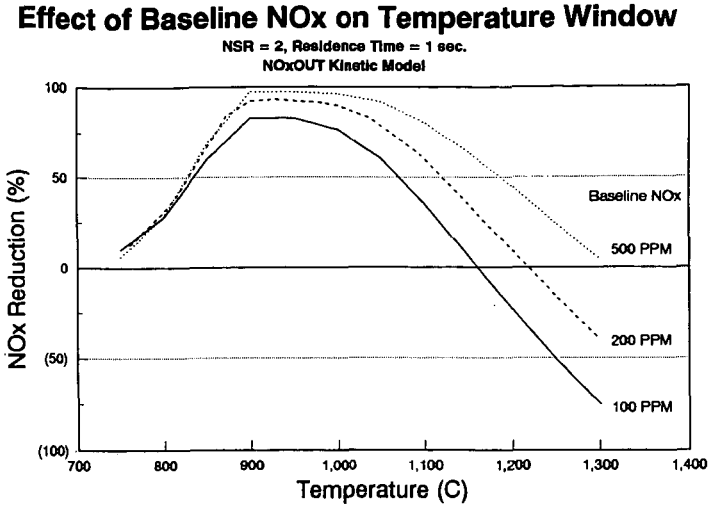
Effect of Baseline NOx on Temperature Window
NSR = 2, Residence Time = 1 sec.
NOxOUT Kinetic Model
NOx Reduction (%)
100
50
0
(50)
(100)
700
800
900
1,000
1,100
1,200
1,300
1,400
Temperature (C)
Baseline NOx
500 PPM
200 PPM
100 PPM

Fig. 7

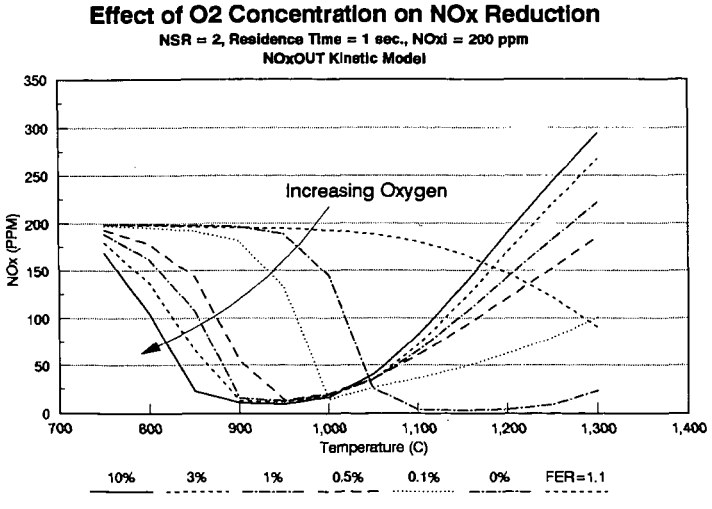
Effect of O2 Concentration on NOx Reduction
NSR = 2, Residence Time = 1 sec., NOxi = 200 ppm
NOxOUT Kinetic Model
NOx (PPM)
350
300
250
200
150
100
50
0
700
800
900
1,000
1,100
1,200
1,300
1,400
Temperature (C)
Increasing Oxygen
10%
3%
1%
0.5%
0.1%
0%
FER=1.1

Fig. 8

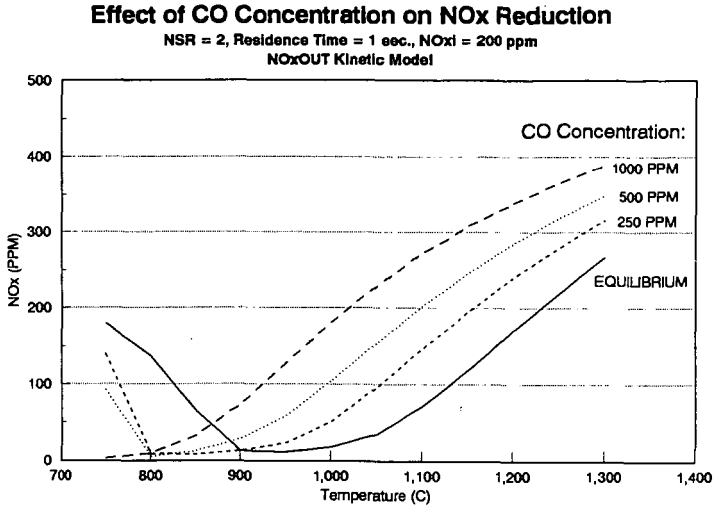
Effect of CO Concentration on NOx Reduction
NSR = 2, Residence Time = 1 sec., NOxI = 200 ppm
NOxOUT Kinetic Model
CO Concentration:
1000 PPM
500 PPM
250 PPM
EQUILIBRIUM
NOx (PPM)
Temperature (C)
0
100
200
300
400
500
700
800
900
1,000
1,100
1,200
1,300
1,400

Fig. 9

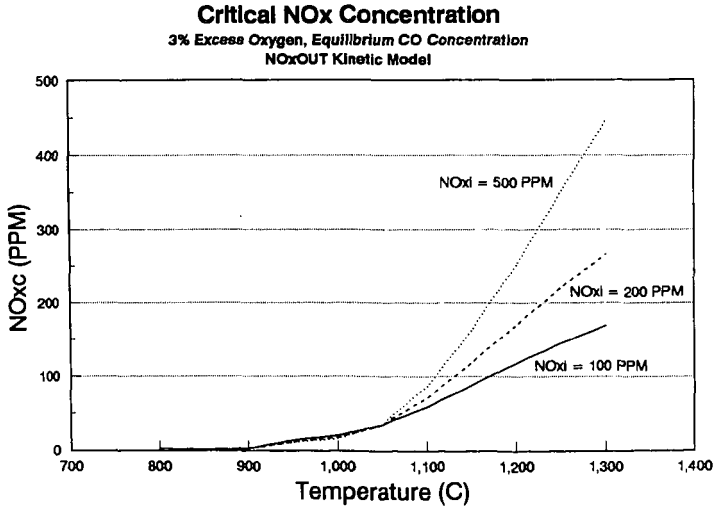
Critical NOx Concentration
3% Excess Oxygen, Equilibrium CO Concentration
NOxOUT Kinetic Model
NOxI = 500 PPM
NOxI = 200 PPM
NOxI = 100 PPM
NOxc (PPM)
Temperature (C)
0
100
200
300
400
500
700
800
900
1,000
1,100
1,200
1,300
1,400

Fig. 10

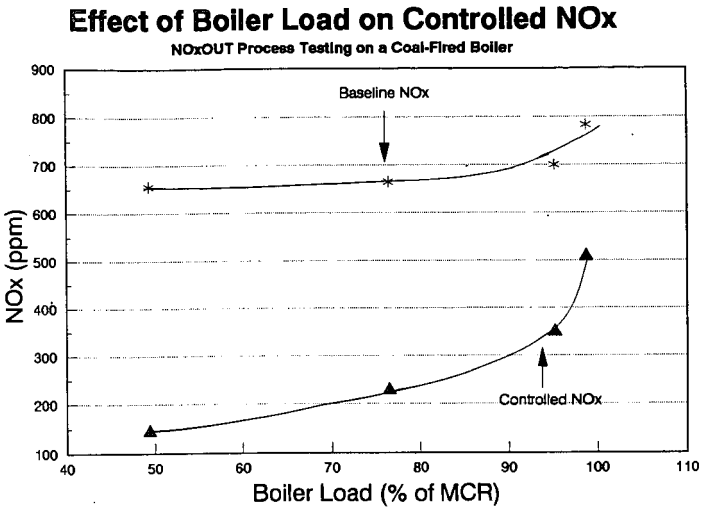
Effect of Boiler Load on Controlled NOx
NOxOUT Process Testing on a Coal-Fired Boiler
Baseline NOx
Controlled NOx
NOx (ppm)
Boiler Load (% of MCR)
900
800
700
600
500
400
300
200
100
40
50
60
70
80
90
100
110

Fig. 11

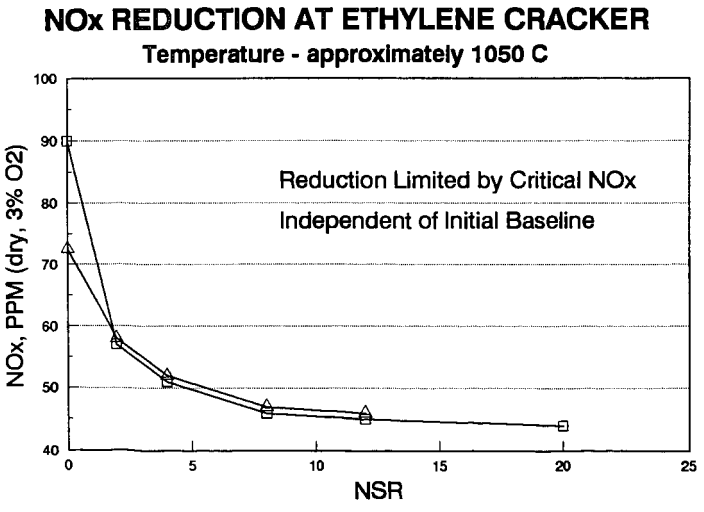
NOx REDUCTION AT ETHYLENE CRACKER
Temperature - approximately 1050 C
Reduction Limited by Critical NOx
Independent of Initial Baseline
NOx, PPM (dry, 3% O2)
NSR
100
90
80
70
60
50
40
0
5
10
15
20
25

Fig. 12

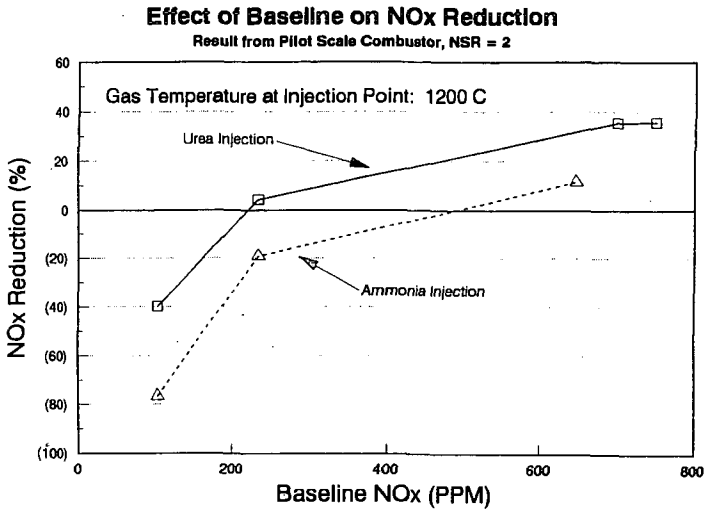
Effect of Baseline on NOx Reduction
Result from Pilot Scale Combustor, NSR = 2
Gas Temperature at Injection Point: 1200 C
Urea Injection
Ammonia Injection
NOx Reduction (%)
Baseline NOx (PPM)
60
40
20
0
(20)
(40)
(60)
(80)
(100)
0
200
400
600
800

Fig. 13

N_2O DECOMPOSITION CATALYZED IN THE GAS PHASE BY SODIUM

S. L. Chen, R. Seeker, R. K. Lyon, and L. HO
Energy and Environmental Research Corp
18 Mason
Irvine, CA. 92718

Key words: N_2O, sodium atom, fluid bed combustion, urea injection

INTRODUCTION

The concentration of N_2O in the atmosphere is observed to be increasing at a rate of 0.18% to 0.26% annually. This increase in the N_2O concentration is presumably the result of one or more human activities, though the activities responsible have not been identified with certainty. Whatever the source of the N_2O its increase in the atmosphere is a matter of concern both because N_2O is a greenhouse gas and because it has a major and unfavorable influence on the ozone layer (1,2,3).

Until recently it was believed that in additions to its problems with NO, NO_2, and SO_2 emissions pulverized coal firing also had a severe problem with N_2O emissions. Weiss and Craig (4), Pierotti and Rasmussen (5), Hae et al (6), and C. Castaldinin et al (7), have all reported measurements of N_2O emissions by pulverized coal fired utility boilers (8). N_2O levels of approximately 25% of the NO emissions were found. If one accepted this 25% correlation between N_2O and NOx emissions, the observed increase in N_2O concentration could be accounted for with reasonable accuracy as coming from pulverized coal firing (5). Thus in addition to its problems with NO, NO_2 and SO_2 emissions pulverized coal firing appeared to be an unacceptable technology because of its N_2O emissions.

Lyon and coworkers (9) have, however, shown that when samples of combustion gases are allowed to stand for periods of hours, chemical reactions occur which form N_2O. Since the studies mentioned above all involved taking samples for later analysis, they were all subject to this artifact and it was possible that the N_2O which was apparently present in gases from pulverized coal firing was in fact absent. Later measurements of N_2O emissions for numerous pulverized coal fired utility boilers and other large combustion systems confirmed this expectation, i.e. none of the long established combustion technologies were found to produce significant quantities of N_2O (10). Given N_2O is unstable at extremely high temperatures and that all the long established combustion technologies involve extremely high temperatures, this result is not surprising.

For the much lower temperatures involved in fluid bed combustion, however, N_2O production is quite high (11) and this may be a barrier to extending the industrial use of this technology.

N_2O emissions are also a problem in the NOxOUT and RAPRENOx technologies for controlling NOx emissions, but not in the Thermal DeNOx process. In the latter NH_3 is injected into hot flue gas, and NO is reduced by the

NH_2+NO reaction. In RAPRENOx, however, HNCO is injected, the NCO radical can be formed, and N_2O can be formed via the NCO+NO=N_2O+CO reaction. Since the urea injected in the
NOxOUT process decomposes to equimolar amounts of NH_3 and HNCO this technology also has a problem with N_2O production.

This paper reports the discovery of a promising new method of controlling the emissions of N_2O. This discovery has been demonstrated on a 0.9 MBTU/hr natural gas fired research combustor and has been examined by computer modeling.

APPARATUS, EXPERIMENTAL PROCEDURES AND COMPUTER MODELING PROCEDURES

Experiments were done in a 15.2 centimeter diameter by 2.4 meter long refractory lined tunnel furnace which has been described in detail elsewhere (12).
Computer modeling experiments were done using the reaction mechanism shown in Table 1 with the PC version of Chemkin. While this program is nominally limited to gas phase specie, the presence of liquid phase materials such as Na_2CO_3 was easily handled by assuming a fictional gas phase specie with thermodynamic properties such that at equilibrium it produced the same gas phase species in the same amounts as does the vaporization of the liquid phase material.

EXPERIMENTAL RESULTS

A series of experiments was done in which the effects of various additives on the reduction of NO by urea injection was examined. Figure 1 shows the results of an experiment comparing NO reduction by urea and by urea mixed with monosodium glutamate (MSG). The urea-MSG mixture achieves a deeper reduction of NO over a wider temperature range than did pure urea. While results similar to this were obtained with other mixtures of urea with organic compounds, as shown in Figure 2 the addition of MSG was also found to greatly decrease the production of N_2O.

Figure 3 shows the effect on N_2O production during NO reduction by urea of adding Na_2CO_3 and Na_2SO_4.

Figure 4 shows the results of an experiment in which solid Na_2CO_3 was injected into the post combustion gases at a point at which their temperature was 2150°F and N_2O was injected at a downstream point for which the temperature was 1800°F. Not only do these results show that Na_2CO_3 injection is an effective method for N_2O removal, they show that in some manner the Na_2CO_3 acts as a catalyst for N_2O removal, many N_2O molecules being removed for each injected Na_2CO_3.

Figure 5 shows computer modeling calculations which will be discussed later and experimental data for the temperature dependence of Na_2CO_3 catalyzed N_2O decomposition. It is interesting to note that within experimental error the rate of N_2O decomposition is independent of whether 50 or 100ppm Na_2CO_3 is used to catalyze the decomposition.

Figure 6 shows the effect of SO_2 on the Na_2CO_3 catalyzed decomposition of N_2O. While the presence of SO_2 does to some extent reduce the ability of Na_2CO_3 to catalyze the decomposition of N_2O, even high ratios of SO_2 to Na_2CO3 are not able to completely inhibit this catalyzed reaction.

COMPUTER MODELING RESULTS

At high temperatures the thermodynamically most favorable path for Na_2CO_3 vaporization is the reaction $Na_2CO_3 = 2Na + 1/2O_2 + CO2$. Figure 7 shows the calculated equilibrium for this reaction. The rate of the reaction between sodium atom and N_2O has been measured by a number of investigators and is relatively well established as are all of the other reactions shown in Table 1 with the exception of $Na+Na+O_2=NaO+NaO$. Since this reaction is analogous to a number of reactions which are known to be extremely rapid, it is assumed to occur with a rate equal to the three body collision rate.

In doing these calculations it was also assumed that the vaporization of Na_2CO_3 achieves equilibrium instantaneously.

The predictions of this computer model agree with experiment in that the model shows that Na_2CO_3 can cause rapid N_2O decomposition, that this N_2O decomposition is catalytic, and that it occurs only above a threshold temperature which the model approximately predicts.

In qualitative terms this reaction mechanism also explains the fact that SO_2 inhibited Na_2CO_3 catalyzed N_2O decomposition, i.e. SO_2 reacts readily with Na_2CO_3 converting it to nonvolatile Na_2SO_4. Once the Na_2CO_3 becomes coated with a layer of Na_2SO_4 its ability to exert its vapor pressure would be reduced.

CONCLUSIONS

The injection of sodium carbonate has been shown to be an effective method of preventing the emission of N_2O in combustion systems. This decomposition is catalytic but occurs in the gas phase. Computer modeling studies suggest that in this catalytic gas phase decomposition the reactions $Na+N_2O=NaO+N_2$ and $2NaO=2Na+O_2$ are important.

REFERENCES

1 Weiss., R.F., J. Geophy. Res., 86,7185-7195 (1981).

2 Khalil, M.A. and Rasmussen, R.A., Tellus, 35B, 161-169 (1983).

3 Marland, G., and Rotty, R.M. J.A.P.C.A., 35, 1033-1038 (1985).

4 Weiss, R.F. and Craig, H., Geophys. Res. Lett., 3, 751-753, (1976).

5 Pierotti, D. and Rasmussen, R.A., Geophys. Res. Lett., 3, 265-267 (1976).

6 Hao, W.M., Wofsy, S.C., McElroy, N.B., Beer, J.M., Toqan, M.A., J. Geophy. Res., 92, 3098-3194 (1987).

7 Castaldini, C., Waterland, L.R., and Lips, H.I., EPA-600-7-86-003a, 1986.

8 Ryan, J. V., and R. K. Srivastava, EPA/IFP workshop on the emission of nitrous oxide from fossil fuel combuetion (Rueil-Malmaison, France, June 1-2, 1988), Rep. EPA-600/9-89-089, Environ. Prot. Agency, Research Triangle Park, N.C., 1989. (Available as NTIS PB90-126038 from Natl. Technol. Inf. Serv., Springfield, Va.)

9 Lyon, R. K., Kramlich, J. C.,et. al., 23rd Symposium (International) on Combustion, in press. also see Lyon, R. K., and Cole, J. A., Combustion and Flame, 77, 139 (1989) and Kramlich, J. C. and Muzio, L.-J., Geophysical Research Letters, 15, 1369-1372, (1988)

10 Levine, J. S., 1991 Joint Symposium on Stationary Combustion NOx Control -- EPA/EPRI March 1991, Washington, D.C.

11 Amand, L. E., and Leckner, B., Combustion and Flames, 84, 181-196, (1991) Also see references 8 and 10.

12 S. L. Chen, M. P. Heap, D. W. Pershing, and G. B. Martin, Fuel 61, 1218 (1982)

Table 1
Rate Constants Used for Computer Modeling

CO+OH=CO2+H	(W&D)	1.5E+7	1.3	-770.0
CO+HO2=CO2+OH	(W&O)	5.75E13	0.0	22930.
H2+O2=2OH	(SLACK = 1.0E13)	3.0E13	0.0	43000.
OH+H2=H2O+H	(D-LSW)	1.17E9	1.3	3626.
H+O2=OH+O	(JAM,JCP 1981)	5.13E16	-0.816	16507
O+H2=OH+H	(LEEDS)	1.8E10	1.0	8890.
H+O2+M=HO2+M	(SLACK)	2.1E18	-1.0	0.0
H2O/21./ H2/3.3/ O2/1.5/N2/0.0/				
N+O2=NO+O	(SLACK = 3.9E19)	3.9E19	-1.35	0.0
OH+HO2=H2O+O2		5.0E13	0.0	1000.
H+HO2=2OH	(LEEDS)	2.5E14	0.0	1900.
O+HO2=O2+OH		4.8E13	0.0	1000.
2OH=O+H2O	(COHEN-WEST.)	6.0E+8	1.3	0.
H2+M=H+H+M		2.23E12	0.5	92600.
H2O/6/H2/3/N2/1.5/				
O2+M=O+O+M	(LEEDS)	1.85E11	0.5	95560.
H+OH+M=H2O+M		7.5E23	-2.6	0.
H2O/20/				
H+O+M=OH+M	(WESTBROOK)	1.0E16	0.0	0.0
H+HO2=H2+O2	(LEEDS)	2.5E13	0.0	700.
HO2+HO2=H2O2+O2	(LEEDS)	2.0E12	0.0	0.
H2O2+M=OH+OH+M	(LEEDS)	1.2E17	0.0	45500.
H2O2+H=HO2+H2	(LEEDS)	1.7E12	0.0	3800.
H2O2+OH=H2O+HO2	(LEEDS)	1.0E13	0.0	1800.
H+H2O2=H2O+OH	(WARNATZ)	1.0E13	0.0	3580.
O+H2O2=HO2+OH	(WARNATZ)	2.8E13	0.0	6400.
N2O+M=N2+O+M	(HANSON)	7.59E13	0.0	15100.0
N2O+M=N2+O+M	(GLARBORG, 86)	1.6E14	0.0	51600.0
N2O+O=N2+O2	(GLARBORG, 86)	1.0E14	0.0	28200.0
NAOH+M=NA+OH+M	(NBS)	1.51E21	-1.00	78344.0
NA+N2O=NAO+N2	(NBS)	1.15E14	0.0	2987.0
NA+NA+O2=NAO+NAO	(GUESS)	2.23E24	0.0	0000.0
NAO+O=NA+O2	(NBS)	2.23E14	0.0	0000.0
NAOH+H=NA+H2O	(NBS)	2.45E14	0.0	43470.0

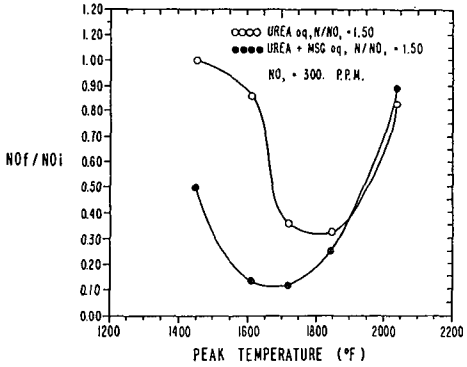

Figure 1

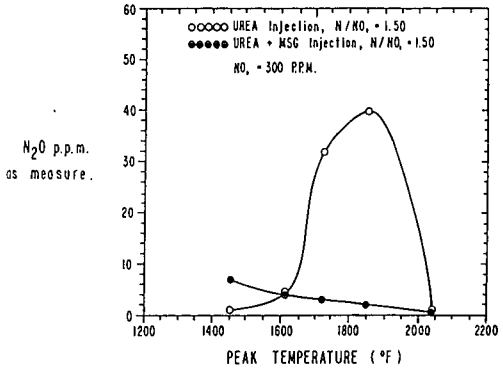

Figure 2

N_2O Reduction

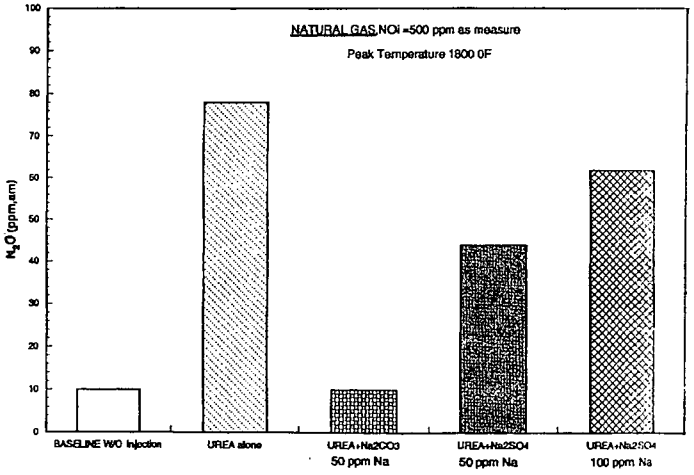

Figure 3

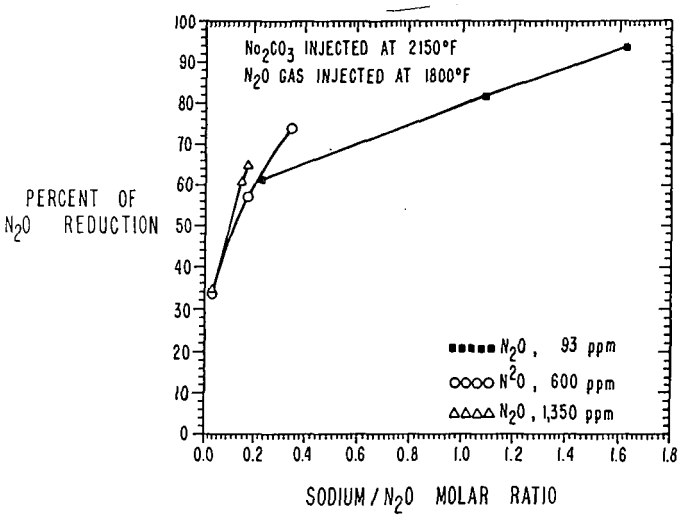

FIG. 4

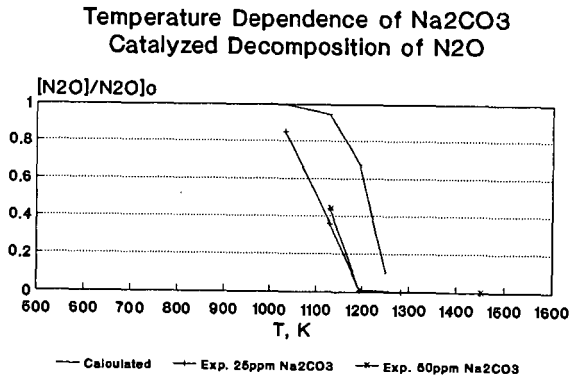

Calculations done for [N2O]o = 100ppm,
t = 0.1sec. 3.8%O2, 8.1%CO2, 16.2%H2O
[Na] = equilibrium for Na2CO3

Figure 5

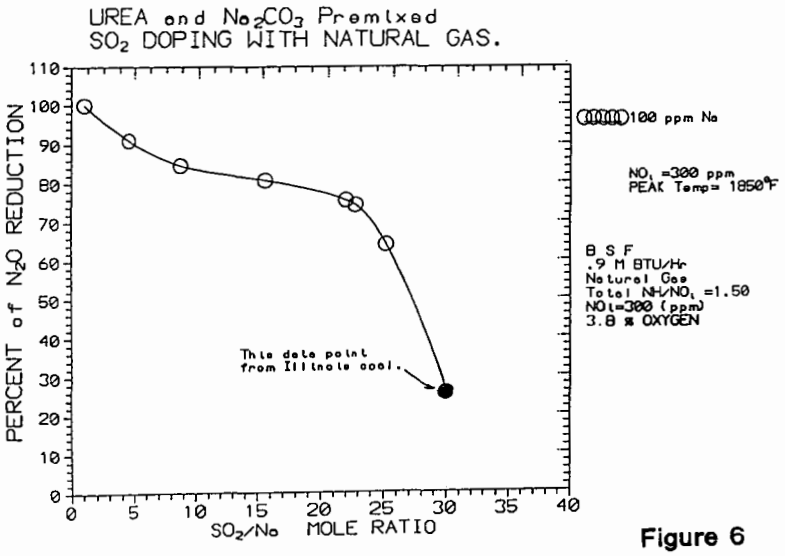

Figure 6

Equilibrium Calculation for
Na2CO3 ▪ 2Na + 1/2O2 + CO2

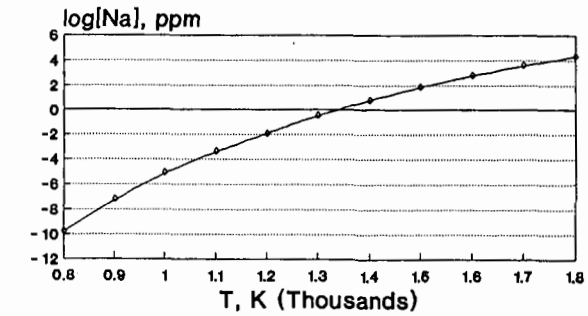

O2 ▪ 3.8%
CO2 ▪ 8.1%
Figure 7